8-2007

Effect of Length on the Performance of Lean NO_X Traps

Vitaly Y. Prikhodko
University of Tennessee - Knoxville

To the Graduate Council:

I am submitting herewith a thesis written by Vitaly Y. Prikhodko entitled "Effect of Length on the Performance of Lean NO_x Traps." I have examined the final electronic copy of this thesis for form and content and recommend that it be accepted in partial fulfillment of the requirements for the degree of Master of Science, with a major in Mechanical Engineering.

Ke Nguyen, Major Professor

We have read this thesis and recommend its acceptance:

Stuart Daw, J. Roger Parsons, David K. Irick

Accepted for the Council:
Dixie L. Thompson

Vice Provost and Dean of the Graduate School

(Original signatures are on file with official student records.)

To the Graduate Council:

I am submitting herewith a thesis written by Vitaly Y. Prikhodko entitled “Effect of Length on the Performance of Lean NO_x Traps.” I have examined the final electronic copy of this thesis for form and content and recommend that it be accepted in partial fulfillment of the requirements for the degree of Master of Science, with a major in Mechanical Engineering.

Ke Nguyen

Major Professor

We have read this thesis
and recommend its acceptance:

Stuart Daw

J. Roger Parsons

David K. Irick

Acceptance for the Council:

Carolyn R. Hodges

Vice Provost and
Dean of Graduate School

(Original signatures are on file with official student records)

EFFECT OF LENGTH ON THE PERFORMANCE OF LEAN NO_X TRAPS

A thesis
Presented for the
Master of Science
Degree
The University of Tennessee, Knoxville

Vitaly Y. Prikhodko
August 2007

ACKNOWLEGMENTS

I would like to express my deep gratitude to Prof. Ke Nguyen and Dr. Stuart Daw for their support and guidance during my tenure in graduate school. Special thanks to Dr. Stuart Daw for encouraging me to pursue higher education, and the opportunity he has provided me to work at National Transportation Research Center. I would like to thank Dr. David K. Irick and Dr. J. Roger Parsons for serving on my thesis committee. I would also like to thank the entire Fuels, Engines and Emissions Research group at ORNL for their assistance in my research; especially, Jae-Soon Choi for the advise, expertise and time he shared with me during my experimental work, and Josh Pihl for the assistance in running the Bench Flow Reactor. Thanks also to Todd Toops, Sam Lewis, Sreekanth Pannala, Kalyan Chakravarthy, Bill Partidge, Scott Eaton, Scott Smith and Hakyong Kim for their encouragement and friendship throughout my project.

I would like to express my appreciation to the U.S. Department of Energy, Office of FreedomCAR and Vehicle Technologies for providing funding for my work. I would like to thank EmeraChem and Umicore for providing the catalyst samples used in this project.

ABSTRACT

The effect of monolith length on the NO_x performance of two different Lean NO_x Traps has been investigated using a bench flow reactor (BFR). The washcoat composition of one of the catalysts consists of Pt/K/γ-Al_2O_3; the major components of the other catalyst include Pt, Pd, Rh, barium, ceria and zirconia supported on γ-alumina washcoat. Samples of 2.22-cm in diameter and length of 2.54, 5.08 and 7.62-cm within each LNT were evaluated with long and short-cycle experiments at a fixed gas hourly space velocity, and results were compared between samples of different lengths. No significant difference in performance was observed in long and short-cycle experiments with full regeneration. On a contrary, significant difference was observed in short-cycle experiments with partial regeneration: the longer the sample the better the performance.

The intra-catalyst concentration of H_2 measured at different axial locations in short-cycle experiments indicated higher H_2 consumption in shorter samples. A series of experiments was carried out to ascertain different mechanisms of H_2 consumption, and results indicated different degrees of lean and rich front back-mixing for samples of different sizes. Higher back-mixing in shorter samples resulted in a higher H_2 loss via its oxidation by O_2 and lesser H_2 availability for reducing stored NO_x, which in turn affected catalyst's performance when regeneration was limited by amount of H_2 available.

TABLE OF CONTENTS

LIST OF TABLES

LIST OF FIGURES

CHAPTER 1

INTRODUCTION

Combustion of fossil fuels such as coal, oil and natural gas used in industrial processes, transportation and powering amenities of modern life is essential to human existence, but combustion is not without undesirable side effects. Pollutants emitted during combustion are responsible for smog, acid rain, global warming and ozone depletion which are a serious threat to vegetation, wild life and human health.

Major components of fossil fuels are carbon and hydrocarbons (coal is mostly carbon; oil and natural gas are mainly hydrocarbons) which in ideal combustion process yield carbon dioxide and water as shown in Equations 1.1 and 1.2:

$$C + O_2 \rightarrow CO_2 \quad (1.1)$$

$$C_xH_y + a\ O_2 \rightarrow x\ CO_2 + (y/2)\ H_2O \quad \text{where } a = x + y/4 \quad (1.2)$$

In reality, combustion of fossil fuels generate small quantities of undesirable products such as carbon monoxide, oxides of nitrogen and particulate matter, which in large amounts (more than normally occurs naturally) have harmful effects on human health and environment.

The largest source of air pollution is the motor vehicles. Three main pollutants emitted by the vehicles are hydrocarbons (HC), carbon monoxide (CO) and nitrogen oxides (NO_x):

- Hydrocarbon emissions are products of incomplete combustion. They react with oxides of nitrogen to form ground level ozone (O_3), which is the primary component of smog. Ozone irritates eyes, causes shortness of breath, wheezing, fatigue, headaches and nausea, and aggravates respiratory problems. Some of the hydrocarbons are also toxic.

- Carbon monoxide (CO) is also a product on incomplete combustion. It is colorless, odorless and poisonous gas. Carbon monoxide restricts the flow of oxygen to the body's organ, and at high levels, it can be fatal.
- Nitrogen oxides (NO and NO_2 or collectively NO_x) are formed via oxidation of nitrogen under high pressure and temperature conditions of combustion inside the engine cylinder. NO_x emissions contribute to formation of ground level ozone, acid rain, and also cause various health problems.

The increase of the air pollution at alarming rates and the rising awareness of its harmful effects on human health and environment led to the establishment of the emissions standards by government agencies dictating the acceptable level of harmful emissions. In the USA, the Clean Air Act of 1970 set permissible limits for concentration levels of HC, CO and NO_x in vehicle exhausts. In order to comply with government regulations, automakers have made many refinements in engine design and exhaust system. The adoption of the catalytic converters in 1975 significantly reduced hydrocarbon and carbon monoxide emissions. In response to even tighter emission standards in 1980s, automakers equipped new cars with three-way catalysts (TWC) which simultaneously eliminate hydrocarbons, carbon monoxide and NO_x. These catalysts consist of a ceramic structure coated with a metal catalyst, usually platinum, rhodium and/or palladium. Three-way catalysts are optimized for the engine operating around stoichiometric, producing a net oxygen-free exhaust. Theoretically, at stoichiometric air-to-fuel ratio (for gasoline engine this ratio is about 14.7:1) all of the fuel reacts with all of the oxygen in the air. However, in reality, the fuel air mixture varies from slightly lean (excess of oxidant) to slightly rich (excess of fuel). Three-way catalysts use oxygen and NO_x in the slightly lean mixture to reduce HC and CO in the slightly rich mixture to form nontoxic CO_2, H_2O and N_2. Most modern cars today are equipped with TWC and through years of research and development emissions of HC, CO and NO_x have been

declining significantly since 1970. As a result, today's vehicles emit only a fraction of pollutants they used to emit in 1970s.

In recent years, the USA Environmental Protection Agency (EPA) started to view carbon dioxide (CO_2), a product of ideal combustion, as a pollutant. Even though CO_2 is not toxic and does not directly impair human health, small increases in its concentration have effect on the environment by changing the average global temperature. When solar radiation reaches the earth, it mostly gets absorbed by the earth's surface. The earth radiates part of the absorbed energy back into outer space as infrared radiation. Certain atmospheric gases block the heat radiated from the earth and keep the earth warm. This process is known as the greenhouse effect and gases responsible for blocking the heat are called greenhouse gases with CO_2 being the primary component. The greenhouse effect is natural, and it makes the life on earth possible by keeping the earth at the proper temperature. However, excessive amounts of greenhouse gases would trap too much energy causing an increase in earth's average temperature – an undesirable effect known as global warming. Scientists predict that a rise of 2°C in average earth's temperature would cause severe changes in weather patterns with storms and heavy rains at some parts of the world and droughts in others resulting in disturbance of ecosystems and adverse side effects on human life. A major source of greenhouse gas emissions is transportation. These emissions can be reduced by improving engine efficiency which would lead to lower fuel consumption and reduction in carbon dioxide emissions. That can be achieved through the use of lean-burn engines.

Lean-burn engines operate under fuel-lean conditions resulting in complete combustion of fuel which leads to improved overall fuel economy and lesser amounts of HC, CO and CO_2 emissions, but since exhaust from lean-burn engine contains excess oxygen, removal of NO_x becomes troublesome. The three-way catalyst is incapable of reducing NO_x levels to acceptable amounts in oxygen-rich environment; therefore new technology is needed that is able to

remove NO_x from lean-burn engine exhaust. Several technologies have been proposed to do that task: Selective Catalytic Reduction (SCR), Lean NO_x Catalyst (LNC) and Lean NO_x Trap (LNT).

SCR and LNC rely on selectivity of injected reductant to react with NO_x rather than O_2 in oxygen-rich exhaust. In SCR technology, ammonia (NH_3) injected into the exhaust stream reacts with NO_x to form N_2 and H_2O. Ammonia SCR has been successfully implemented in stationary applications. However, adopting this technology for mobile applications would require onboard storage of ammonia and ammonia distribution network which, perhaps, the main weakness of SCR. Lean NO_x Catalyst uses hydrocarbons as reductants, avoiding the need for added infrastructure, but fuel penalty, narrow operating temperature window, insufficient durability and low NO_x conversion are the obstacles for LNC use in exhaust aftertreatment.

In Lean NO_x Trap technology, NO_x reduction is achieved by storing NO_x during normal lean exhaust conditions and then reducing the stored NO_x during periodic rich excursions of short duration. LNT offers higher NO_x conversion efficiency and wider operating temperature window than its competitors, making LNT an attractive candidate for NO_x abatement in lean-burn engine exhaust. The main drawbacks of LNT are fuel penalty for rich excursions, sulfur poisoning and sophisticated engine control strategies.

A typical LNT catalyst consists of honeycomb-like ceramic monolith coated with three primary components: precious metals such as Pt, Pd and Rh, alkali or alkaline earth metals such as Ba and K, and a high surface area support material such as γ-Al_2O_3. During normal lean exhaust conditions, NO is oxidized to NO_2 over the precious metal catalysts and stored on alkali/alkaline earth metals in the form of nitrates. During periodic rich excursions, NO_x is released from the storage sites and (ideally) reduced to N_2 over precious metals as shown in Figure 1.1.

In the present study, the effect of monolith length on the performance of Lean NO_x Trap is investigated. Conventional census rules out the performance

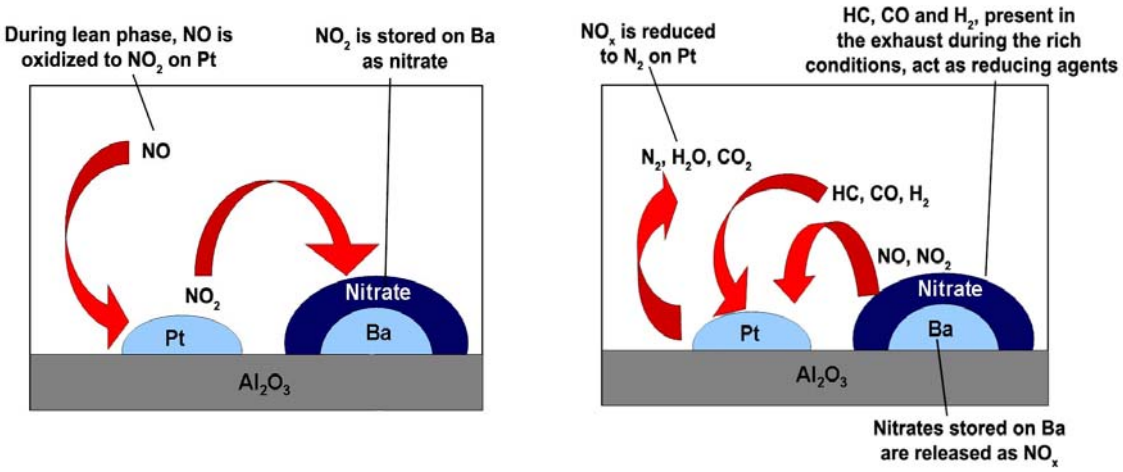

Figure 1.1. Schematic of LNT Operation

dependence on the length at a given gas hourly space velocity. As seen in the dimensionless form of the fluid phase mole balance for each species in the mixture, Equations 1.3 to 1.5, reacting system is governed by residence time (reciprocal of space velocity) and mass transfer coefficient. In a fully-developed

$$-\frac{\partial C_A^*}{\partial z^*} - \tau k_{m,A} a_c (C_A^* - C_{As}^*) = \frac{\partial C_A^*}{\partial t^*} \tag{1.3}$$

$$C_A^* = 1 \quad \text{at } z^*=0 \tag{1.4}$$

$$\frac{\partial C_A^*}{\partial z^*} = 0 \quad \text{at } z^*=1 \tag{1.5}$$

laminar flow, mass transfer coefficient is constant ($k_{m,A}$, m/s); therefore, reacting system is governed by residence time only (a_c is the ratio of wetted perimeter to cross-sectional area of the channel, m/m^2). Since LNT is designed to operate in a laminar flow regime (Re<2100) for preventing large pressure drops, changing the sample length should not affect the catalyst performance as long as space velocity or residence time is kept constant. However, significantly different results are often obtained from LNT evaluation experiments performed under the same conditions, i.e., same catalyst formulation, temperature, space velocity and gas mixture composition. As different sample sizes are often used in LNT

evaluation as restricted by reactor design, length is suspected as the culprit of LNT performance disparity.

To investigate the effect of monolith length on Lean NO_x Trap performance, samples of 2.22-cm in diameter and 2.54, 5.08 and 7.62-cm-long cored from two LNTs of different formulation and physical properties were evaluated at a fixed space velocity of 30,000 h^{-1} (flow had to be increased with increasing length to keep the same space velocity) using a bench flow reactor (BFR). Evaluation consisted of two sets of cycling experiments: long and short-cycle experiments. Short-cycle experiments were intended to approximate the catalyst operation in engine exhaust applications while long cycling were performed to explore the processes which are not, otherwise, observed in short-cycle experiments. Both sets of cycling experiments were performed at three different temperatures. Two reductant concentrations were used in short-cycle experiments: one to represent partial regeneration and the other full regeneration. The reductant concentration for partial regeneration experiments represents the concentration of the reductant that is below the theoretical amount needed to reduce the integral amount of NO_x that enters during the trapping part of the cycle. Full regeneration uses significantly higher reductant concentration than theoretical one to insure that regeneration of the catalyst is not limited by the amount of reductant. Hydrogen (H_2) was used as a reductant in all of the experiments.

The results of the cycling experiments are compared between samples of different lengths; no significant difference in performance is observed in long-cycle experiments and in short-cycle experiments with full regeneration. On the other hand, significant difference in performance is observed in short-cycle experiments with partial regeneration: the longer the sample the better the performance (as measured by NO_x conversion efficiency). The intra-catalyst concentration of H_2 measured at different axial locations in short-cycle experiments indicates higher H_2 consumption in shorter samples. Since availability of H_2 appears to cause the differences in LNT performance in short-

cycle experiments, investigation was carried out to ascertain mechanisms of H_2 consumption. To investigate the amount of H_2 consumed by O_2 stored on the surface of the catalyst, short-cycle experiments without NO in the lean phase (oxygen storage capacity or OSC experiments) were performed and results followed the trend previously observed in short-cycle experiments: more H_2 is consumed in shorter samples. The results of the OSC experiments seem to indicate that the consumption of H_2 might possibly occur via other mechanisms in addition to oxygen stored on the catalyst's surface. The catalytic reaction between H_2 and O_2 at the interface between the lean and rich phases may contribute significantly to H_2 consumption; the extent of which depends on the degree of mixing at the lean/rich interface. To evaluate the extent of back-mixing, OSC experiments with a nitrogen purge of ten seconds between lean and rich pulse (referred to as back-mixing experiments) were performed. Nitrogen purge creates an inert environment between the lean and rich front, which should eliminate H_2 consumption due to lean/rich front back-mixing, and indeed nitrogen purge resulted in a decrease of H_2 consumption in shorter samples, making H_2 trends similar between samples of three different lengths.

Back-mixing occurs to a higher degree in a slower moving front resulting in higher H_2 consumption and less H_2 availability to reduce stored NO_x, thereby lowering catalyst's NO_x conversion when regeneration is limited by amount of H_2 available as in the case of partial regeneration.

CHAPTER 2

LITERATURE REVIEW

This chapter contains a description of LNT operating principles in NOx emissions abatement. A discussion of the composition and operating principles of a typical LNT are presented in Sections 2.1 and 2.2, respectively. Section 2.3 focuses on effects of space velocity and reactor size.

2.1 Composition of LNT

A honeycomb monolith is a commonly used configuration for Lean NO_x Trap (LNT) catalyst. Such a configuration offers a high surface-to-volume ratio and a low-pressure drop across the catalyst. The monolith substrate is usually made from high-temperature resistant ceramic materials such as cordierite. Cordierite mainly consists from kaolin ($Al_2O_3 \cdot 2SiO_2 \cdot 2H_2O$), talc ($3MgO \cdot 4SiO_2 \cdot H_2O$) and alumina ($Al_2O_3$), and it has low coefficient of thermal expansion, high temperature stability, desirable porosity and excellent oxidation resistance [1]. The surface of the monolith is coated with a layer of high surface area material, commonly referred to as the washcoat, in which the catalytic components are dispersed. Commonly used washcoat material is γ-Al_2O_3 due to its high surface area. Often, other oxides are added to the washcoat to improve performance characteristics of the catalyst. A small amount of titanium oxide (TiO_2), for example, added to the alumina coating suppresses deactivation of the LNT caused by sulfur compounds such as SO_2 or SO_3 present in the exhaust gases [2]. To improve the hydrothermal stability of the catalyst and dispersion of the catalytic components resulting in an increased trapping performance of LTN, ceria (CeO_2) and zirconia (ZrO_2) are frequently added in the washcoat [3].

The catalytic components of Lean NO_x Trap are typically composed of at least one precious metal component (Pt, Pd, and Rh) and one alkali or alkaline

earth metal component (Ba, K, Cs, etc.), supported on a high surface area γ-Al_2O_3. Precious metals are used as oxidation and reduction catalysts. The precious metals normally used in the LNT are predominantly platinum (Pt) with smaller amount of either palladium (Pd) and rhodium (Rh). Platinum has highest activity in the catalytic oxidation of NO to NO_2, whereas Pd and Rh are much more active in NO_x reduction [4]; therefore, some LNT catalyst formulations include a mixture of these precious metals. The effectiveness of NO_x storage strongly depends on the basicity of the NO_x storage components: the stronger the metal basicity the more stable the stored NO_x [2, 5, 6]. The activity of NO_x storage components was found to decrease in the following order when testing was performed at 300˚C: Cs > K > Ba > Na > Mg [2]. On the other hand, activity of precious metals decreases in the presence of strongly basic storage components; thus, the selection of basicity of the NO_x storage components is important for optimum operation of LNT. Furthermore, the amount of NO_x that can be stored at a given temperature varies with the type of the storage material. For example, catalysts containing potassium have higher NO_x conversion than catalysts with barium at temperatures above 350˚C; on the other hand, barium-based catalysts have higher activity at temperatures below 350˚C [2].

2.2 Principle of Operation

In Lean NO_x Trap, NO_x reduction is achieved by storing NO_x during normal lean exhaust conditions and then reducing the stored NO_x during periodic rich excursions of short duration. Discussion of NO_x storage and NO_x reduction is given in Sections 2.2.1 and 2.2.2, respectively.

2.2.1 NO_x Storage

The principle of NO_x storage during normal lean exhaust conditions can be described by a two-step process. First, NO is oxidized to NO_2 over the precious metal catalysts via the following reaction [7]:

$$NO + ½\ O_2 \rightarrow NO_2 \quad (2.1)$$

The resulting NO_2 is subsequently stored on alkali/alkaline earth metals in the form of nitrites and/or nitrates.

Since NO_x exists mainly as NO in engine exhaust – approximately 90% – and with NO_2 being a precursor for the storage process [5, 8, 9, 10] the effectiveness of the first reaction strongly affects the overall performance of Lean NO_x Trap catalyst. As discussed previously in Section 2.1, precious metals have different activities for NO oxidation with Pt being the most effective oxidation catalyst; thus, the overall performance of the LNT is greatly affected by the choice of precious metals. Furthermore, the NO oxidation to NO_2 can be either kinetically or thermodynamically limited. At low temperatures NO oxidation is kinetically-limited preventing the reaction in Equation 2.1 from reaching equilibrium (at the thermodynamic equilibrium, NO_2 is the dominant species when the temperature is below 200˚C based on 250ppm of NO_x, 8% O_2 and a balance of N_2). As the temperature increases NO oxidation becomes equilibrium-limited [7, 11].

The second step in NO_x storage involves reaction of NO_2 with the sorbent compounds to form nitrites and/or nitrates. Several spectroscopic studies confirm the presence of nitrite and nitrate compounds on the catalyst surface with nitrates becoming the prevalent adsorbed species at high temperatures and long exposure times [12, 13, 14]. Multiple reaction pathways or mechanisms have been proposed to explain the nitrate formation, and they are applicable to any alkali or alkali-earth metals [11]:

- Formation of nitrite from BaO, NO and oxygen atom, and subsequent oxidation to the nitrate

$$BaO + 2NO + O^* \rightarrow Ba(NO_2)_2 \quad (2.2)$$

$$Ba(NO_2)_2 + 2O^* \rightarrow Ba(NO_3)_2 \quad (2.3)$$

- Formation of nitrate from BaO, NO_2 and oxygen atom

$$BaO + 2NO_2 + O^* \rightarrow Ba(NO_3)_2 \quad (2.4)$$

- Formation of nitrate from BaO, NO and multiple oxygen atoms

$$BaO + 2NO + 3O^* \rightarrow Ba(NO_3)_2 \quad (2.5)$$

- Intermediate barium peroxide reacts with NO_2 to form the nitrate

$$BaO_2 + 2NO_2 \rightarrow Ba(NO_3)_2 \quad (2.6)$$

- As N_2O_4 forms, it reacts with BaO and NO_2 to form a mixture of nitrites and nitrates. Nitrites are subsequently oxidized by oxygen to form nitrates as in Equation 2.3

$$2NO_2 \rightarrow N_2O_4 \quad (2.7)$$

$$2BaO + N_2O_4 + 2NO_2 \rightarrow Ba(NO_3)_2 + Ba(NO_3)_2 \quad (2.8)$$

- Reaction of NO_2 and BaO to form a mixture of nitrites and nitrates

$$2BaO + 4NO_2 \rightarrow Ba(NO_3)_2 + Ba(NO_3)_2 \quad (2.9)$$

The reactions given by Equations 2.2 to 2.9 are reversible or equilibrium reactions, and the equilibrium is shifted toward the NO_x storage with NO_2 presence in the gas stream. The reactions 2.2 to 2.5 require (O*) for the formation of the nitrite and nitrate species. Monatomic oxygen, O*, originates either from O_2 dissociated on precious metals in close proximity to storage component or from another NO_2 molecule [11]. In all of the reactions – 2.2 to 2.9 – barium oxide (BaO) is the precursor state; the actual form of the barium depends on the composition of the exhaust gases. For example, when CO_2 and H_2O are present in exhaust gases barium hydroxide ($Ba(OH)_2$) and barium carbonate ($BaCO_3$) are dominant compounds on the catalyst surface. Initially, BaO, $Ba(OH)_2$ and $BaCO_3$ coexist at the catalyst surface, and NO_x storage occurs first on BaO, then $Ba(OH)_2$ and finally $BaCO_3$ [15]. Continuous presence of CO_2 in the exhaust results in transformation of BaO and $Ba(OH)_2$ sites into more stable $BaCO_3$, causing a decrease in LTN trapping capacity. The presence of H_2O has similar effects; however, its presence reduces the negative impact of

CO_2 on NO_x storage since H_2O increases the amount of hydroxides at the surface via the equilibrium reaction given by Equation 2.10 [11, 15].

$$BaCO_3 + H_2O \rightarrow Ba(OH)_2 + CO_2 \quad (2.10)$$

The Lean NO_x Trap catalyst has a certain capacity to store NO_x, and once the storage sites approach saturation NO_x starts to break through. Before NO_x slip reaches unacceptable amount, the catalyst is exposed to a brief rich excursion causing the release and reduction of stored NO_x.

2.2.2 NO_x Reduction

Operation of LNT catalyst requires periodic regeneration of the surface to recover some or all of the original storage capacity. The regeneration of the catalyst surface is accomplished by exposing LNT to a mixture of reduced species such as hydrocarbons (HC), hydrogen (H_2) and carbon monoxide (CO). These reductants can be obtained by injecting fuel into the exhaust upstream of the catalyst (referred to as in-pipe injection regeneration) or by altering the combustion process of the lean-burn engine so that periodic fuel-rich exhaust is produced (referred to as in-cylinder regeneration). Different reductant compositions are obtained depending on a strategy used to deliver reductants [16], but the end result is to have enough reductants to create a net reducing environment which requires elimination of O_2 in the gas phase and O_2 stored on the catalyst surface, to release NO_x and subsequently reduce it to N_2 [11]. Insufficient surface regeneration results in continuous accumulation of nitrite or nitrate species over subsequent cycles and decrease in LNT trapping efficiency up to a steady-state level where amount of NO_x being released and stored is nearly constant. The complete catalyst regeneration can be achieved by using longer rich period or greater reductant concentration and higher temperature [11].

The absence of O_2 and NO in the gas stream during rich phase drives the equilibrium in Equation 2.2 to 2.9 towards reactants releasing the stored NO_x. However, NO_x is not released in significant amounts by simply shutting off O_2 and NO and exposing the catalyst to inert gases at the temperatures at which

adsorption was carried out. On the other hand, exposing catalyst to rich conditions results in significant NO_x release even at temperatures below that of adsorption and effective reduction under near isothermal conditions [17]. This indicates that release and reduction of stored NO_x involves the activation of reductant such as H_2 on Pt sites resulting in destabilization of nitrate species, and it does not involve, as a preliminary step, thermal decomposition of stored NO_x [17]. Thermal decomposition becomes important when significant heat is released due to the exothermic reaction between reductant and oxygen stored on the catalyst's surface; a temperature rise as high as 150˚C has been previously observed at the middle of the LNT during switching from lean to rich conditions [18].

A number of NO_x reduction mechanisms in the regeneration phase has been proposed. Nova et al [17] proposed that reductant (H_2) is first activated on Pt sites followed by spillover onto the washcoat toward nitrate species causing them to decompose and to subsequently be reduced on Pt. Another proposed mechanism involves the surface diffusion of adsorbed NO_x species toward reduced Pt sites and their subsequent reduction. The reduction of NO_x is selective to N_2 under typical operating conditions [12]; however, at low temperatures and high reductant concentrations formation of NH_3 and N_2O can reach significant amounts [19].

2.3 Effect of Length on LNT performance

In literature, gas hourly space velocity (GHSV) not size dimensions is often used as a parameter for comparing LNT data from different sources given that other operating conditions are the same, i.e., same catalyst formulation, temperature and gas mixture composition. Even though changing gas hourly space velocity affects NO_x conversion in LNT – NO_x conversion increases with decreasing GHSV since gaseous species spend more time inside the catalyst [11, 20] – NO_x conversion should not be affected by changing size of the sample as long as the space velocity remains constant. However, significantly different

results are often obtained from LNT evaluation experiments performed under the same conditions, i.e., same catalyst formulation, temperature, space velocity, and gas mixture composition [21]. As different sample sizes are often used in LNT evaluation, length is suspected as the culprit of LNT performance disparity.

A review of the literature on Lean NO_x Traps reveals that no work has been published on the effect of catalyst size on the performance of LNT. The lack of work in this area stems from the conventional view that rules out the performance dependence on the LNT's size at a given gas hourly space velocity as previously discussed in Chapter 1. The goal of the work presented in this thesis is to determine if and how monolith length affects LNT performance. Samples of three different lengths and same diameter were evaluated at a fixed gas hourly space velocity using a bench flow reactor. To keep same GHSV, flow had to be increased with increasing length. Details of the experiments used in catalyst evaluations are given in Chapter 3 followed by results and discussion in Chapter 4 and conclusions in Chapter 5.

CHAPTER 3

EXPERIMENTAL APPARATUS AND PROCEDURE

In the present study, a bench flow reactor (BFR) located at Oak Ridge National Laboratory's National Transportation Research Center (NTRC) was used to investigate the effect of monolith length on Lean NO_x trap (LNT) performance. The BFR is designed to allow exposure of catalyst monolith samples to simulated exhaust gases, while maintaining precise control of the flow, temperature, and composition of the gases. Such control is needed to ensure the experimental reproducibility needed for studies of this type. Section 3.1 gives an overall description of the BFR setup, followed by Section 3.2 with a detailed description of its components.

Two LNT bricks (that is, segments of LNT monolith) of different formulation and physical properties were used in the present investigation. Their chemical and physical characteristics are given in Section 3.3. LNT monolith samples of 2.22-cm in diameter and length of 2.54, 5.08 and 7.62-cm were extracted from full size monoliths and evaluated using both long-period and short-period cycling experiments. Section 3.4 gives details of the short and long cycle experiments.

Reductant consumption trends during short cycles show different degrees of lean and rich front back-mixing for samples of different sizes. Higher back-mixing results in a higher reductant loss via its oxidation by O_2 which in turn affects catalyst's performance. To investigate the extent of back-mixing, short cycles with and without neutral purge between lean and rich pulse were performed. Details about these experiments can be found in section 3.4.

3.1 Overall Description of the Bench Flow Reactor

The bench flow reactor, located at Oak Ridge National Laboratory's (ORNL's) NTRC, is illustrated schematically and in a photograph in Figures 3.1 and 3.2, respectively. Individual components of simulated exhaust gases are introduced to the reactor via mass flow controllers. The outlets of the mass flow controllers are connected to three separate manifolds which are used for mixing oxidizing species (NO and O_2), reducing species (H_2) and inert gases (N_2 and CO_2). For lean/rich cycling a four-way valve is used to introduce the lean or rich pulse into the reactor. The gases from the inert manifold are directed to the water evaporator through a heated line. A peristaltic pump is used to deliver liquid water to the water evaporator in which liquid water absorbed onto quartz wool evaporates and is swept by inert gasses. Directly downstream of the water evaporator, inert gases and water vapor are combined with lean or rich gases and introduced to the reactor.

Three high-temperature manual valves are used to direct the gas flow to either one of two tubular furnaces or bypass line. Three additional high-temperature valves installed downstream of tube furnaces and bypass line are used to direct the gas flow to the desired furnace. The bypass line is used to flow gases during initial startup and to measure inlet concentrations of the gas species in the simulated exhaust gases prior to the experiment. A tube furnace contains the catalyst sample housed in a quartz-tube reactor. The reactor is outfitted with three type K thermocouples and a pressure transducer. Capillary probes 185 μm in diameter are installed upstream of the catalyst and connected to a spatially-resolved capillary inlet mass spectrometer (SpaciMS), which is capable of measuring spatially-resolved concentrations of various species.

Exits of both reactors and bypass line are connected to a heated exhaust line leading to the room's ventilation system. Gases are pulled from the exhaust line to the FTIR cell and NO_x analyzers for analysis. A diaphragm pump is used to draw gas through the FTIR cell; whereas NO_x analyzers are equipped with internal pumps. Upstream of the NO_x analyzers, an ammonia scrubber is used to

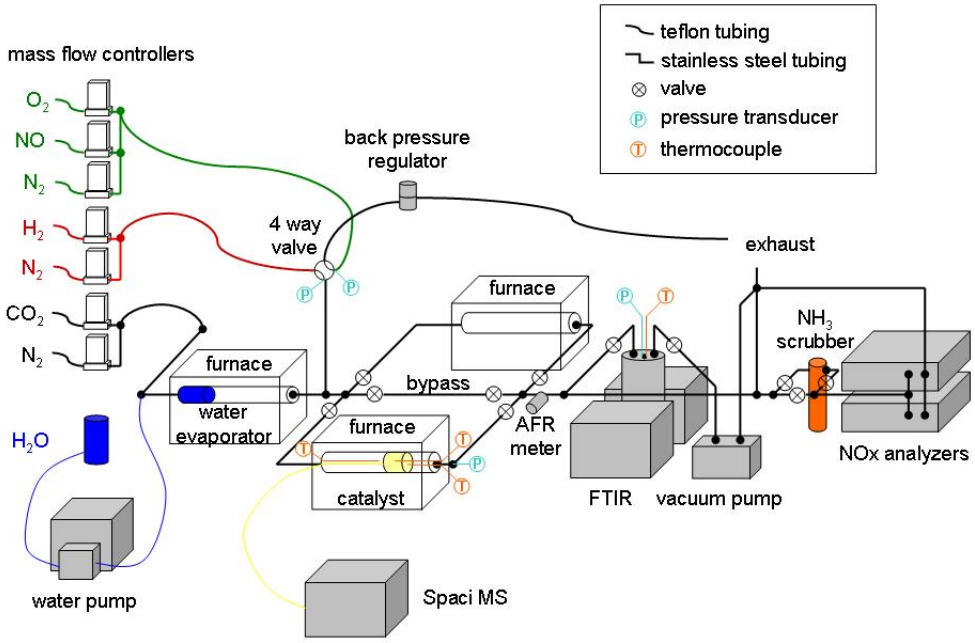

Figure 3.1. Schematic of the Bench Flow Reactor

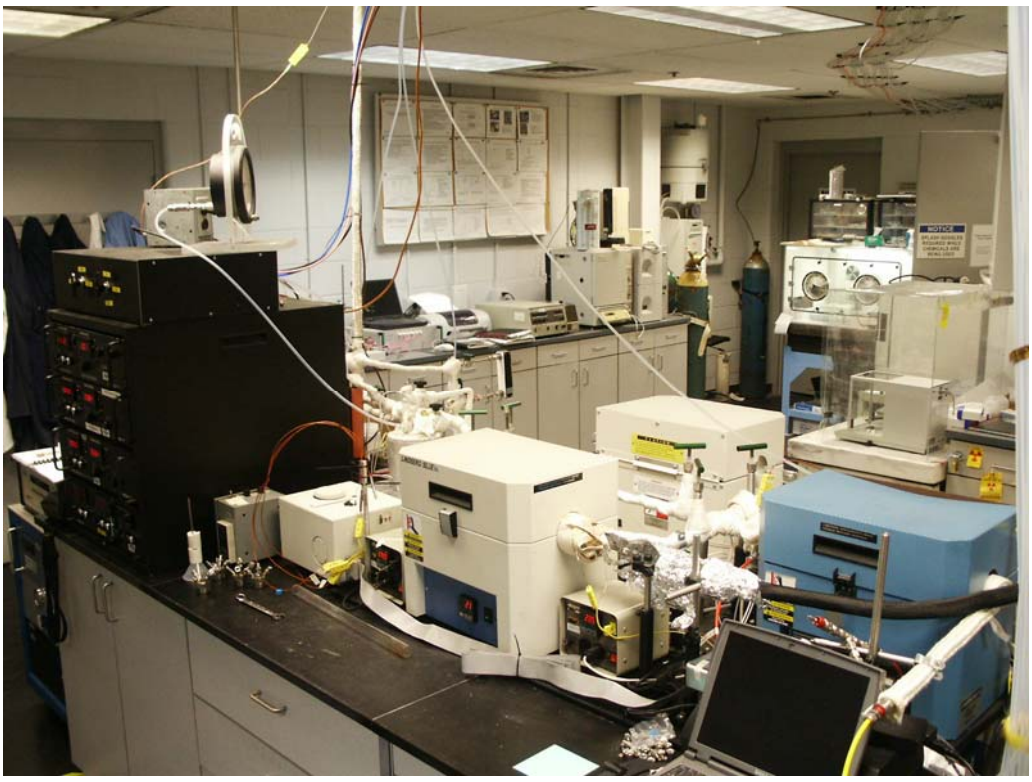

Figure 3.2. Photograph of the Bench Flow Reactor

prevent ammonia from interfering with NO_x measurements. National Instruments hardware and software are used to control the experiments and to acquire data during the experimental runs.

3.2 Individual Components of the Bench Flow Reactor

3.2.1 Mass Flow Controllers and Gas Manifolds

Unit Instruments 7300 and 7360 mass flow controllers (MFCs) are used to regulate the flow of individual components in the simulated exhaust gases to the reactor. The Unit 7360 model is specifically designed for corrosive gases such as NO. Since the mass flow controllers are calibrated with N_2 at standard temperature and pressure (STP), a correction factor is applied when other gases are used. The mass flow controllers are controlled by National Instruments LabView.

Each mass flow controller is connected to a gas cylinder with its outlet connected to one of the three separate mixing manifolds. One manifold is dedicated for inert gases (N_2 and CO_2), while the other two are for oxidizing (NO and O_2) and reducing species (H_2), respectively. The front and back panels of the manifold setups are shown in Figures 3.3 and 3.4, respectively. The front panel shows the mass flow controllers inlets and outlets, and manifold inlets and outlets. The back panel shows the mass flow controllers and manifold mixing chambers.

Swagelok quick-connect fittings and 0.64-cm Teflon tubing are used to connect the exits of the mass flow controllers and the manifold inlets. This setup gives a flexibility of connecting mass flow controllers to different manifolds. Outlets of the lean and rich manifolds lead to a four-way valve that controls the choice of lean or rich pulse introduction to the reactor. The inert manifold connects to a heated gas line that leads to the water evaporation system.

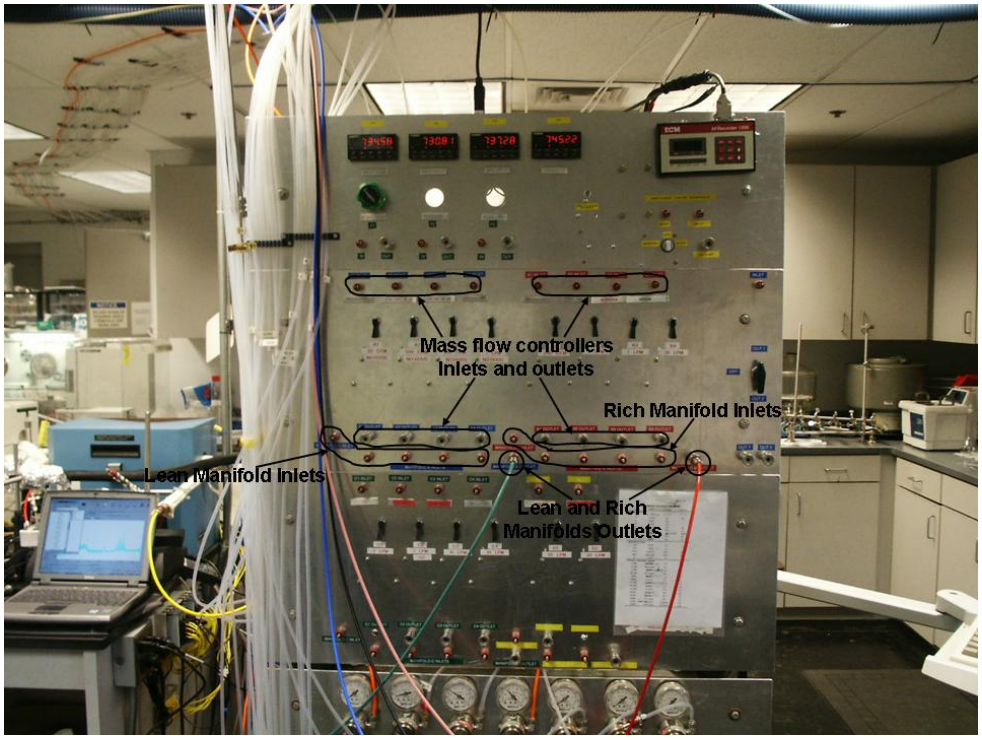

Figure 3.3. Front Panel of the Manifold Setups

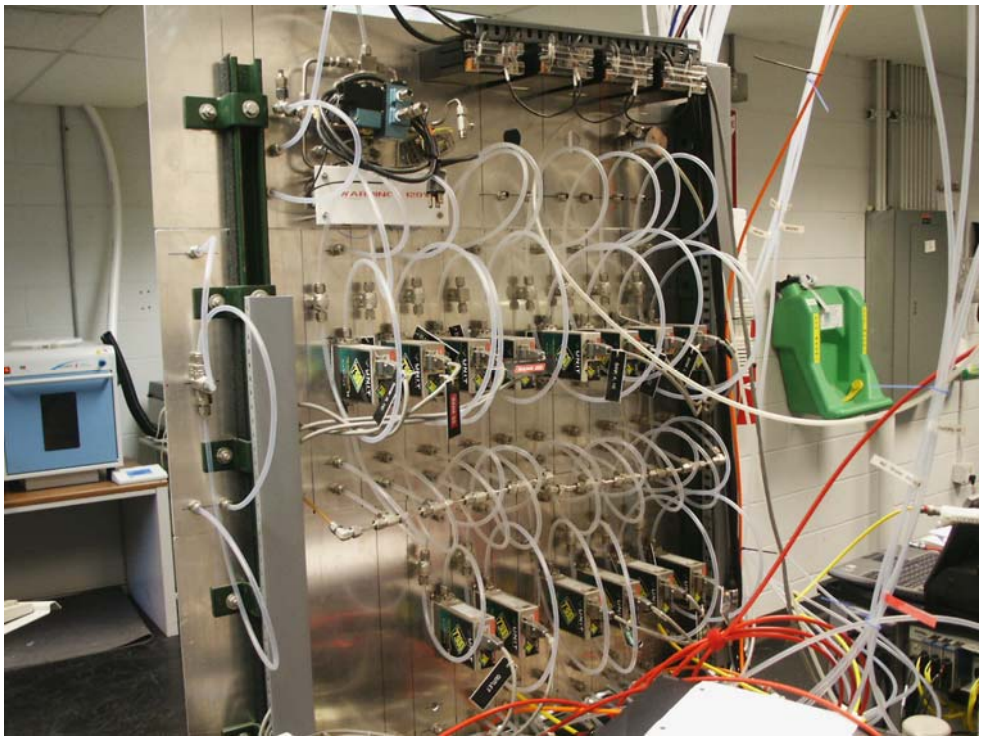

Figure 3.4. Back Panel of the Manifold Setups

3.2.2 Heated Gas Lines

Stainless steel tubes, 0.64-cm OD, with stainless steel Swagelok fittings are used to connect all of the components of the bench-flow reactor. The tubes are heated to different temperatures depending on their location in the BFR. The section before the water evaporator is heated to temperatures above 100˚C. The temperature in this section is varied depending on the flow rate used in the experiment. By varying the heating temperature the flow water pulsation is eliminated and a constant steam flow rate is maintained.

The line leading to the reactor is heated to the operating temperature of the catalyst. Since this section usually operates at temperatures up to 600˚C, Swagelok VCR-type connectors are employed. The VCR connector uses metal gasket face fittings which are easy to dissemble when catalyst samples are changed. The tubes downstream of the reactor are heated above 100˚C to prevent water condensation. The gas lines are heated with Thermolyne BriskHeat model BIH051-040LD flexible electric heating tapes controlled by either a variable voltage transformers or Yokogawa model UP150 programmable temperature controllers, and insulated by Zetex ceramic fiber tape.

3.2.3 Four-Way Valve and Back Pressure Regulator

A Numatics MicroAir Series direct solenoid actuated four-way valve is utilized to introduce either the lean or rich pulse into the reactor. This valve allows fast switching times (0.1 – 0.2 seconds) between lean and rich pulses. As shown in Figure 3.5, the valve has two inlets connected to the lean and rich manifolds, and three exits: the one in the middle leads to the reactor and the other two connect to the exhaust line. Two Omega PX811-020AV pressure transducers are used to measure pressures at the exit of the reactor and at the exits leading to the exhaust line. A Swagelok model KBP1A1C5CA40 back pressure regulator, connected to the exhaust line, is used to keep these two pressures equal. The valve's fast switching times and the use of back pressure

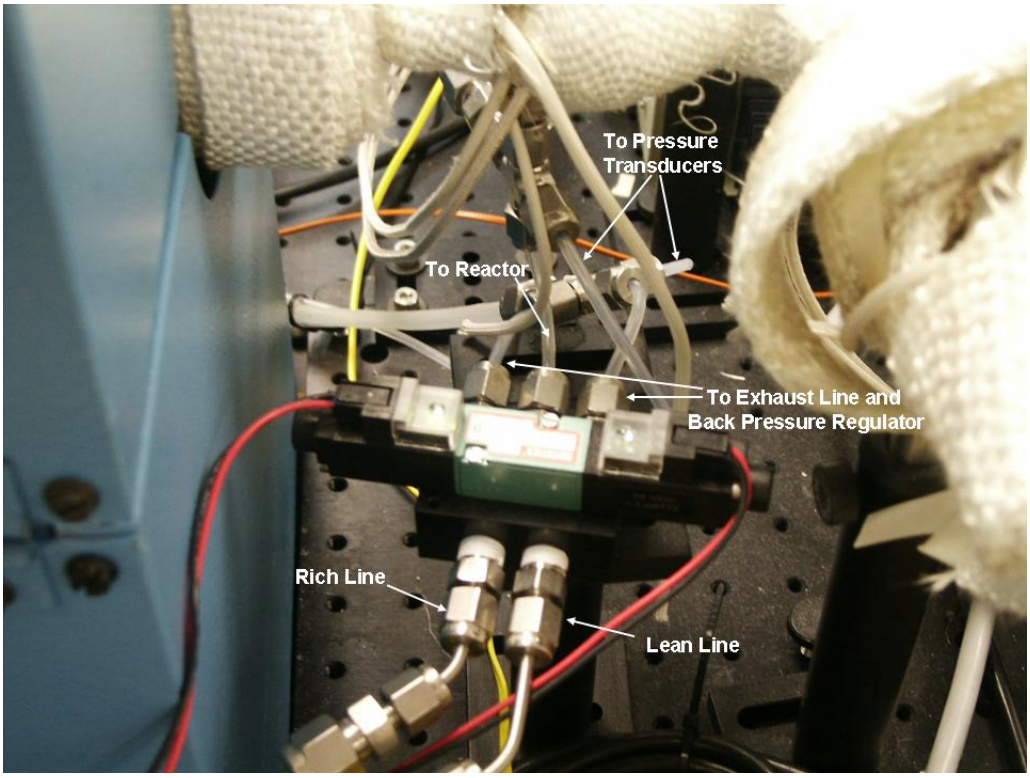

Figure 3.5. Four-Way Solenoid Valve

regulator ensures step-like changes and a constant flow of lean/rich gases to the reactor.

3.2.4 Water Vapor Delivery System

The water vapor delivery system consists of two main components: a Cole-Parmer MasterFlex peristaltic pump and a water evaporator. The pump is used to deliver liquid water to the water evaporator. Inside the water evaporator, liquid water evaporates and is swept by inert carrier gases.

Figure 3.6 shows a photograph of the pump with its main components labeled. De-ionized water is drawn from a container and delivered to the water evaporator via 0.89-mm ID PVC tubing. Pump manufacturer software called WinLin is used to control the pump. The pump is calibrated prior to each experiment to ensure that the rotation of the pump head gives desired flow rate of liquid water. The tubing transporting the liquid water connects to the 0.16-cm

stainless steel tube of the water evaporator. A photograph of the water evaporator is shown in Figure 3.7. A 1.26-cm OD stainless steel tube is placed inside of a tube furnace maintained at 350˚C. The front 1.5-cm of the stainless steel tube is packed with quartz wool while the rest is filled with glass beads. The tube is connected to a Swagelok union tee type fitting. One end of the fitting is connected to a 0.64-cm OD heated line of the inert carrier gases; the other to a bored 0.16-cm Swagelok fitting. A 0.16-cm OD stainless steel tube is inserted through the bored Swagelok fitting with its end buried inside the quartz wool. The other end is connected to the PVC tubing carrying liquid water from the water pump. Injected liquid water is absorbed onto the quartz wool, evaporates and is swept away by inert carrier gases.

3.2.5 Bypass Line

The bypass line is used to purge the bench-flow reactor with nitrogen during initial startup and to measure inlet concentrations of the gas species used in each experiment. Six Swagelok high-temperature bellows-sealed valves (SS-4UW), rated up to 650˚C—three upstream and three downstream of tubular furnaces and bypass line—are used to direct the gas flow to either one of two tubular furnaces or the bypass line.

3.2.6 Reactor Setup

LNT catalyst samples studied in the NTRC BFR are typically cut to 2.22-cm in diameter and wrapped in Zetex ceramic fiber strips to prevent gas bypass and then inserted in a 2.54-cm OD quartz-tube. The tube in turn is placed inside a Linberg/Blue M model TF55035COMA-1 Mini-Mite tubular furnace with a maximum operating temperature of 1100˚C. The catalyst sample is typically positioned 25.4-cm from the quartz-tube inlet. The section upstream of the catalyst sample is filled with glass beads to promote mixing and uniform heating of the gases. A mass spectrometer capillary is also inserted through the front end fitting as shown in Figure 3.8.

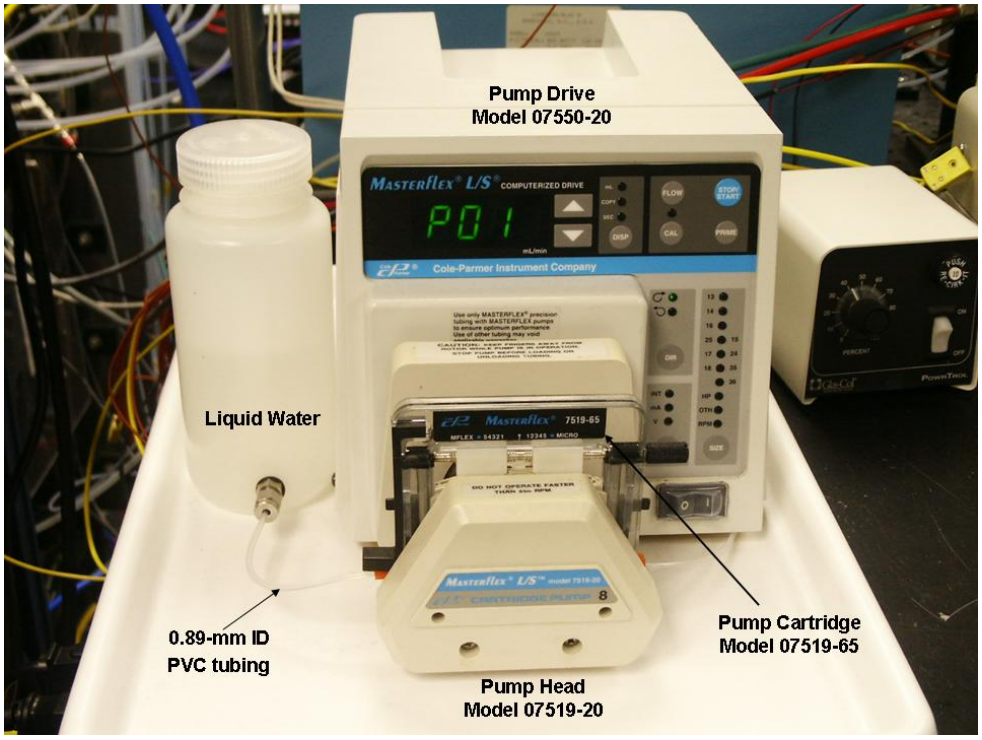

Figure 3.6. MasterFlex Peristaltic Pump

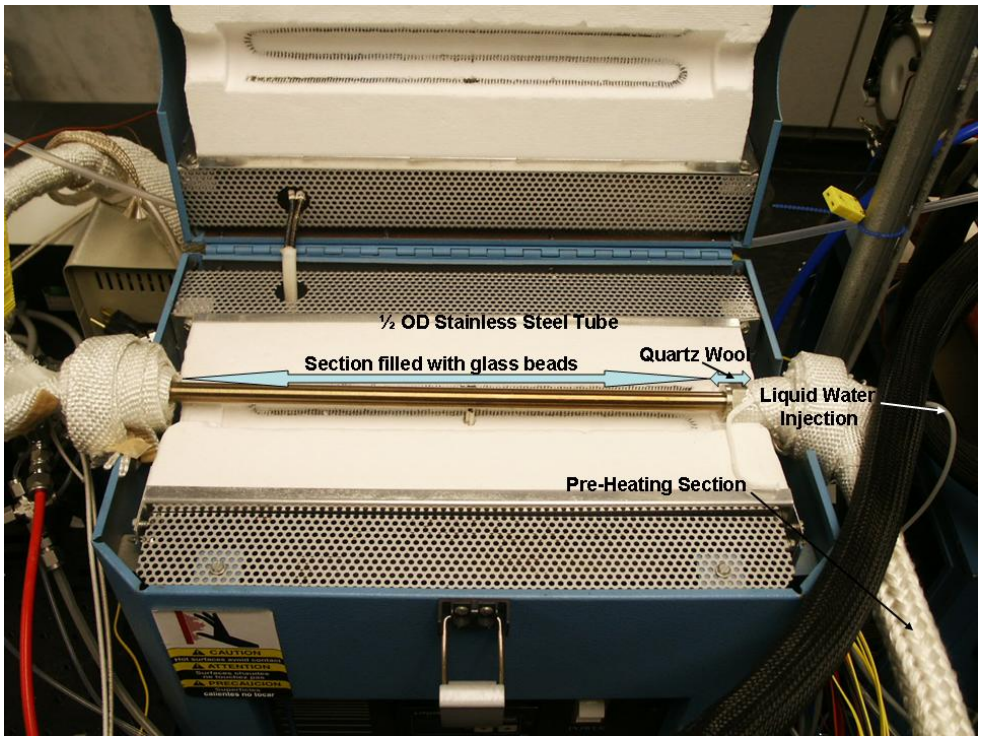

Figure 3.7. Water Evaporator

Three Omega type-K thermocouples are used to measure the inlet and exit gas temperatures as well as the temperature at the middle of the LNT catalyst sample while the reactor exit pressure is measured with an Omega PX811-020AV pressure transducer. For measuring the inlet gas temperature a thermocouple of 1.6 mm in diameter is inserted through the reactor front end fitting and positioned at a location approximately 1.5 mm from the sample inlet. The remaining two thermocouples, smaller in diameter (0.5 mm), are inserted through the reactor back end fitting and positioned in the radial center of the reactor: one located 1.5 mm away from the sample exit is used for measuring the exit gas temperature, and the other to measure the temperature at the middle of the sample.

Two custom-made end fittings are used to seal the quart-tube reactor. The disassembled fitting shown in Figure 3.9, consists of a 2.54-cm Swagelok end cap with five smaller Swagelok fittings welded onto it. These smaller fittings are used for connecting gas lines and pressure transducers, and for inserting thermocouples and mass spectrometer capillaries. Graphite ferrules seal the reactor and are proved to be leak free for conditions used in this investigation.

3.2.7 Spatially-Resolved Capillary Inlet Mass Spectrometer (SpaciMS)

One specialized measurement employed in the present study was the Spatially Resolved Capillary Inlet Mass Spectrometer or SpaciMS. SpaciMS was developed at the NTRC for application to the BFR and other types of emissions and engine measurements where extractive sampling is possible, and the basic setup is shown in Figure 3.10. It allows transient, spatially-resolved measurements of various species such as H_2 and NO_x with better temporal resolution than conventional analyzers. It uses capillary probes, 185 μm OD, to transport gas mixtures from the reactor to the mass spectrometer for analysis. The sampling end of the capillary probe is inserted through the front end fitting of the reactor and positioned in the radial center at different locations along the

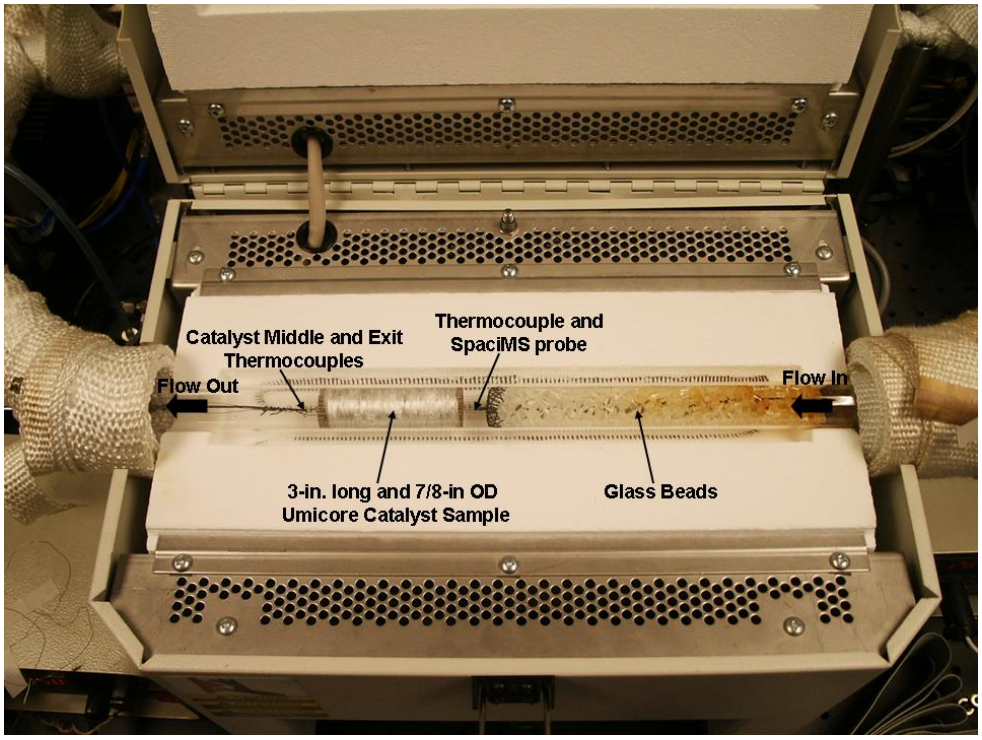

Figure 3.8. Reactor Setup

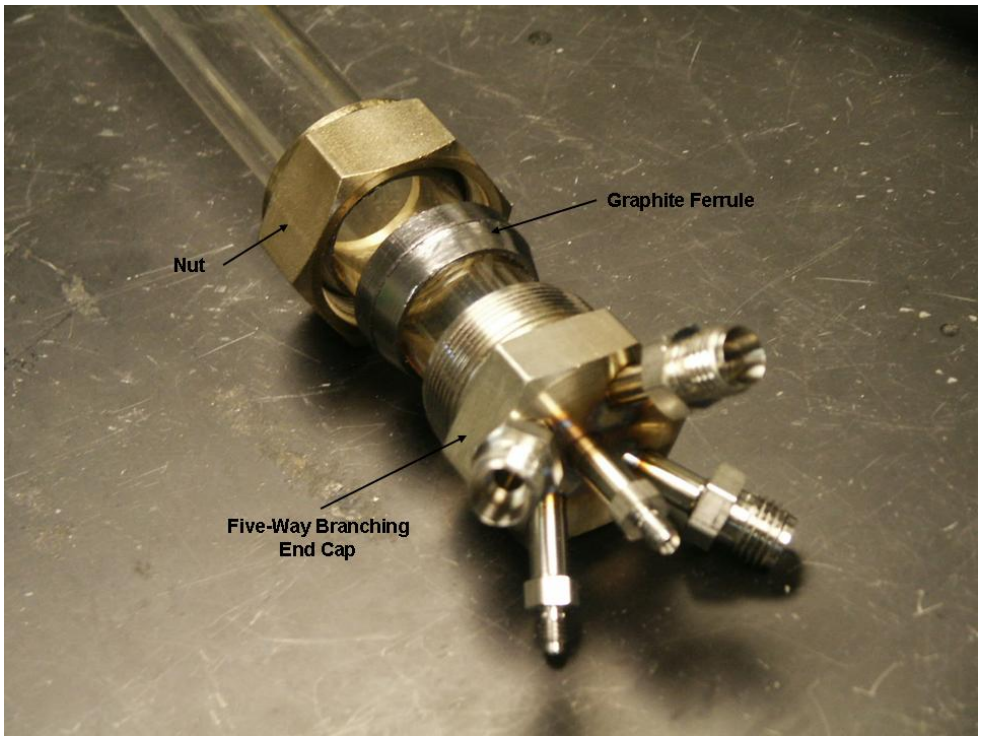

Figure 3.9. Reactor End Fitting

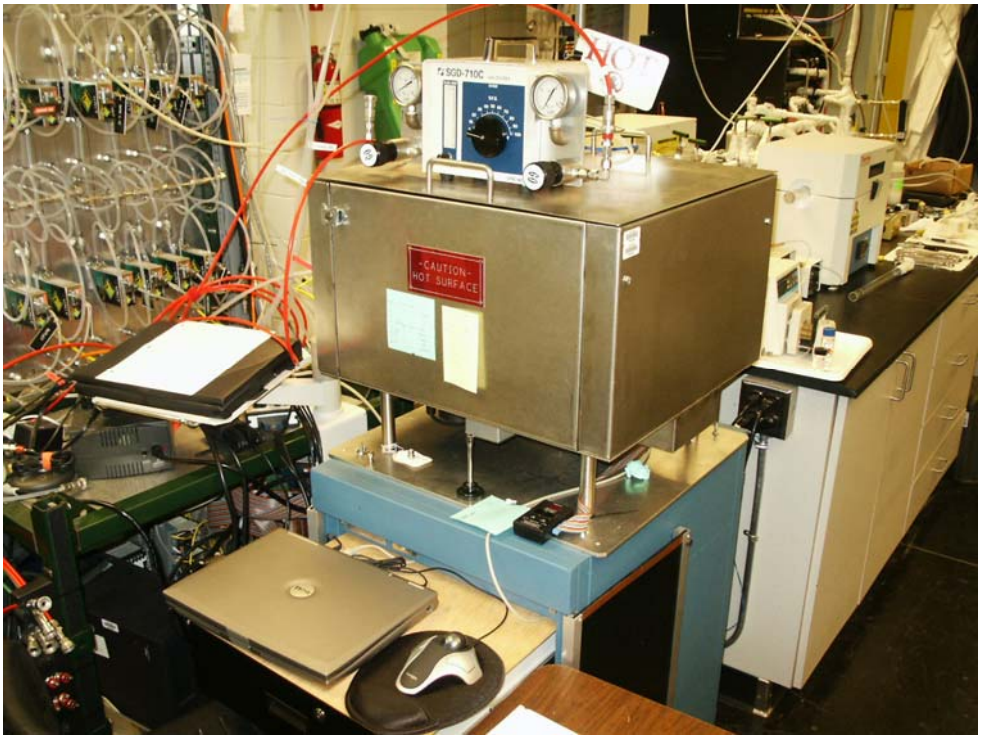

Figure 3.10. Spatially-Resolved Capillary Inlet Mass Spectrometer

catalyst length. The other end is connected to a multiple-port valve leading to spectrometer's ionization chamber. Between the reactor and mass spectrometer, the probe capillary is housed in a heated sheath to prevent water condensation. Even though multiple capillaries can be used at the same time, only one was employed in this investigation. This capillary was manually positioned at four different locations in the catalyst sample: catalyst inlet, quarter-way and half-way from the inlet, and exit.

The mass spectrometer ionization chamber is maintained at a vacuum (~10^{-6} Torr) by means of turbo-molecular and roughing pumps. The resulting vacuum creates a pressure gradient for transporting the gas mixture through the capillary from the reactor to the ionization chamber at a rate of 10 μL/min. The sample gas mixture is ionized by a filament, and the gaseous ions are separated by a magnetic sector mass filter according to their mass-to-charge ratios. The separated ions are then detected by a continuous-dynode electron multiplier.

After each experiment, the SpaciMS is calibrated by sending a known concentration of a particular gas diluted in N_2 through Horiba model SGD-710 gas divider. Since the mass spectrometer has linear response, only two points are needed for its calibration. A more detailed discussion on the principle and the operation of SpaciMS can be found in the paper by Partridge et al. [22].

3.2.8 Fourier Transform Infrared Spectrometer (FTIR)

A MIDAC model M2000 Fourier Transform Infrared Spectrometer (FTIR) equipped with a Gemini Specialty Optics gas absorption cell is used for measuring the concentration of the following species: NO_2, N_2O, NH_3, CO, CO_2 and H_2O. Figure 3.11 shows a photograph of the FTIR setup used in this study. The FTIR gas cell has a volume of 375 mL and a pathlength of 3 m. It is wrapped in a heating jacket connected to a Yokogawa model UP150 programmable temperature controller and maintained at 117˚C. A diaphragm pump is used to draw the gas mixtures from the exhaust line through the FTIR cell. Two Swaglok needle valves are installed at the FTIR gas cell's inlet and outlet and used to maintain a 2 L/min flow rate through the cell at 700 Torr (the same conditions are used to obtain calibration and background spectra). The flow rate and pressure are measured by a Gilmont Accucal model GF-6340-1130 flow meter and an Omega PX811-020AV pressure transducer, respectively. MIDAC's AutoQuant Pro software is used to acquire, analyze and quantify spectra.

In general, a spectrometer measures the extent to which electromagnetic radiation of a particular wavelength is absorbed by a gas sample. Infrared radiation typically changes the intensity of the rotations and vibrations of the molecules. IR records peaks at wavelengths at which absorption occurs, which in turn are used to identify the molecules present. The intensity of absorbance is proportional to the concentration of absorbing species.

The calibration used for quantifying the gas mixture is performed by sending known concentrations of a particular compound through the FTIR, and

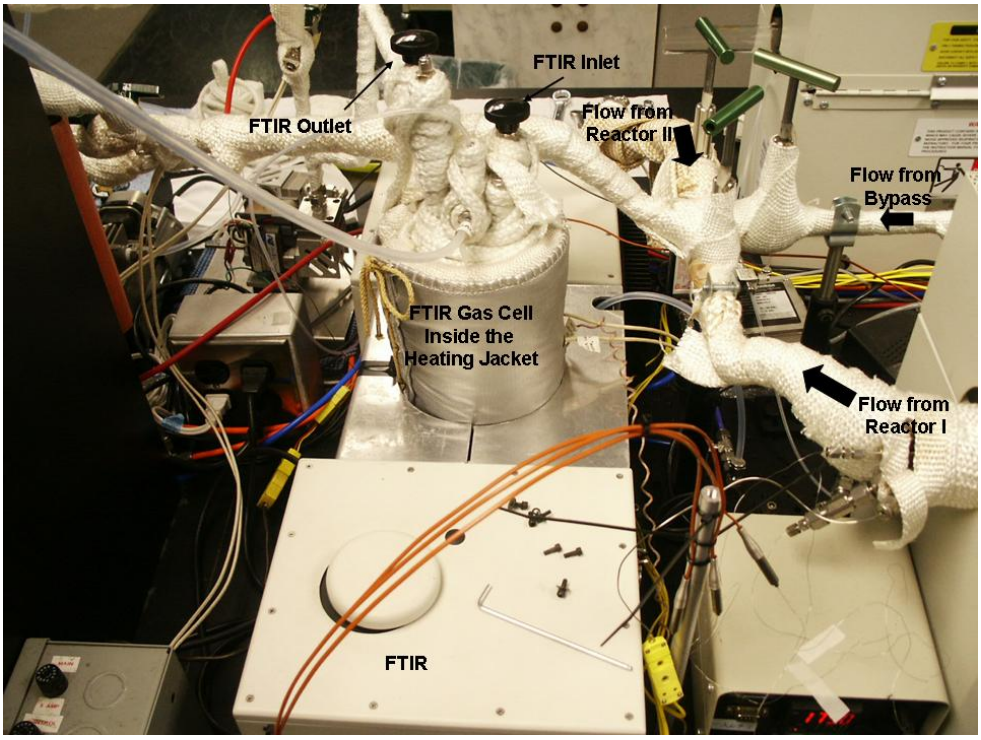

Figure 3.11. FTIR

the reference spectra of that compound are recorded. Once the reference spectra for all gases of interest are obtained, regions for analysis were selected. More details on FTIR's theory of operation and how calibration methods are implemented can be found in the master's thesis by Josh Pihl [19].

3.2.9 NO_x Analyzers and Ammonia Scrubber

Two California Analytical Instruments model 400 HCLD NO_x chemiluminescence analyzers are utilized to measure NO and NO_x concentrations in the gas mixture. These analyzers equipped with internal pumps draw sample of gas mixture from the exhaust line. NO in the gas mixture reacts with ozone generated internally by the analyzer to produce NO_2 in an electronically excited state. When NO_2 drops back to the ground state, light is emitted. The intensity of this light is proportional to the concentration of NO in the gas mixture. To measure NO_x, the gas mixture is first passed through the catalyst inside of the analyzer that converts all NO_2 in the gas mixture to NO.

Some experiments performed in this investigation produce ammonia which would interfere with NO_x measurements. Ammonia decreases the efficiency of the catalyst used to convert NO_2 in the gas mixture to NO, leading to low NO_x measurements. To overcome this problem, a Perma Pure model AS-200-08-SS ammonia scrubber is installed upstream of the NO_x analyzers. These scrubbers can be removed as needed when high levels of temporal resolution are needed in the NO_x measurements.

3.2.10 Data Acquisition System

National Instruments hardware and software are used to control the experiments and to acquire data. A Dell personal computer is equipped with data acquisition cards and LabView 7.1 software. Two LabView graphical interfaces are used to control experiments. One is used to control the flow rates of individual components of the simulated exhaust gas mixture via mass flow controllers and position of the four-way valve, the other to acquire and record data as received from nearly all of the components of the bench flow reactor. In addition two stand-alone computers are utilized to control SpaciMS and FTIR.

3.3 Catalysts

The two LNT catalysts used in this study are described in this section.

3.3.1 Catalyst A

Catalyst A manufactured by EmeraChem is mainly used in the power generating industry under the trade name of $SCONO_x$. It consists of a cordierite substrate washcoated with $Pt/K/\gamma\text{-}Al_2O_3$. Square catalyst monolith (15.24x15.24x15.24 cm) with a cell density of 31 cells per square centimeter is supplied by the manufacturer. A number of 2.54-cm long and 2.22-cm in diameter samples cored from that brick were “degreened” and tested for sample-to-sample variation using the measured NO_x concentration profiles. The “degreening” was performed for 8 hours at 550˚C under short cycling conditions

(see Section 3.4.1.1). Three 2.54-cm cores with similar performance were then selected and used in the performance evaluation of 2.54, 5.08 and 7.62-cm samples.

3.3.2 Catalyst B

Catalyst B supplied by Umicore is commercially available and designed for gasoline direct injection (GDI) engine applications. It is also the reference LNT catalyst utilized by the DOE Crosscut Lean Exhaust Emissions Reduction Simulation (CLEERS) program [23]. The major washcoat components include platinum, palladium, rhodium, barium, ceria, zirconia and γ-alumina. For this study, a cylindrical catalyst monolith, 11.84-cm in diameter and 15.24-cm long with a cell density of 97 cells per square centimeter was "degreened" in a furnace at 700˚C under a flow of 10% H_2O in air for 16 hours [19]. A core, 7.62-cm long and 2.22-cm in diameter was then obtained from the "degreened" brick and used for the evaluation. Once the 7.62-cm sample was evaluated, the front 2.54-cm of it was sectioned out and the 5.08-cm sample evaluated. Upon completion of the evaluation of the 5.08-cm sample, the 2.54-cm sample was prepared in a similar manner and evaluated.

3.4 Experimental Procedure

Prior to each set of experiments standard procedure requires all of the individual BFR components to be checked for possible malfunctions. After the initial checkup, all of the gas lines including the FTIR cell are purged with a flow of nitrogen (~15 L/min) for at least 30 minutes. During the purge, all of the heat tape controllers, except the one at the reactor inlet, and the water evaporator furnace are turned on. The total flow rate is adjusted for the planned experiments, and the BFR is allowed to reach steady state operating temperatures. During this time, the FTIR gas cell is adjusted to the same conditions at which calibration spectra is obtained (700 Torr, 117˚C and a 2 L/min flow rate). After the FTIR is aligned and a background spectrum is taken, CO_2

and H_2O are sent through the bypass line. Once the concentrations of these two species reach steady state, as monitored by FTIR, the reactor furnace and the furnace inlet heating tape are turned on, and the flow is switched to the reactor. The NO_x analyzers are zeroed and spanned, and SpaciMS is turned on.

Before each cycling experiment, the catalyst is heated to 500˚C and exposed to the regeneration condition, which consists of 1% H_2, 5% H_20, 5% CO_2 and a balance of N_2 for 15 minutes to get a clean initial catalyst surface. The catalyst is then cooled to the operating temperature for the planned experiments.

All of the experiments performed in this study employed operating conditions similar to the ones proposed by the CLEERS LNT Focus Group, which is a technical collaborative research group that focuses on the development of the LNT simulation science [23].

3.4.1 Short-Cycle Experiments

The short-cycle experiments reasonably approximate the catalyst operation in engine exhaust applications. Both catalysts, A and B, of three different lengths were evaluated at three different temperatures and two different reductant concentrations and at a space velocity of 30,000 hr^{-1}. One reductant concentration is chosen to represent partial regeneration and the other to represent full regeneration. The reductant concentration for partial regeneration experiments represents the concentration of the reductant that is below the theoretical amount needed to reduce the integral amount of NO_x that enters during the trapping part of the cycle. Full regeneration uses significantly higher reductant concentration than theoretical one to insure that regeneration of the catalyst is not limited by the amount of reductant. The theoretical amount of reductant is calculated based on the assumption that all of the NO_x entering the reactor is stored as $Ba(NO_3)_2$ during lean phase, and reduced to N_2 during rich phase, as shown in Equations 3.1 and 3.2.

$$BaCO_3 + 2NO + 1.5O_2 \rightarrow Ba(NO_3)_2 + CO_2 \quad (3.1)$$

$$Ba(NO_3)_2 + 5H_2 + CO_2 \rightarrow BaCO_3 + N_2 + 5H_2O \quad (3.2)$$

Based on the equations 3.1 and 3.2, for each one mole of NO entering the reactor 2.5 moles of hydrogen are required to reduce stored NO_x to N_2. The reductant concentration calculations for Catalyst A and B are shown in Sections 3.4.1.1 and 3.4.1.2, respectively.

Short cycles without NO in the lean phase were performed in order to determine catalysts' oxygen storage capacity (OSC). OSC experiments with a nitrogen purge of ten seconds (referred as back-mixing experiments) between lean and rich pulse were also performed, and results were used to determine the reductant consumption due to reaction between reductant and O_2 at the interface between the rich and lean pulses.

During these experiments, the FTIR was set to acquire one scan per data point per second, and the species concentrations were calculated in real time. Once NO/NO_x profiles did not change from cycle to cycle, the FTIR was then changed to acquire data at high-speed mode (one scan per data point, as fast as possible and without any analysis). Temperature, pressure, flow rates of individual mass flow controllers and NO/NO_x concentrations were acquired at 2 samples per second. SpaciMS data was collected at 20 samples per second, and at least 5 cycles are collected at each capillary probe position. The operating conditions for catalysts A and B are given in Sections 3.4.1.1 and 3.4.1.2, respectively.

3.4.1.1 Catalyst A Operating Conditions

The short-cycle experiments were performed at three different temperatures: 200, 300 and 400˚C. Each experiment consisted of 120 lean/rich cycles with each cycle consisting of 56 s lean and 4 s rich. Two reductant concentrations were used at each test temperature: 1% H_2 representing partial regeneration (which is below theoretical concentration) and 2% representing full

regeneration (double the partial regeneration amount). The theoretical reductant concentration calculation is presented in Equation 3.3.

$$0.03\%\ \text{NO} \times 56\ \text{s lean} \times \frac{5\ \text{moles H}_2}{2\ \text{moles NO}} \times \frac{1}{4\ \text{s rich}} = 1.05\%\ \text{H}_2 \qquad (3.3)$$

The operating conditions for short cycling are shown in Table 3.1, for oxygen storage short cycling in Table 3.2 and for back-mixing short cycling in Table 3.3.

3.4.1.2 Catalyst B Operating Conditions

The short-cycle experiments were performed at temperatures: 230, 325 and 500˚C. Catalyst B is designed to operate at higher temperatures than Catalyst A. 500˚C was chosen as highest testing temperature; 230 and 325C were calculated based on CLEERS LNT Focus Group protocol [23]. At least 140 lean/rich cycles were performed to account for extra time needed to measure H_2 and NO_x concentrations by SpaciMS. Each cycle consisted of 60 s lean and 5 s rich. The theoretical concentration of H_2 needed to reduce the integral amount of NO_x that enters during the lean part of the cycle is calculated as shown in Equation 3.4.

$$0.03\%\ \text{NO} \times 60\ \text{s lean} \times \frac{5\ \text{moles H}_2}{2\ \text{moles NO}} \times \frac{1}{5\ \text{s rich}} = 0.9\%\ \text{H}_2 \qquad (3.4)$$

To account for reductant loss due to its oxidation by stored oxygen, higher reductant concentration was used for partial reduction experiments (1.4% H_2) than the one calculated. 3.4% H_2 was used for full regeneration cycling experiments.

The operating conditions for short cycling are given in Table 3.4, for oxygen storage short cycling in Table 3.5 and for back-mixing short cycling in Table 3.6.

Table 3.1. Catalyst A, Short Cycling Operating Conditions

Mode	Time	Gas Composition
Lean	56 s	300 ppm NO, 10% O_2, 5% H_2O, 5% CO_2, balance N_2
Rich	4 s	1% H_2, 5% H_2O, 5% CO_2, balance N_2
Lean	56 s	300 ppm NO, 10% O_2, 5% H_2O, 5% CO_2, balance N_2
Rich	4 s	2% H_2, 5% H_2O, 5% CO_2, balance N_2

Table 3.2. Catalyst A, Oxygen Storage Short Cycling Operating Conditions

Mode	Time	Gas Composition
Lean	56 s	10% O_2, 5% H_2O, 5% CO_2, balance N_2
Rich	4 s	1% H_2, 5% H_2O, 5% CO_2, balance N_2
Lean	56 s	300 ppm NO, 10% O_2, 5% H_2O, 5% CO_2, balance N_2
Rich	4 s	2% H_2, 5% H_2O, 5% CO_2, balance N_2

Table 3.3. Catalyst A, Back-Mixing Short Cycling Operating Conditions

Mode	Time	Gas Composition
Lean	56 s	10% O_2, 5% H_2O, 5% CO_2, balance N_2
Purge	10 s	5% H_2O, 5% CO_2, balance N_2
Rich	4 s	1% H_2, 5% H_2O, 5% CO_2, balance N_2
Lean	56 s	10% O_2, 5% H_2O, 5% CO_2, balance N_2
Purge	10 s	5% H_2O, 5% CO_2, balance N_2
Rich	4 s	2% H_2, 5% H_2O, 5% CO_2, balance N_2

Table 3.4. Catalyst B, Short Cycling Operating Conditions

Mode	Time	Gas Composition
Lean	60 s	300 ppm NO, 10% O_2, 5% H_2O, 5% CO_2, balance N_2
Rich	5 s	1.4% H_2, 5% H_2O, 5% CO_2, balance N_2
Lean	60 s	300 ppm NO, 10% O_2, 5% H_2O, 5% CO_2, balance N_2
Rich	5 s	3.4% H_2, 5% H_2O, 5% CO_2, balance N_2

Table 3.5. Catalyst B, Oxygen Storage Short Cycling Operating Conditions

Mode	Time	Gas Composition
Lean	60 s	10% O_2, 5% H_2O, 5% CO_2, balance N_2
Rich	5 s	1.4% H_2, 5% H_2O, 5% CO_2, balance N_2
Lean	60 s	300 ppm NO, 10% O_2, 5% H_2O, 5% CO_2, balance N_2
Rich	5 s	3.4% H_2, 5% H_2O, 5% CO_2, balance N_2

Table 3.6. Catalyst B, Back-Mixing Short Cycling Operating Conditions

Mode	Time	Gas Composition
Lean	60 s	10% O_2, 5% H_2O, 5% CO_2, balance N_2
Purge	10 s	5% H_20, 5% CO_2, balance N_2
Rich	5 s	1.4% H_2, 5% H_2O, 5% CO_2, balance N_2
Lean	60 s	10% O_2, 5% H_2O, 5% CO_2, balance N_2
Purge	10 s	5% H_2O, 5% CO_2, balance N_2
Rich	5 s	3.4% H_2, 5% H_2O, 5% CO_2, balance N_2

3.4.2 Long-Cycle Experiments

Long cycling experiments were performed to explore processes that were not, otherwise, seen during short cycles. Typically, each long cycling experiment consisted of three cycles of 15 minute lean and 10 minute rich. The FTIR was set to acquire four scans per data point as fast as possible, and the species concentrations were calculated in real time. Temperature, pressure, flow rates of individual mass flow controllers and NO/NO_x concentrations were acquired at 2 samples per second. SpaciMS was not used for these experiments. The operating conditions for catalysts A and B are given in Tables 3.7 and 3.8, respectively.

Table 3.7. Catalyst A, Long Cycling Operating Conditions

Mode	Time	Gas Composition
Lean	15 min	300 ppm NO, 10% O_2, 5% H_2O, 5% CO_2, balance N_2
Rich	10 min	0.2% H_2, 5% H_2O, 5% CO_2, balance N_2
Lean	15 min	300 ppm NO, 10% O_2, 5% H_2O, 5% CO_2, balance N_2
Rich	10 min	0.5% H_2, 5% H_2O, 5% CO_2, balance N_2
Temperature: 200, 300 and 400˚C Space Velocity: 30,000 hr^{-1}		

Table 3.8. Catalyst B, Long Cycling Operating Conditions

Mode	Time	Gas Composition
Lean	15 min	300 ppm NO, 10% O_2, 5% H_2O, 5% CO_2, balance N_2
Rich	10 min	0.4% H_2, 5% H_2O, 5% CO_2, balance N_2
Temperature: 230, 325 and 500˚C Space Velocity: 30,000 hr^{-1}		

CHAPTER 4

RESULTS AND DISCUSSION

The results and discussion of experiments described in Chapter 3 are presented in this chapter. Section 4.1 presents results of experiments performed on Catalyst A. This includes the results of the experiments that were performed to determine the "degreening" protocol and the effect of "breakage". The evaluation of samples of different lengths with two sets of cycling experiments is also presented in this section. Cycling experiments were performed at different temperatures and reductant concentrations, and results are compared between samples of different lengths. Comparisons are presented in terms of NO_x (NO and NO_2), NH_3 and N_2O profiles. Finally, the results of reductant consumption trends are used to explain the differences observed in performance of samples of different lengths. Section 4.2 presents results of experiments performed on Catalyst B, which was evaluated in a similar way as Catalyst A.

4.1 Catalyst A ($SCONO_x$) Evaluation

4.1.1 Determination of "Degreening" Protocol

Generally, fresh catalyst initially shows high performance activity, which severely deteriorates during first couple of hours of operation when catalyst is exposed to elevated temperatures. After the initial very rapid catalyst decay, the catalyst activity reaches a stable level [24]. It is, therefore, necessary to "degreen" the fresh catalyst to achieve stable and reproducible levels of its activity.

Prior to the catalyst evaluation, each 2.54-cm-long Catalyst A's sample was "degreened" by performing storage-reduction cycles at 550˚C, which is 150˚C higher than the highest operating temperature used in this study. Each cycle consists of a 56-second storage (300 ppm NO, 10% O_2, 5% H_2O, 5% CO_2

and balance N_2) and a 4-second reduction (1.2% H_2, 5% H_2O, 5% CO_2 and balance N_2). The cycling proceeds until steady state NO_x conversion is obtained. To determine the time duration needed for Catalyst A to reach steady state conditions, the catalyst activity for NO_x conversion is checked after 0, 1, 3, 7 and 11 hours of "degreening" with baseline experiments.

The baseline experiments consist of short and long-cycle experiments performed at 300˚C. Short-cycle experiment consists 120 lean/rich cycles with each cycle consisting of 56 s lean (300 ppm NO, 10% O_2, 5% H_2O, 5% CO_2 and balance N_2) and 4 s rich (1.0% H_2, 5% H_2O, 5% CO_2 and balance N_2). Long-cycle experiment consists of three cycles, each with a 15-minute storage phase (300 ppm NO, 10% O_2, 5% H_2O, 5% CO_2 and balance N_2) and a 10-minute reduction phase (0.2% H_2, 5% H_2O, 5% CO_2 and balance N_2).

Figures 4.1 and 4.2 show exit NO_x concentration obtained from a typical lean/rich cycle at different "degreening" times for long and short-cycle baseline experiments, respectively. Results for short-cycle experiment are presented toward the end of the 120-cycle run, at which NO_x profile shows no cycle-to-cycle variations. For long-cycle experiment exit NO_x concentrations in the third cycle at different "degreening" times are presented. The NO_x profiles and conversion efficiencies for long-cycle experiments vary considerably in the first 7 hours of "degreening"; however the variation is small with additional 4 hours of "degreening". In the present study NO_x conversion efficiency is defined as the amount of NO_x converted as a percentage of the total inlet NO_x over the lean portion of the cycle. Even though NO_x conversion efficiencies during short-cycle experiments are not affected by "degreening" (2.2% decrease is observed), the shape of the NO_x curves changes during the first 7 hours of "degreening" – increase in slope of the NO_x curve during lean period and disappearance of second peak during rich period – and not during additional 4 hours. It is, therefore, concluded that Catalyst A needs to be "degreened" for at least 7 hours to reach stable conditions. Each 2.54-cm-long Catalyst A used in this investigation is "degreened" for 8 hours at conditions described above.

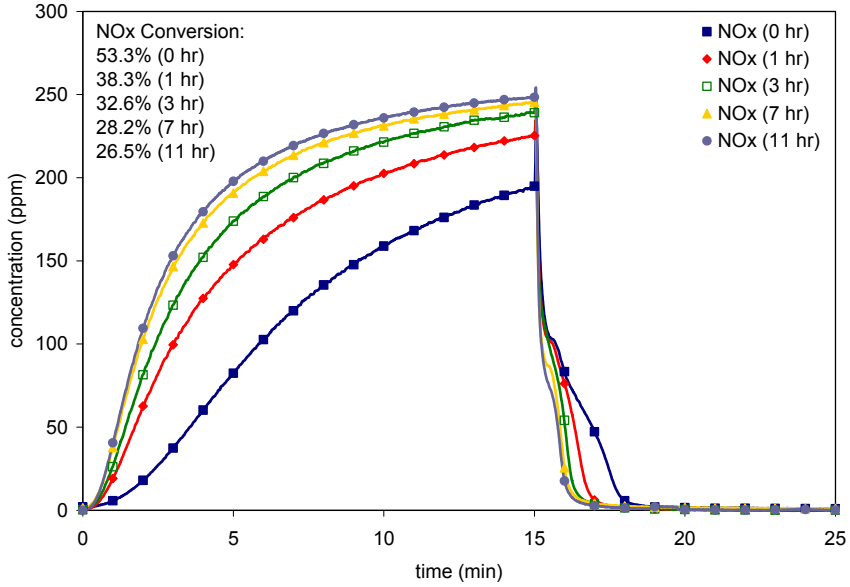

Figure 4.1. Catalyst A's outlet concentrations of NO_x for 2.54-cm-long sample in long-cycle baseline experiments with 0.2% H_2 in rich phase at 300˚C and 30,000 h^{-1} space velocity after different "degreening" times

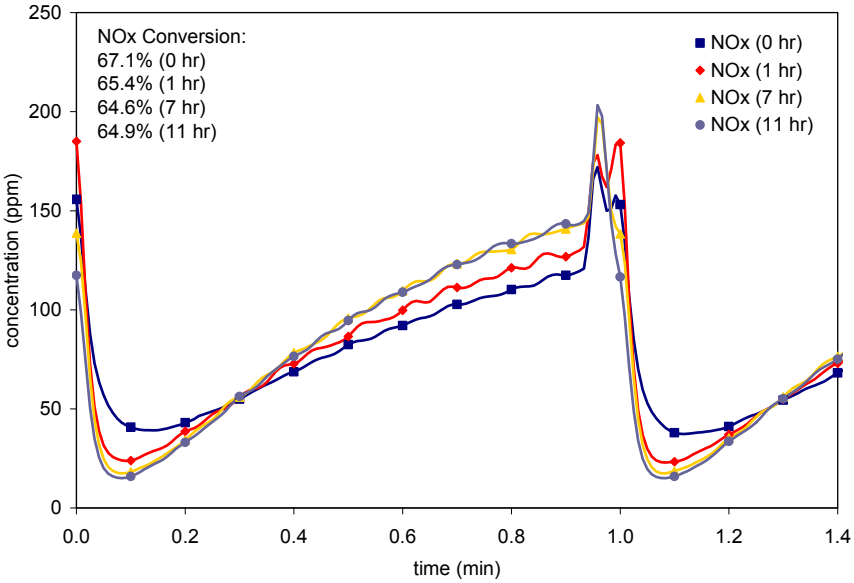

Figure 4.2. Catalyst A's outlet concentrations of NO_x for 2.54-cm-long sample in short-cycle baseline experiments with 1.0% H_2 in rich phase at 300˚C and 30,000 h^{-1} space velocity after different "degreening" times

4.1.2 Breakage Effect

Samples of 5.08 and 7.62-cm-long used in this study were obtained by placing 2.54-cm long samples in tandem. The resulting sample was then wrapped in Zetex ceramic fiber strips and positioned in a 2.54-cm OD quartz-tube reactor – as described in section 3.2.6 – for testing. Even though great care was taken to align all the channels of the 2.54-cm samples and to minimize the gap between them, the effect of channel misalignment and "breakage" on catalyst performance needed to be assessed to meaningfully compare samples of different lengths. To that effect NO_x profiles and conversion efficiencies of a "non-segmented" 5.08-cm-long sample are compared to a "segmented" 5.08-cm sample.

A "non-segmented" 5.08-cm-long sample was "degreened" for 8 hours at conditions described in Section 4.1.1 and evaluated with baseline experiments. After evaluation, the 5.08-cm sample was sectioned into two 2.54-cm-long samples. These two 2.54-cm samples were used to form a "segmented" 5.08-cm sample on which the evaluation was carried out. Figures 4.3 and 4.4 show results of baseline experiments. As seen in the figures the NO_x profiles and conversion efficiencies do not vary between "non-segmented" and "segmented" 5.08-cm-long samples. Consequently, breakage appears to have no effect on the performance of Catalyst A.

4.1.3 Comparison of 2.54 and 5.08-cm Samples

The effect of monolith length on Lean NO_x Trap performance was initially investigated on 2.54 and 5.08-cm-long Catalyst A samples. The results of short and long-cycle experiments and their comparison are shown in this section.

4.1.3.1 Sample-to-Sample Variation

Sample-to-sample variation makes direct comparison of samples with different lengths challenging. To overcome this problem, the performance of a number of "degreened" 2.54-cm-long samples was investigated using baseline

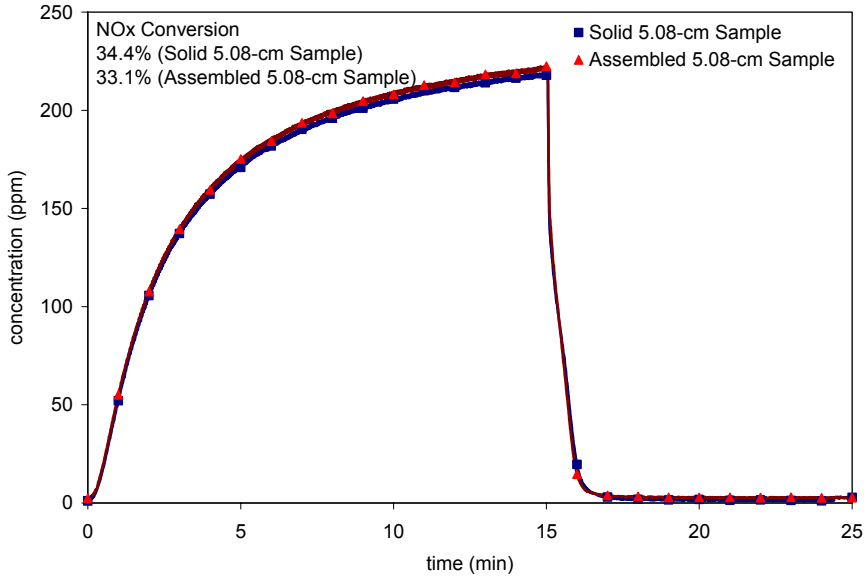

Figure 4.3. Catalyst A's outlet concentrations of NO_x for non-segmented and segmented 5.08-cm-long sample in long-cycle baseline experiments with 0.2% H_2 in rich phase at 300˚C and 30,000 h^{-1} space velocity

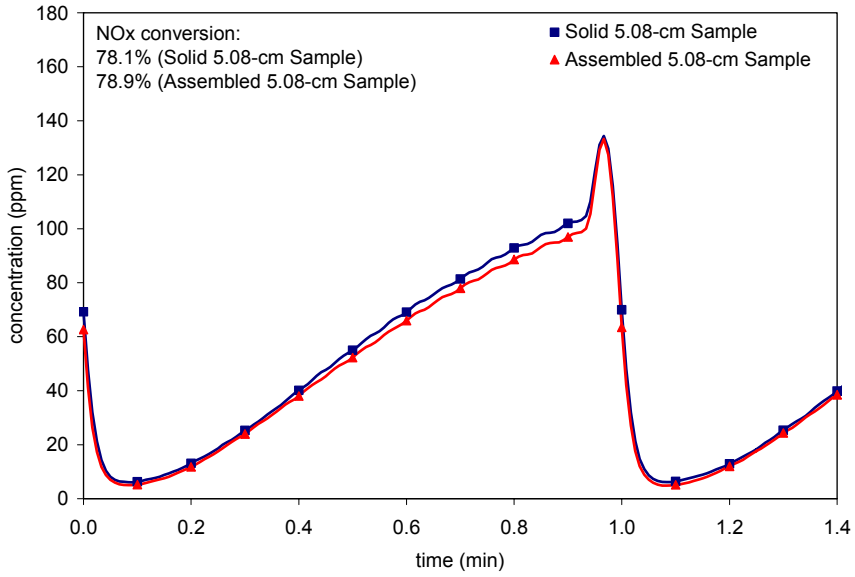

Figure 4.4. Catalyst A's outlet concentrations of NO_x for non-segmented and segmented 5.08-cm-long sample in short-cycle baseline experiments with 1.0% H_2 in rich phase at 300˚C and 30,000 h^{-1} space velocity

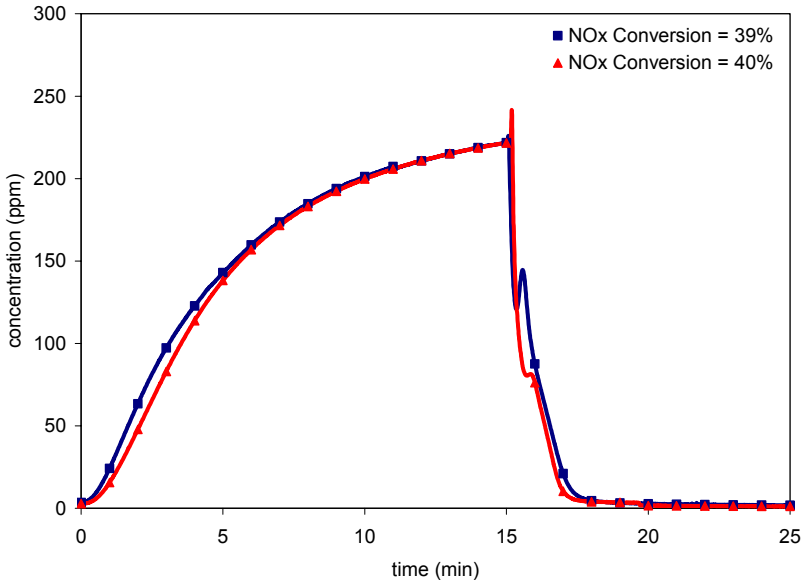

Figure 4.5. Catalyst A's outlet concentrations of NO_x for 2.54-cm-long samples in long-cycle baseline experiments with 0.2% H_2 in rich phase at 300˚C and 30,000 h^{-1} space velocity (sample-to-sample variation)

experiments, and two with similar performance were selected and used to compare the performance of 2.54 and 5.08-cm-long samples. The results of the baseline experiments for a particular set of two 2.54-cm-long samples are shown in Figures 4.5 and 4.6.

NO_x conversion efficiencies and NO_x profiles for long-cycle experiments, shown in Figure 4.5, closely match each other. Short-cycle experiments show a difference of about 6% for NO_x conversion efficiencies in the two 2.54-cm-long samples, which is within the experimental uncertainty. Discrepancies were much greater in other samples that were tested for sample-to-sample variation, and their results are not presented here.

4.1.3.2 Long-Cycle Experiments

Long-cycle experiments were performed at three different temperatures (200, 300 and 400˚C) and two reductant concentrations (0.2 and 0.5%), and results are compared between 2.54-cm and 5.08-cm-long samples. Figures 4.7

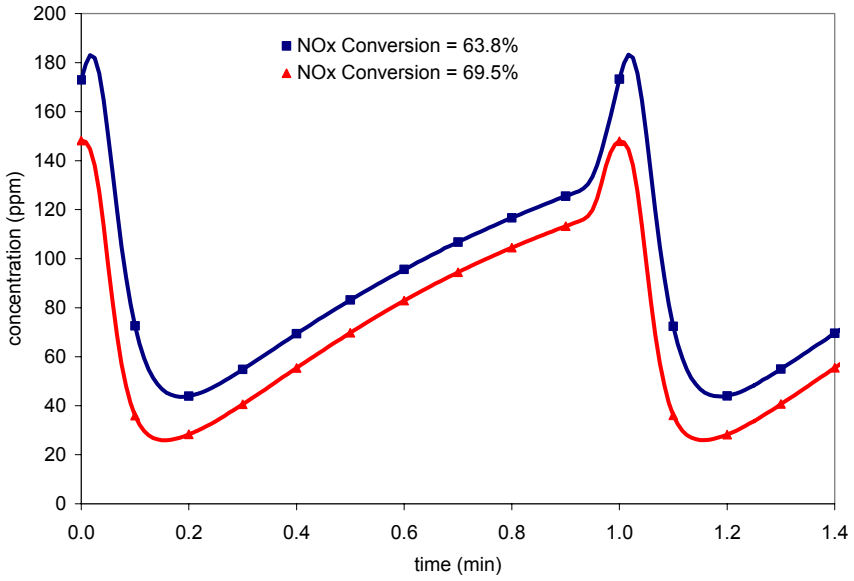

Figure 4.6. Catalyst A's outlet concentrations of NO_x for 2.54-cm-long samples in short-cycle baseline experiments with 1.0% H_2 in rich phase at 300˚C and 30,000 h^{-1} space velocity (sample-to-sample variation)

and 4.8 show the catalyst outlet gas concentrations for 2.54 and 5.08-cm-long samples with 0.2% H_2 in the rich phase of the cycle. Each long cycle consists of 15 minutes capture (300 ppm NO, 10% O_2, 5% H_2O, 5% CO_2 and balance N_2) and 10 min regeneration (0.2% H_2, 5% H_2O, 5% CO_2 and balance N_2). Three cycles were run and the results are shown only for the third cycle.

Figure 4.7 shows the outlet concentrations of NO_2 and NO_x plotted versus time. These data sets show the typical trends of LNT operation. At the beginning of the storage phase, NO_x is not observed at the exit of the catalyst, which suggests that the entire incoming NO is stored on the surface during this period. The time delay in the NO_x outlet concentration is largest at 400˚C (approximately 1 minute) and almost immediate at 200˚C. This is generally considered to originate from the kinetic limitation of the oxidation of NO to NO_2 at lower temperatures. With NO_2 being a precursor for the storage process [5, 8], and since NO oxidation to NO_2 is kinetically-limited at low temperatures [7], NO_x storage is consequently lower. After the breakthrough, rapid increase in NO_x

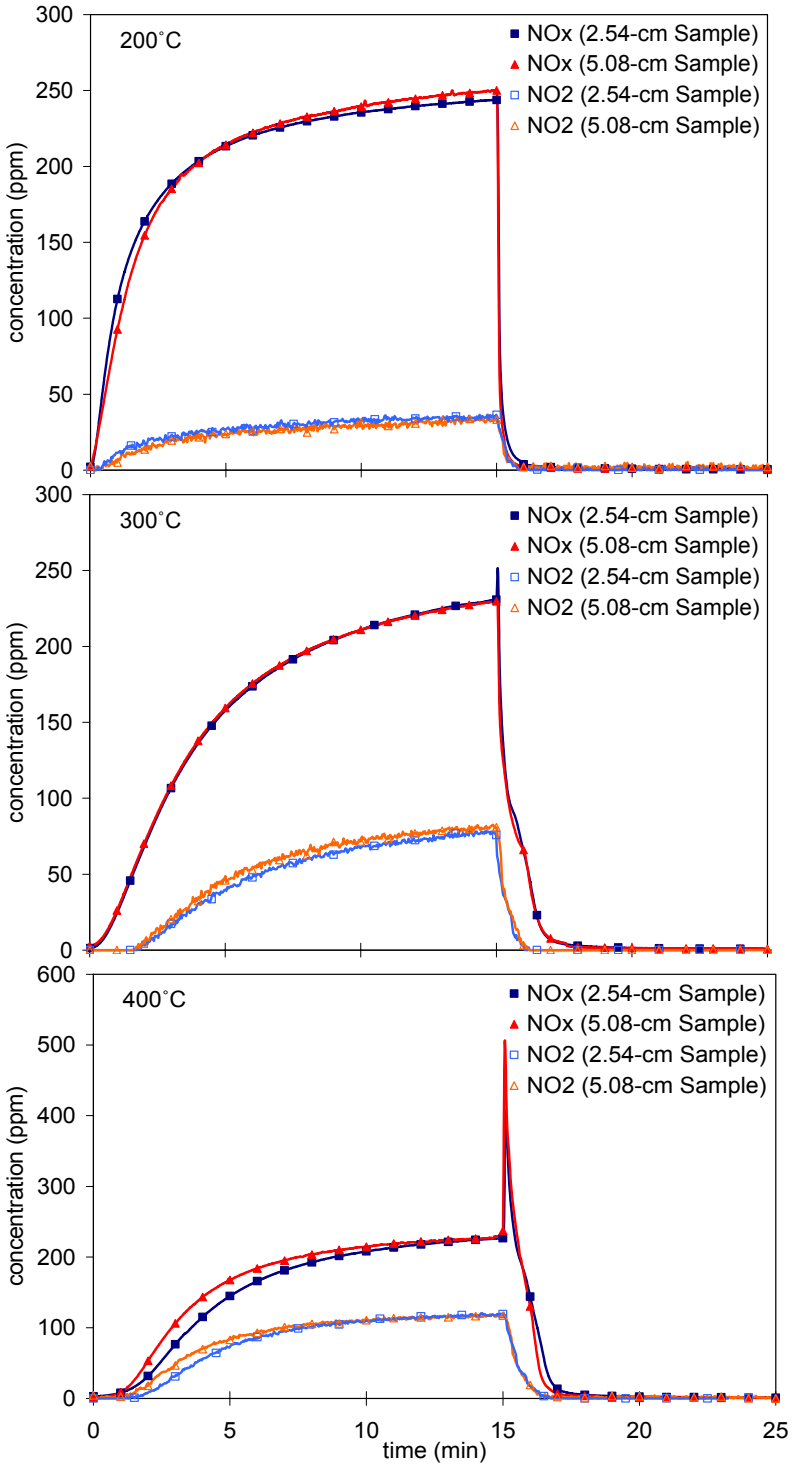

Figure 4.7. Catalyst A's outlet concentrations of NO_2 and NO_x for 2.54 and 5.08-cm-long samples in long-cycle experiments with 0.2% H_2 in rich phase at 200, 300 and 400˚C

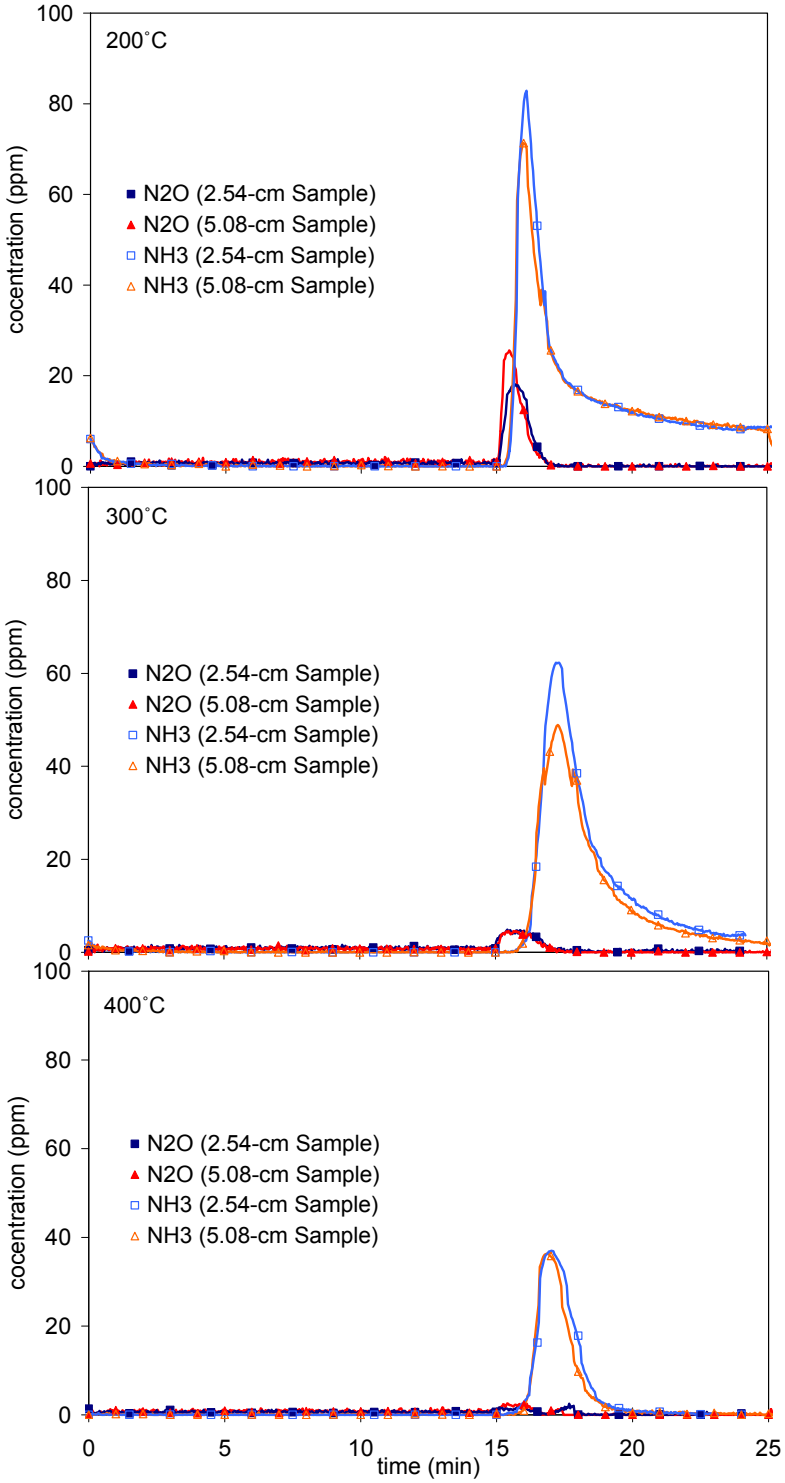

Figure 4.8. Catalyst A's outlet concentrations of N_2O and NH_3 for 2.54 and 5.08-cm-long samples in long-cycle experiments with 0.2% H_2 in rich phase at 200, 300 and 400˚C

outlet concentration is observed with a higher rate at 200˚C due to lower oxidation rate of NO at this temperature. As the NO_x storage sites become saturated, the rate of NO_x storage decreases and outlet NO_x concentration reaches nearly asymptotic level.

Upon switching to rich conditions (15 minutes into the cycle), NO_x is released from the surface and reduced to N_2 (not measured) and other species. A sharp NO_x spike is observed at 300 and 400˚C but not at 200˚C (Figure 4.7). This is probably due to higher rate of nitrate decomposition (NO_x release) than the rate of NO_x reduction at higher temperatures [12].

Many mechanisms governing NO_x release have been reported in the literature. One of them is thermal in nature (thermal release) in which NO_x is desorbed due to heat generated during switch from lean to rich conditions (exothermic reaction between reductant and oxygen stored on the catalyst's surface). Other mechanisms originate from introduction of rich excursion to establish the net reducing environment. Maximum observed temperature increase inside the catalyst (mid T) during lean to rich switching is 13˚C, as shown in Figure 4.9, suggesting that thermal release may be negligible during Catalyst A's operation. No change is observed for the catalyst's inlet gas phase temperature (inlet T); however a maximum increase of 12˚C is seen at the exit gas phase temperature (outlet T) due to heat transfer from the catalyst.

Figure 4.8 shows the outlet concentrations of NH_3 and N_2O. Both species are observed during the regeneration and not during storage period indicating that NH_3 and N_2O are formed from stored NO_x during regeneration. Immediately after switching from lean to rich conditions, N_2O is formed. As N_2O outlet concentration reaches its maximum – between 0.3 and 0.8 minutes into the rich phase – NH_3 begins to appear. The NH_3 concentration increases rapidly and then slowly decays. Long tail of NH_3 concentration is observed at 200 and 300˚C, and it does not go to zero before the end of rich period, indicating that not all of the NO_x is released and reduced during the rich phase. This can be

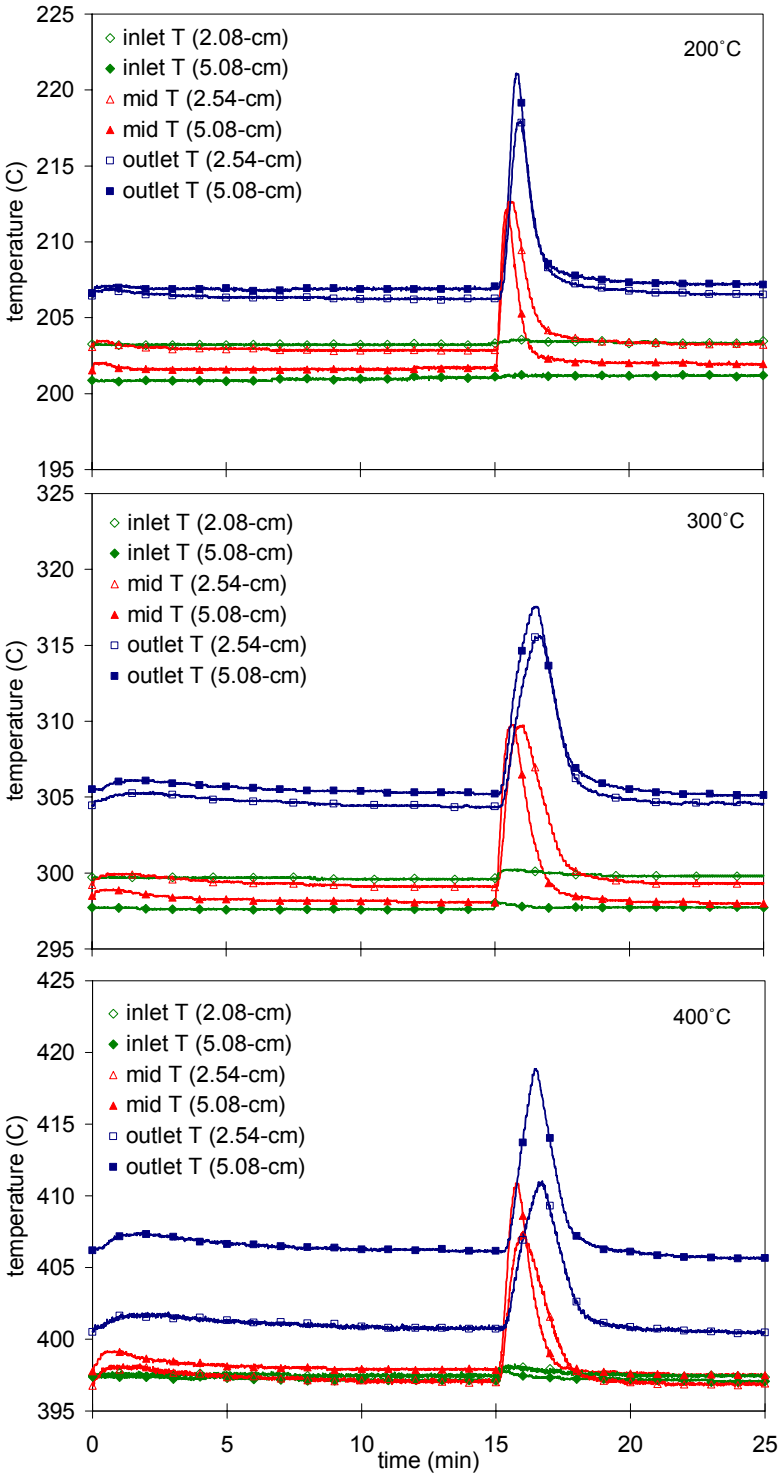

Figure 4.9. Catalyst A's temperature profiles for 2.54 and 5.08-cm-long samples in long-cycle experiments with 0.2% H_2 in rich phase at 200, 300 and 400˚C

attributed to the increase in nitrate stability with decreasing temperature, and thus preventing NO_x release and subsequent reduction at lower temperatures. Also, as seen in Figure 4.8, increasing the temperature decreases the amount of N_2O and NH_3 formed.

Figures 4.7, 4.8 and 4.9 show no significant difference in the catalyst outlet gas concentrations and temperatures between 2.54 and 5.08-cm-long samples with 0.2% H_2 as the reductant. The cycle average NO_x conversion efficiencies for 2.54 and 5.08-cm-long samples, given in Table 4.1, closely match each other at a given temperature with the biggest difference of 3% at 200˚C. Lower average conversion efficiencies at 400˚C than those at 300˚C are due to significant amount of unconverted NO_x release at higher temperature (even though more NO_x is stored at 400˚C). Based on data presented in Figures 4.7 to 4.9 and Table 4.1, it is concluded that the performance of Catalyst A is not affected by sample's length during long-cycle experiments with 0.2% H_2 as the reductant.

A second set of long-cycle experiments was performed with 0.5% H_2 concentration during rich phase. Except for one major difference – NH_3 and N_2O are formed at larger quantities – the trends for these cycles are similar to those with 0.2% H_2 during rich period. Thus, increasing the reductant concentration increases the formation of both NH_3 and N_2O. Figures A.1-A.3 (Appendix A) show the catalyst outlet gas concentrations and temperature profiles for 2.54 and 5.08-cm-long samples with 0.5% H_2 reductant, and average NO_x conversion efficiencies are presented in Table 4.2. As in the case of long-cycle experiments with 0.2% H_2 during rich period, no significant difference is observed between 2.54 and 5.08-cm-long samples with 0.5% H_2 reductant in the rich phase (the highest difference of 5.7% is observed at 200˚C, and it is within the experimental uncertainty). It is, therefore, concluded that at a given temperature and reductant concentration Catalyst A's performance during long cycling is not affected by sample length.

Table 4.1. NO_x conversion efficiencies of Catalyst A in long-cycle experiments with 0.2% H_2 in rich phase

Length \ Temperature	200˚C	300˚C	400˚C
2.54-cm	21.5%	36.0%	33.2%
5.08-cm	24.5%	36.5%	33.1%

Table 4.2. NO_x conversion efficiencies of Catalyst A in long-cycle experiments with 0.5% H_2 in rich phase

Length \ Temperature	200˚C	300˚C	400˚C
2.54-cm	19.6%	33.3%	33.4%
5.08-cm	25.3%	35.6%	34.8%

4.1.3.3 Short-Cycle Experiments

Short-cycle experiments were performed on the same 2.54-cm and 5.08-cm-long samples at the same space velocity (30,000 hr^{-1}) and temperatures (200, 300 and 400˚C) as the long-cycle experiments. Each cycle consisted of 56 s capture with gas composition identical to those used for the long-cycle experiments (300 ppm NO, 10% O_2, 5% H_2O, 5% CO_2 and balance N_2) and 4 s regeneration with higher reductant concentration (1 or 2% H_2, 5% H_2O, 5% CO_2 and balance N_2). A concentration of 1% H_2 represents partial regeneration (which is below theoretical concentration), whereas 2% represents full regeneration (double the partial regeneration amount) as discussed in Section 3.4.1. Figures 4.10 to 4.12 show the catalyst outlet gas concentrations and temperature profiles for short-cycle experiments operating with 1% H_2 during regeneration period, and Figures 4.13 to 4.15 show results for 2% H_2. A total of

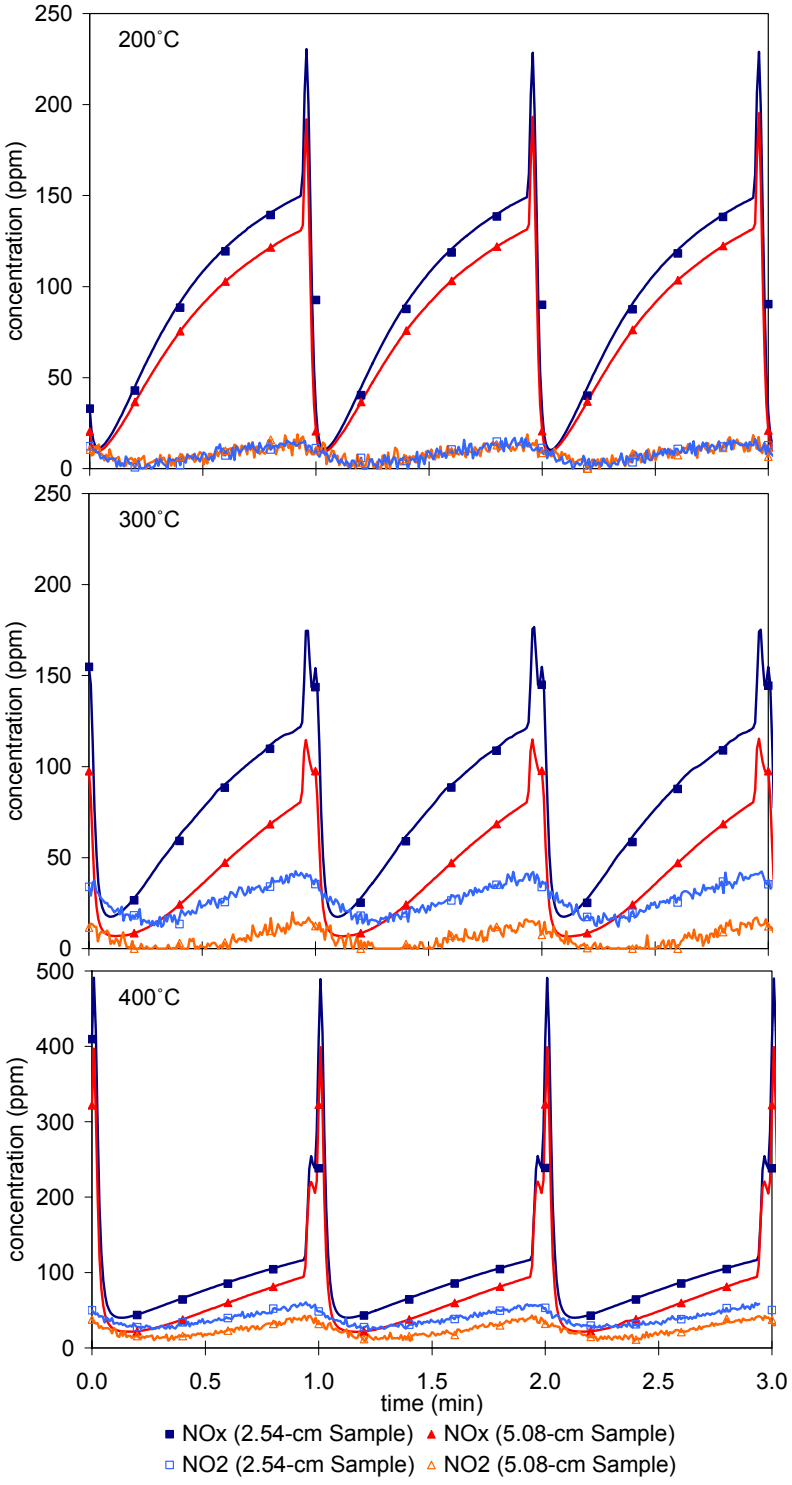

Figure 4.10. Catalyst A's outlet concentrations of NO_2 and NO_x for 2.54 and 5.08-cm-long samples in short-cycle experiments with 1.0% H_2 in rich phase at 200, 300 and 400˚C

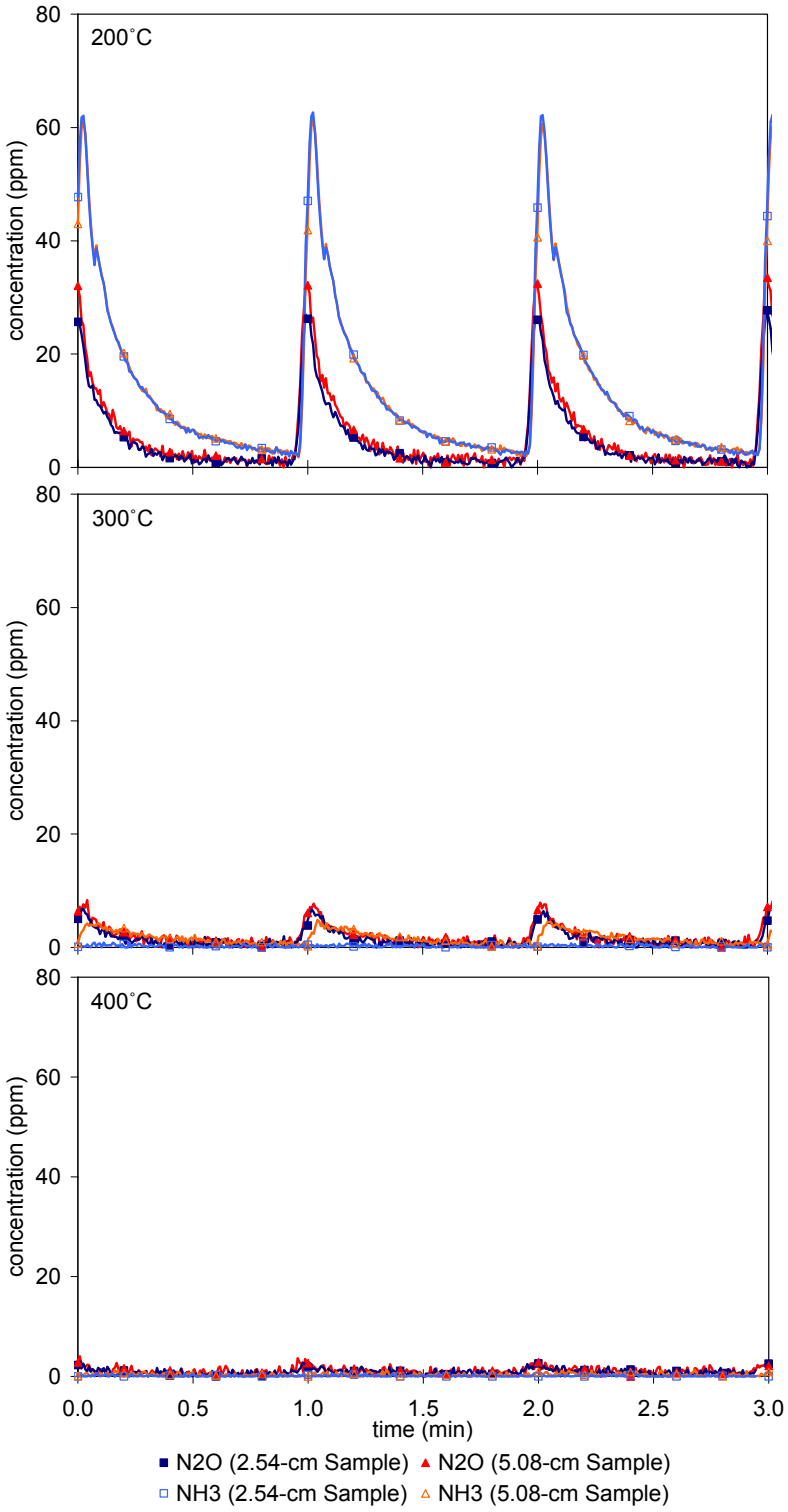

Figure 4.11. Catalyst A's outlet concentrations of N_2O and NH_3 for 2.54 and 5.08-cm-long samples in short-cycle experiments with 1.0% H_2 in rich phase at 200, 300 and 400˚C

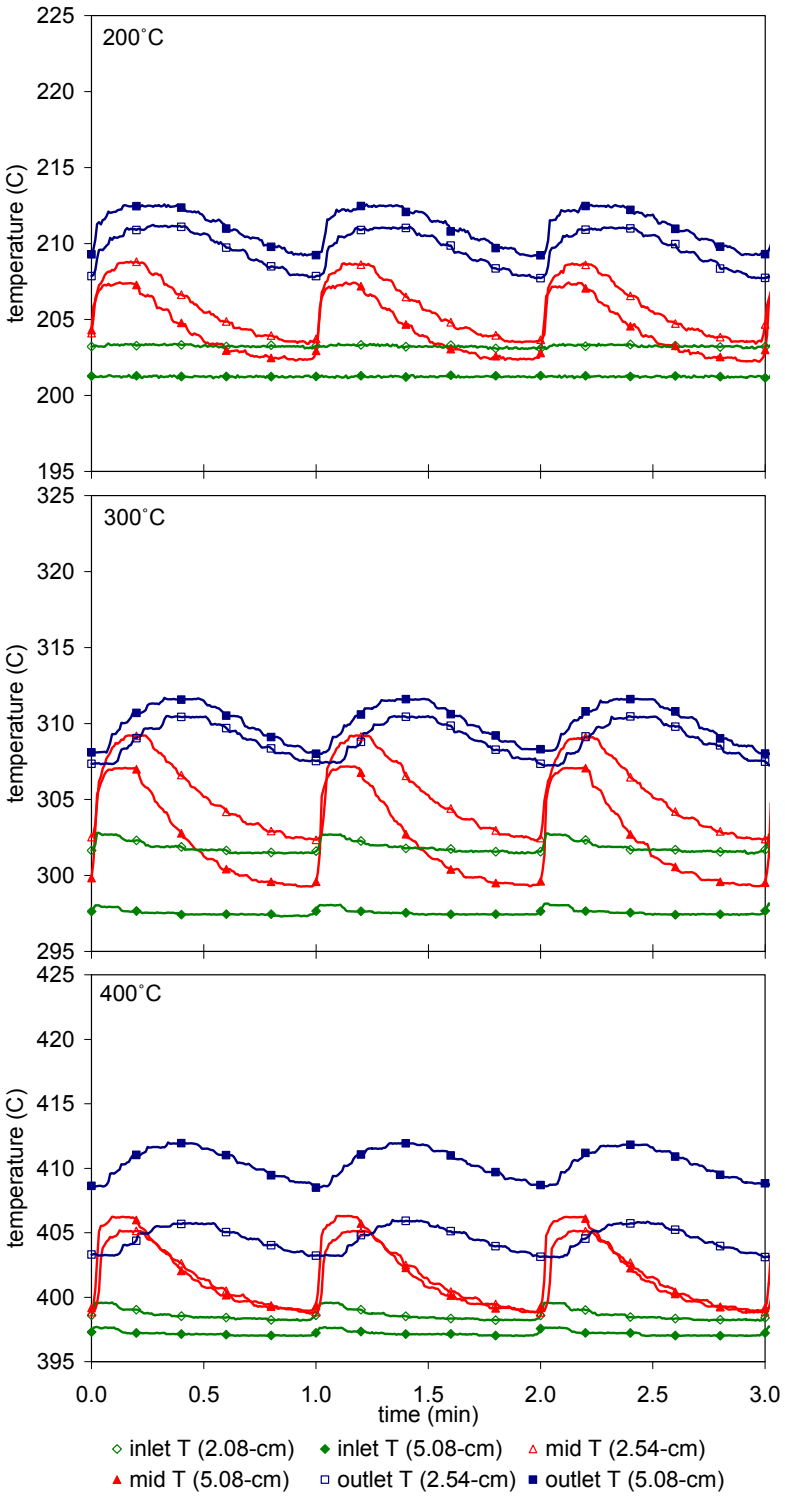

Figure 4.12. Catalyst A's temperature profiles for 2.54 and 5.08-cm-long samples in short-cycle experiments with 1.0% H_2 in rich phase at 200, 300 and 400˚C

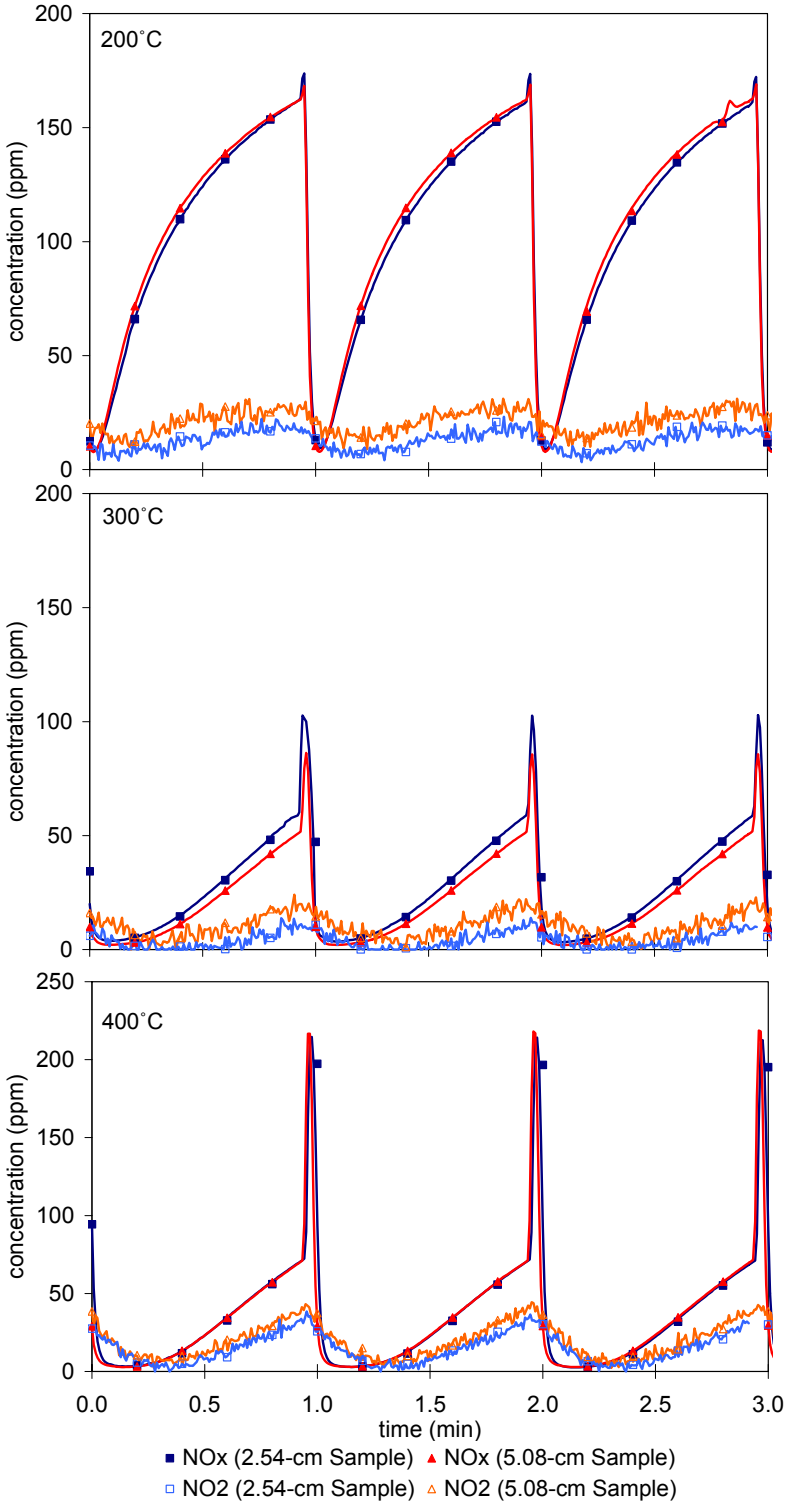

Figure 4.13. Catalyst A's outlet concentrations of NO_2 and NO_x for 2.54 and 5.08-cm-long samples in short-cycle experiments with 2.0% H_2 in rich phase at 200, 300 and 400˚C

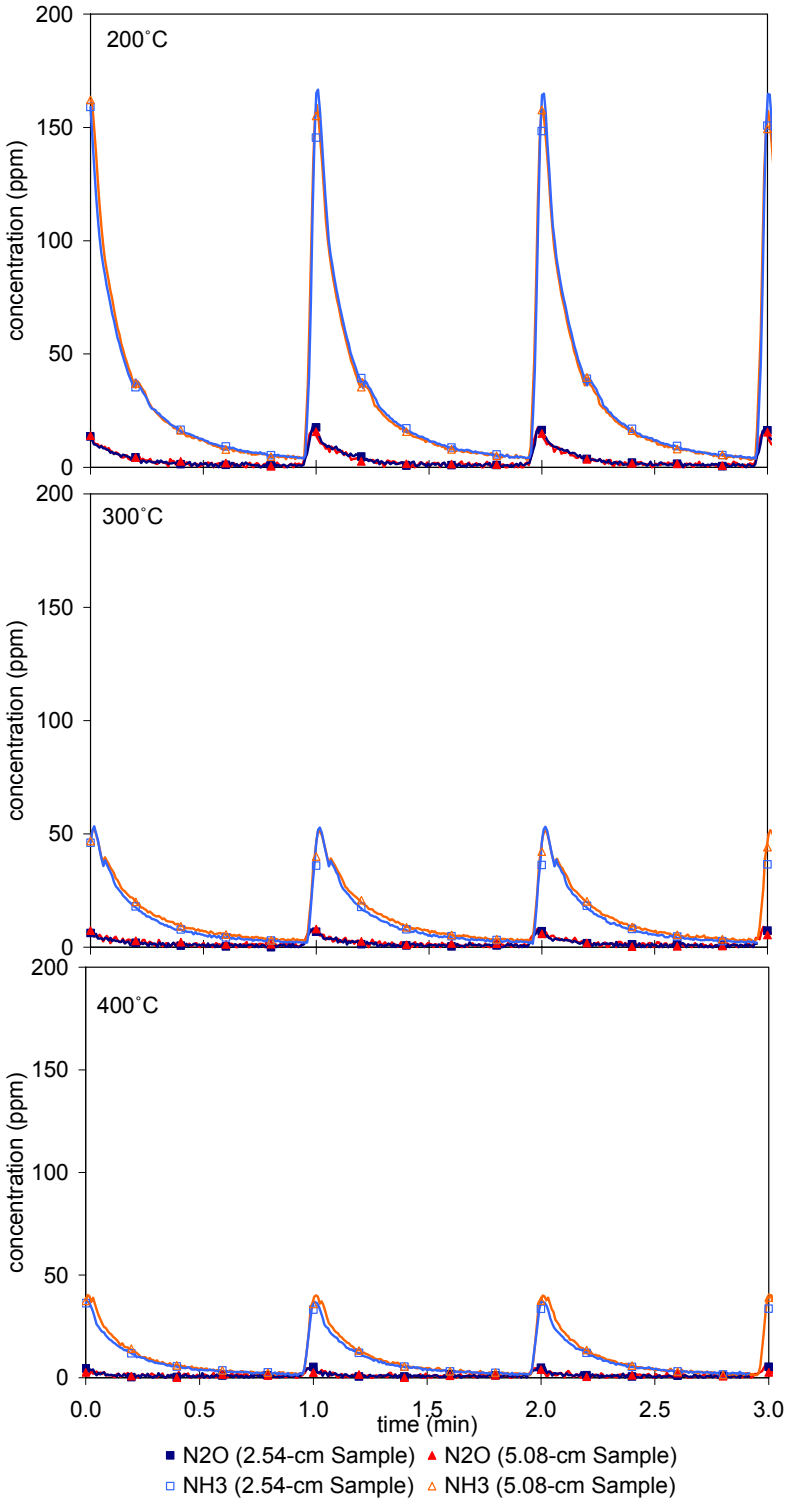

Figure 4.14. Catalyst A's outlet concentrations of N_2O and NH_3 for 2.54 and 5.08-cm-long samples in short-cycle experiments with 2.0% H_2 in rich phase at 200, 300 and 400˚C

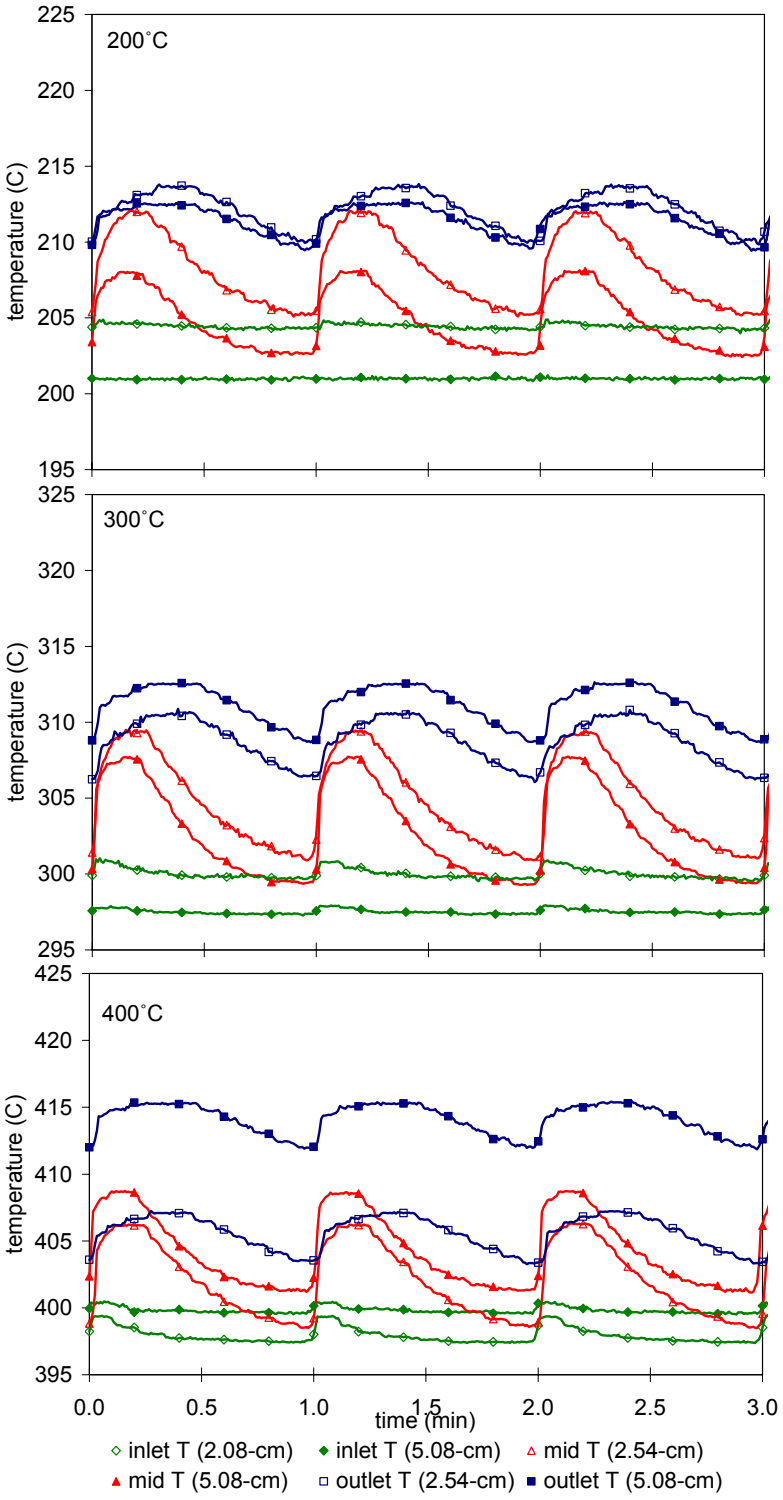

Figure 4.15. Catalyst A's temperature profiles for 2.54 and 5.08-cm-long samples in short-cycle experiments with 2.0% H_2 in rich phase at 200, 300 and 400˚C

Table 4.3. NO_x conversion efficiencies of Catalyst A in short-cycle experiments with 1.0% H_2 in rich phase

Temperature / Length	200˚C	300˚C	400˚C
2.54-cm	61.1%	68.7%	61.1%
5.08-cm	67.4%	83.6%	73.8%

Table 4.4. NO_x conversion efficiencies of Catalyst A in short-cycle experiments with 2.0% H_2 in rich phase

Temperature / Length	200˚C	300˚C	400˚C
2.54-cm	58.5%	89.2%	86.0%
5.08-cm	57.5%	91.0%	86.6%

120 cycles were performed but only 3 cycles recorded toward the end of the 120-cycle run are shown in the figures.

The general trends for the short-cycle experiments are similar to those obtained in the long-cycle experiments. Both NH_3 and N_2O peak at the beginning of regeneration phase, and their concentrations slowly decay into the capture phase of the next cycle. The presence of NH_3 and N_2O during capture is due to the short transient in the short-cycle experiments and the slow response time of the FTIR by which these species are measured. As in long-cycle experiments, the higher the temperature the smaller the amount of NH_3 and N_2O are produced. On the other hand the production of NH_3 and N_2O increases with increasing reductant concentrations; that is, at a given temperature more NH_3 and N_2O are produced with 2% H_2 during regeneration period than with 1% H_2.

Significant release of unconverted NO_x is observed at the beginning of the regeneration phase at each temperature. The cycle average NO_x conversion efficiencies, shown in Tables 4.3 and 4.4, indicate that Catalyst A performs the best at 300˚C at a given reductant concentration. As in the case of long-cycle

experiments, the worse performance at 200˚C is due to kinetically limited nitrate formation (NO to NO_2 oxidation) at this low temperature, and lower performance at 400˚C (than at 300˚C) is attributed to a significant NO_x release at the beginning of rich phase (even though more NO_x is stored at this temperature than any other) due to the weak stability of nitrate species at this temperature.

Most interesting (from perspective of this study) are the differences in performance between 2.54 and 5.08-cm-long samples. No significant difference is observed during short cycling with 2% H_2 in regeneration period (full regeneration), and difference as large as 15% is recorded during cycling with 1% H_2 (partial regeneration). Also, NH_3 is observed in 5.08-cm-long experiment and not during 2.54-cm run operating at 300˚C with 1% H_2 reductant.

The investigation of the effect of length on LNT performance was further extended to include the evaluation of 7.62-cm-long sample. Three different 2.54-cm-long samples were selected and used to evaluate segmented samples of 2.54, 5.08 and 7.62-cm long at 300˚C (temperature at which the largest difference in performance between 2.54 and 5.08-cm-long was observed) with the same experiments as those presented in this section, and results are discussed in Section 4.1.4.

4.1.4 Comparison of 2.54, 5.08 and 7.62-cm Samples

A number of fresh 2.54-cm-long samples was “degreened”, tested for sample-to-sample variation using baseline experiments, and three with similar performance were selected to compare performance of segmented samples of 2.54, 5.08 and 7.62 cm long. The results of the baseline experiments for a set of three 2.54-cm-long samples are shown in Figures A.4 and A.5 (Appendix A). A difference of about 6% for NO_x conversion efficiencies in the three 2.54-cm-long samples is observed in short-cycle experiments and 4% in long-cycle experiments; both are within the experimental uncertainty. Samples with discrepancies greater than 6% were not used in this study. The performance of 2.54, 5.08 and 7.62-cm-long sample was evaluated at 300˚C using long-cycle

and short-cycle experiments described previously in Section 4.1.3. The results of the long and short-cycle experiments are given in Sections 4.1.4.1 and 4.1.4.2, respectively.

4.1.4.1 Long-Cycle Experiments

Catalyst outlet gas concentrations and temperature profiles for 2.54, 5.08 and 7.62-cm-long samples with 0.2% and 0.5% H_2 in the rich phase of the cycle are shown in Figures 4.16 and 4.17, respectively, and their respective NO_x conversion efficiencies are given in Tables 4.5 and 4.6. The general trends are similar to those presented in Section 4.1.3.2.

Table 4.5. NO_x conversion efficiencies of Catalyst A in long-cycle experiments with 0.2% H_2 in rich phase

Temperature / Length	300˚C
2.54-cm	25.4%
5.08-cm	26.4%
7.62-cm	29.1%

Table 4.6. NO_x conversion efficiencies of Catalyst A in long-cycle experiments with 0.5% H_2 in rich phase

Temperature / Length	300˚C
2.54-cm	25.5%
5.08-cm	26.9%
7.62-cm	29.5%

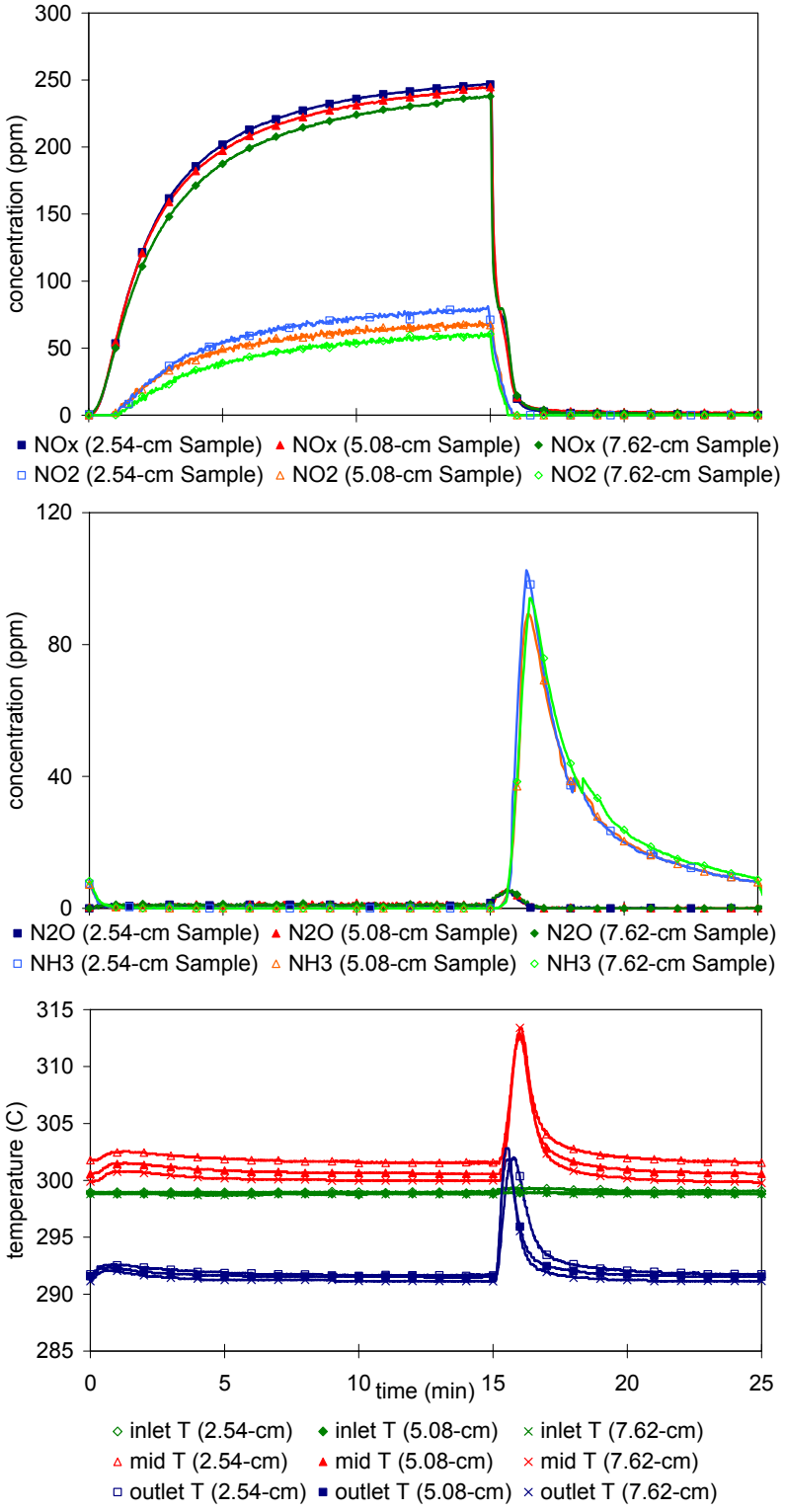

Figure 4.16. Catalyst A's outlet gas concentrations and temperature profiles for 2.54, 5.08 and 7.62-cm-long samples in long-cycle experiments with 0.2% H_2 in rich phase at 300˚C

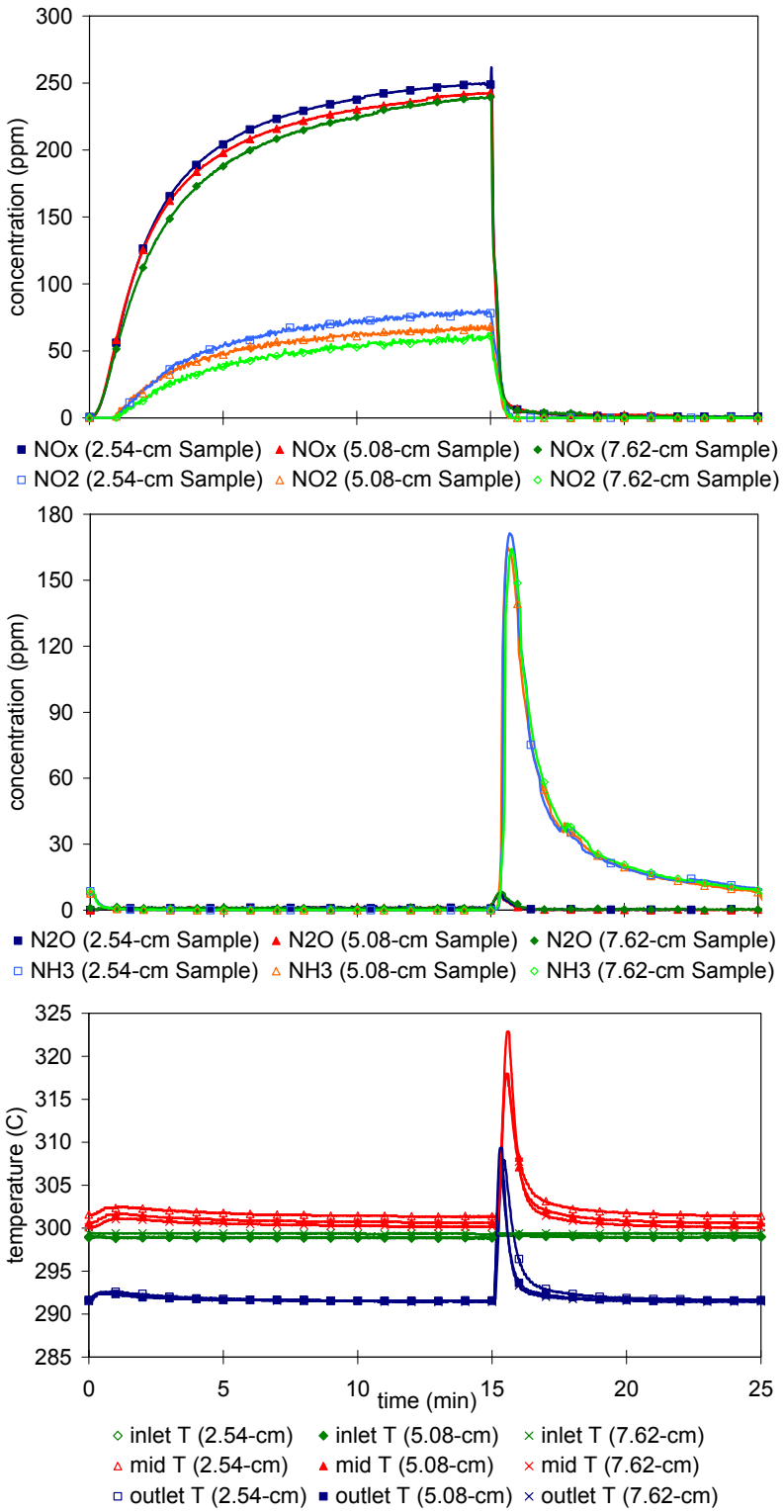

Figure 4.17. Catalyst A's outlet gas concentrations and temperature profiles for 2.54, 5.08 and 7.62-cm-long samples in long-cycle experiments with 0.5% H_2 in rich phase at 300˚C

As in the case of 2.54 and 5.08-cm-long samples discussed in Section 4.1.3.2, no significant difference is observed between 2.54-cm-long sample and segmented samples of 5.08 and 7.62-cm-long in long-cycle experiments at 300˚C with 0.2% or 0.5% H_2 in rich period. The differences in NO_x/NO_2 profiles and NO_x conversion efficiencies between samples of three different lengths follow the previously observed trend in short-cycle experiments in which the longer the sample the better the performance. However, the differences in NO_x conversion efficiencies fall within the experimental uncertainty, which makes it difficult to conclude whether these differences result from length variation or experimental limitations. Based on results presented in this section and Section 4.1.3.2, it is concluded that Catalyst A's performance in long-cycle experiments is not affected by sample length.

4.1.4.2 Short-Cycle Experiments

The segmented samples of 2.54, 5.08 and 7.62 cm long were evaluated with short-cycle experiments at 300˚C using the same gas concentrations as in Section 4.1.3.3. Figure 4.18 and Table 4.7 show the catalyst outlet gas concentrations, temperature profiles and NO_x conversion efficiencies for short-cycle experiments with 1% H_2 in regeneration period, whereas Figure 4.19 and Table 4.8 show results for 2% H_2.

Table 4.7. NO_x conversion efficiencies of Catalyst A in short-cycle experiments with 1.0% H_2 in rich phase

Temperature / Length	**300˚C**
2.54-cm	65.7%
5.08-cm	77.1%
7.62-cm	80.5%

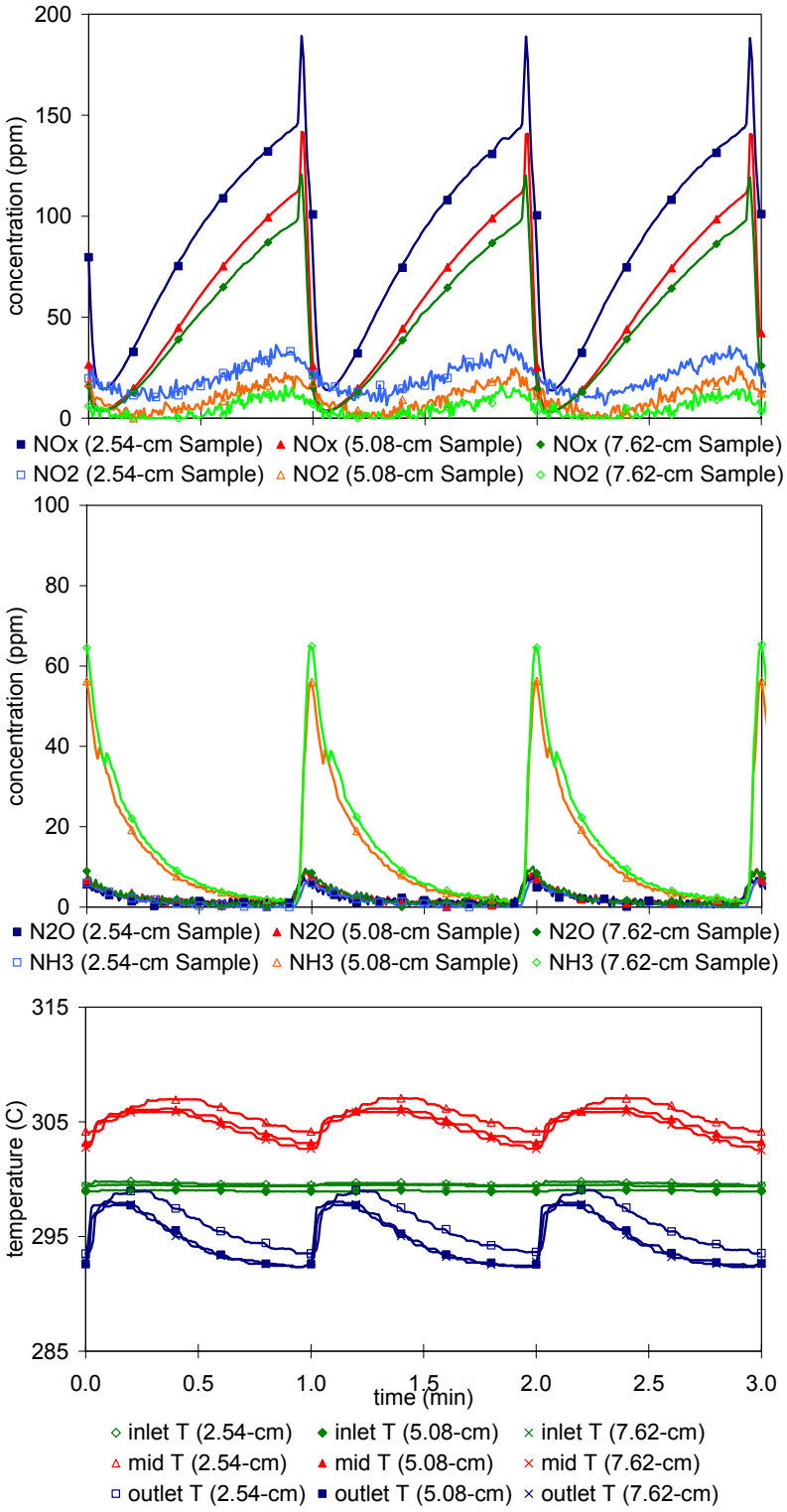

Figure 4.18. Catalyst A's outlet gas concentrations and temperature profiles for 2.54, 5.08 and 7.62-cm-long samples in short-cycle experiments with 1.0% H_2 in rich phase at 300˚C

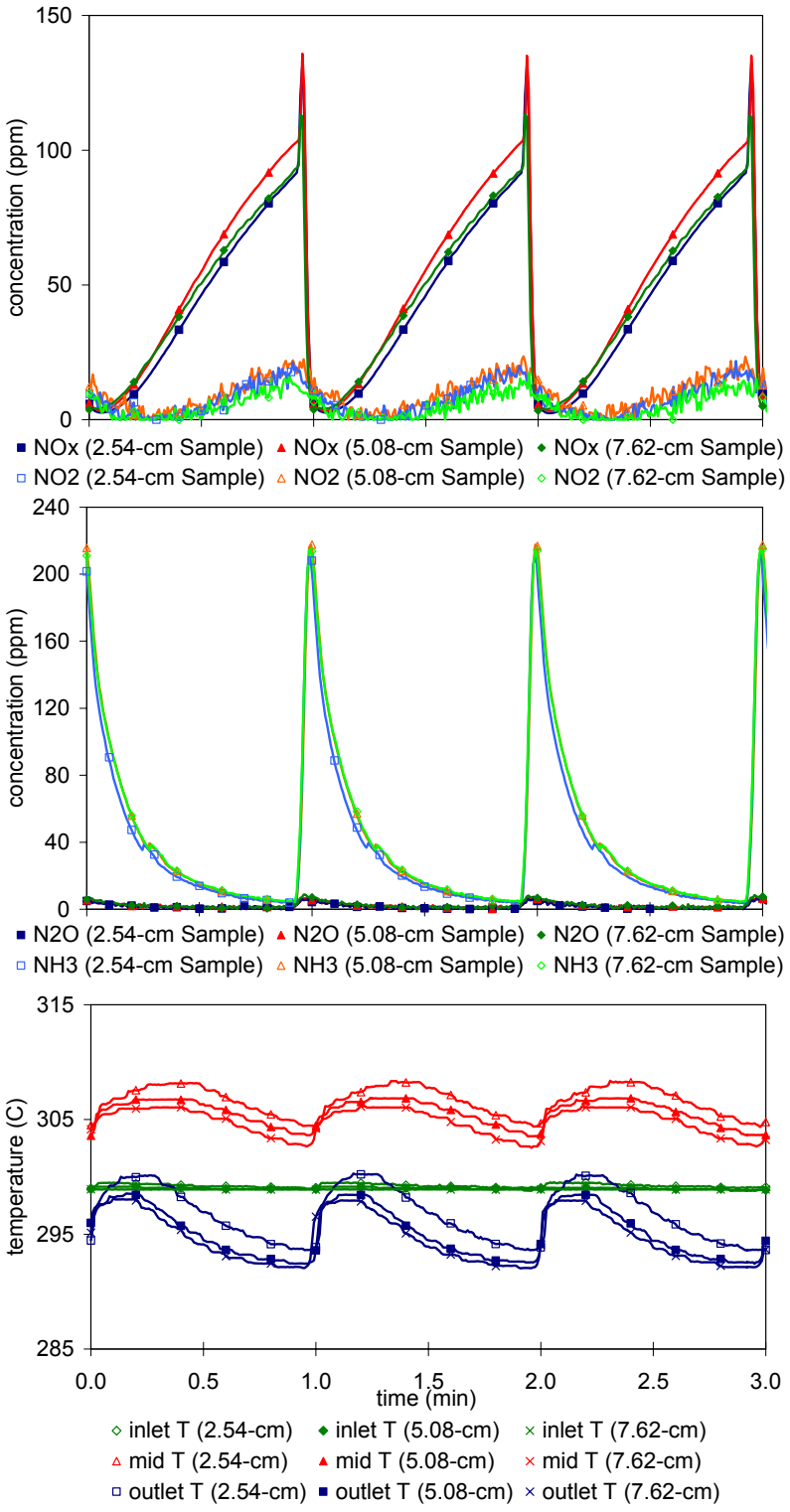

Figure 4.19. Catalyst A's outlet gas concentrations and temperature profiles for 2.54, 5.08 and 7.62-cm-long samples in short-cycle experiments with 2.0% H_2 in rich phase at 300°C

Table 4.8. NO_x conversion efficiencies of Catalyst A in short-cycle experiments with 2.0% H_2 in rich phase

Temperature / Length	300˚C
2.54-cm	82.1%
5.08-cm	79.5%
7.62-cm	81.7%

No significant difference is observed between 2.54, 5.08 and 7.62-cm-long segmented samples in short-cycle experiments with 2% H_2 in regeneration phase and a difference of 15% is observed between 2.54 and 7.62-cm-long samples using 1% H_2 (partial regeneration). On the other hand a difference of only 3.4% is observed between 5.08 and 7.62-cm-long samples with 1% H_2, which is within the experimental uncertainty; and thus it is inconclusive to attribute this difference to variation in length. Level of NH_3 produced in 5.08 and 7.62-cm-long segmented samples is very similar and significantly larger than in 2.54-cm-long sample in experiments with 1% H_2. Results of this section confirm the conclusion drawn in Section 4.1.3.3: Catalyst A's performance is affected by sample length during short-cycle experiments when regeneration is limited by amount of reductant available. On the other hand, increasing the catalyst's length from 5.08 to 7.62 cm appears not to cause significant change in performance regardless of reductant concentration. In Section 4.1.5 the reductant consumption trends in short-cycle experiments are presented, which can be used to explain the differences in performance observed in this section.

4.1.5 Reductant Consumption Trend during Short Cycling

The intra-catalyst concentration of H_2 was measured at three different axial locations – catalyst inlet, mid-section and exit – with SpaciMS. Figures 4.20 and 4.21 show H_2 profiles for short-cycle experiments as described previously in Section 4.1.4.2. These figures provide information on the consumption of H_2

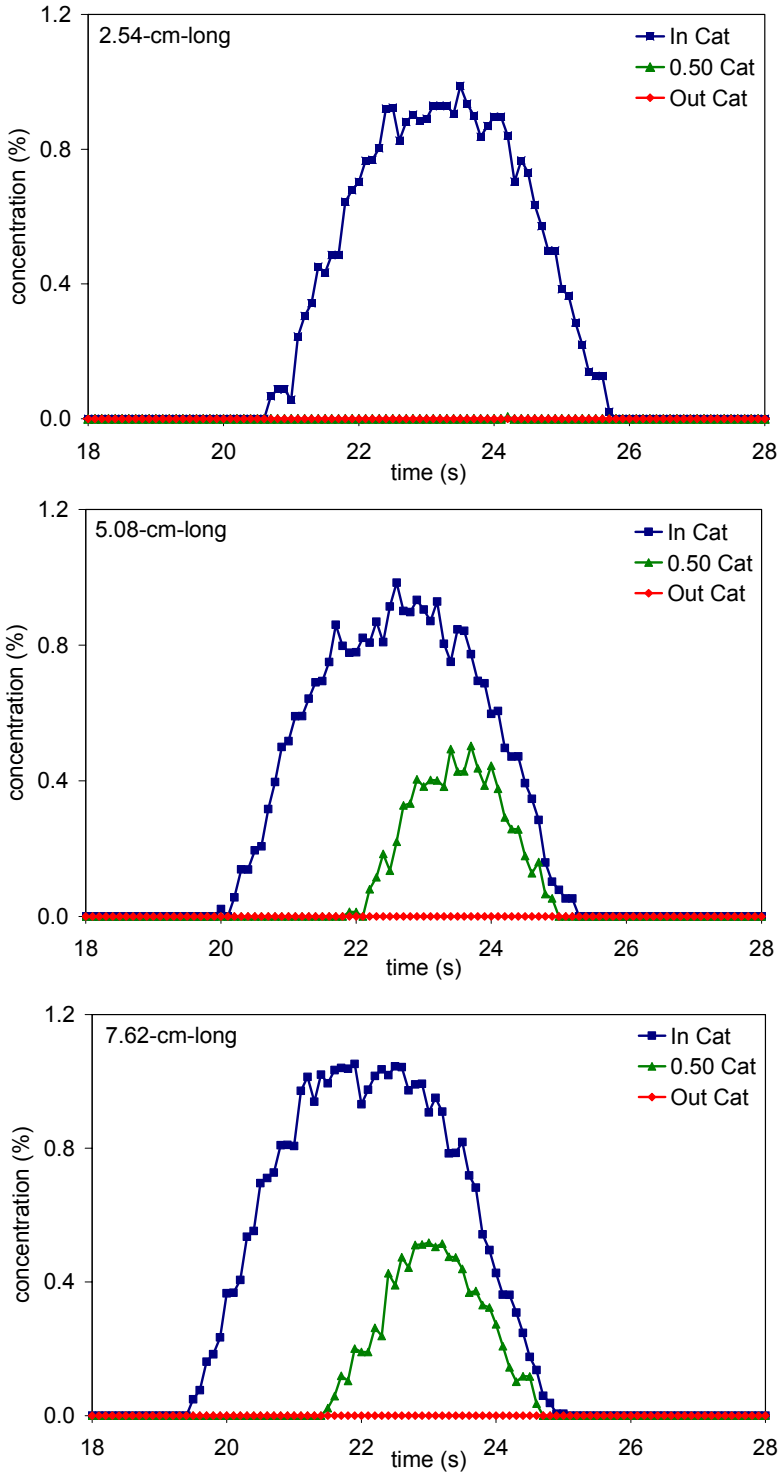

Figure 4.20. Catalyst A's H_2 consumption trends in 2.54, 5.08 and 7.62-cm-long samples in short-cycle experiments with 1.0% H_2 in rich phase at 300˚C

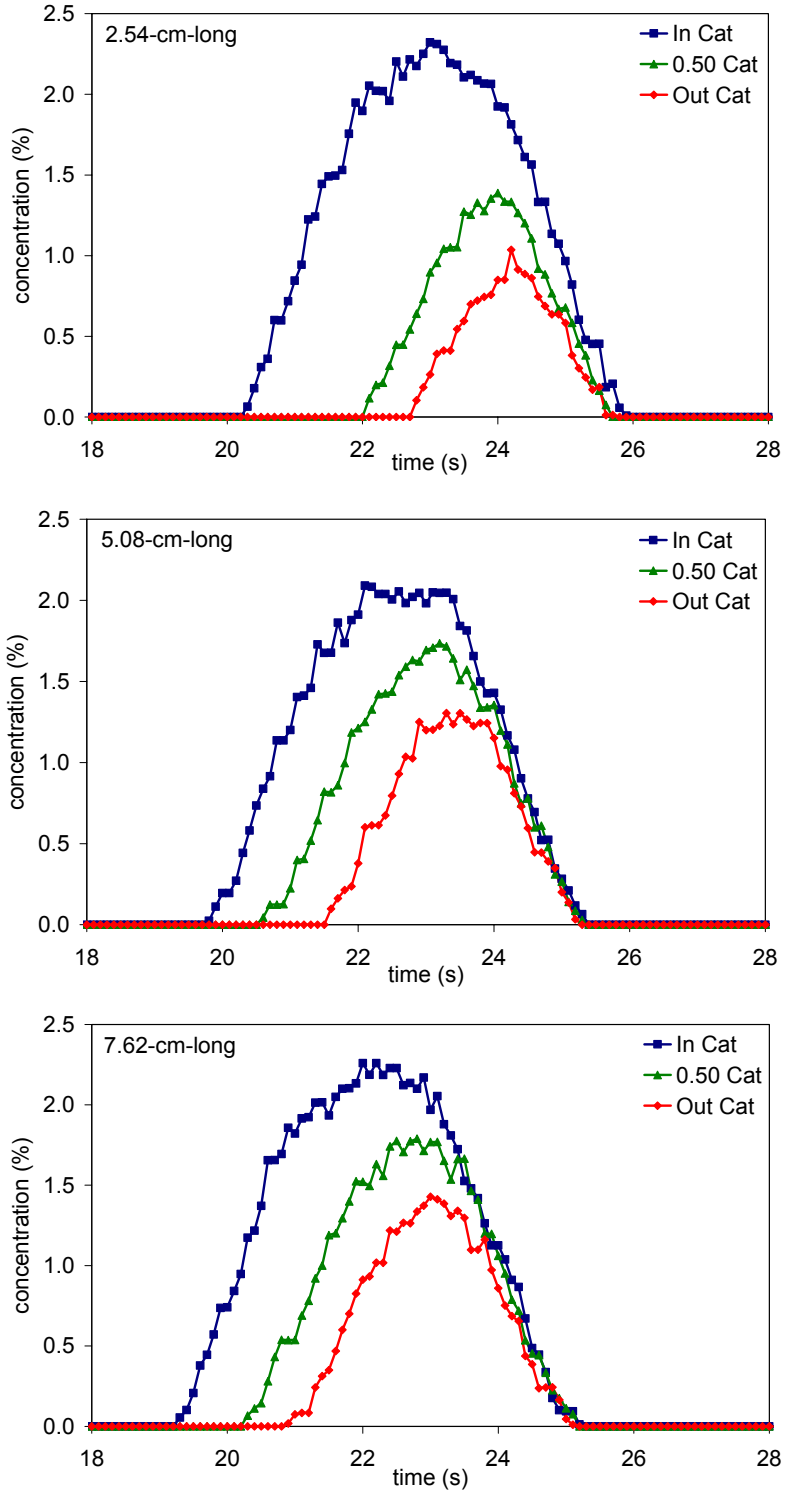

Figure 4.21. Catalyst A's H_2 consumption trends in 2.54, 5.08 and 7.62-cm-long samples in short-cycle experiments with 2.0% H_2 in rich phase at 300˚C

along the length of segmented samples of 2.54, 5.08 and 7.62-cm-long. In short-cycle experiments with 1% H_2 in the rich phase, as seen in Figure 4.20, H_2 is completely consumed in the front half of the 2.54-cm-long sample; whereas about 25% of H_2 remains in the 5.08 and 7.62-cm long samples. With 2% H_2 in the rich phase of the short-cycle experiments, approximately 60% of H_2 is consumed in the entire length of 5.08 and 7.62-cm-long samples, whereas 80% is consumed in 2.54-cm-long sample (see Figure 4.21). Short-cycle experiments with two different concentrations of H_2 in the rich phase follow the same trend: more H_2 is consumed in 2.54-cm-long sample than in 5.08 and 7.62-cm samples, which is in contrast to performance trends observed in Section 4.1.4.2. Higher consumption of H_2 in 2.54-cm-long sample should result in higher NO_x conversion, however the opposite is observed: 2.54-cm-long sample has lower NO_x conversion efficiency than longer samples in short-cycle experiments with 1% H_2, and no difference is observed with 2% H_2.

Catalyst regeneration is limited by the amount of reductant available in short-cycle experiments with 1% H_2 in the rich phase; thus, small variability in inlet level of H_2 (whether due to different combinations of mass flow controllers or other factors) may result in different conversion efficiencies by regenerating the catalyst surface to different extents. Therefore, lower NO_x conversion efficiency and higher H_2 consumption in 2.54-cm-long sample may be due to lower actual (as opposed to commanded) inlet concentration of H_2 available to reduce NO_x. Even though higher H_2 consumption is observed in 2.54-cm-long than in longer samples in short-cycle experiment with 2% H_2, no significant difference is observed in NO_x conversion between the three samples. This result seems to indicate that as long as the catalyst regeneration is not limited by the amount of H_2 available (considerable amount of H_2 is detected at the catalyst outlet in each case), varying sample lengths does not affect the catalyst's performance.

Actual concentration of H_2 at the catalyst inlet was measured by positioning SpaciMS probe at the catalyst inlet and sending the same gases using the same set of mass flow controllers used during the regeneration phase

of the cycling experiments. No variability in inlet H_2 was observed between 2.54, 5.08 and 7.62-cm-long samples; therefore, the difference in reductant consumption trends between these three samples is not due to the use of different mass flow controllers.

Short-cycle experiments without NO in the lean phase were performed in order to determine the role of catalysts' oxygen storage capacity (OSC). Results from this particular set of experiments reveal interesting information concerning reductant consumption. With 1% H_2 in the rich phase approximately 50% of H_2 is consumed in the front half of the 2.54-cm-long sample compared to 18% in the 5.08 and 7.62-cm long samples as shown in Figure 4.22; no significant reductant consumption is observed in the rear half of the catalyst regardless of the length of the sample. Similar results are obtained in OSC experiments with 2% H_2 and are shown in Figure 4.23.

Different H_2 consumption in 2.54, 5.08 and 7.62-cm-long samples in OSC experiments seems to indicate that the consumption of H_2 might possibly occur via other mechanisms in addition to oxygen stored on the catalyst's surface. The catalytic reaction between H_2 and O_2 at the interface between the lean and rich phases may contribute significantly to H_2 consumption; the extent of which depends on the degree of mixing at the lean/rich interface. Even though the present bench flow reactor was specifically designed to minimize this interaction, the possibility of some mixing could not be entirely eliminated. Higher degree of back-mixing would result in higher H_2 consumption and lesser amount of H_2 available for reducing stored NO_x, thereby lowering catalyst's NO_x conversion. Higher consumption of H_2 in 2.54-cm-long sample than in 5.08 and 7.62-cm samples may be attributed to higher degree of back-mixing in a shorter sample; whereas lower and similar H_2 consumption in 5.08 and 7.62-cm-long samples apparently indicates that lesser degree of back-mixing is achieved when the flow rate is increased to the levels used in 5.08 or 7.62-cm samples (at a fixed gas hourly space velocity and catalyst diameter, gas velocity or flow rate increases with increasing sample length).

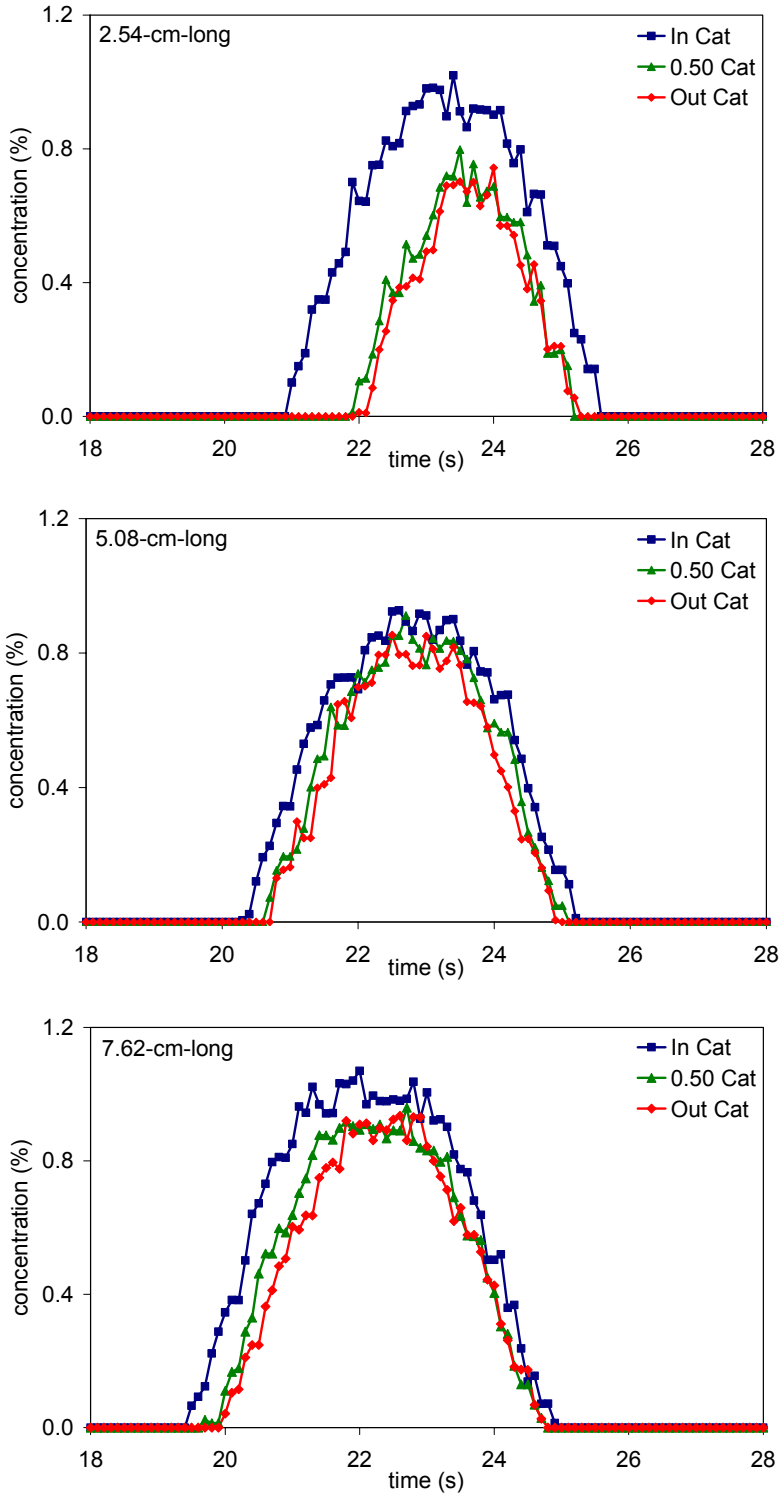

Figure 4.22. Catalyst A's H_2 consumption trends in 2.54, 5.08 and 7.62-cm-long samples in oxygen storage (without NO during lean phase) experiments with 1.0% H_2 in rich phase at 300˚C

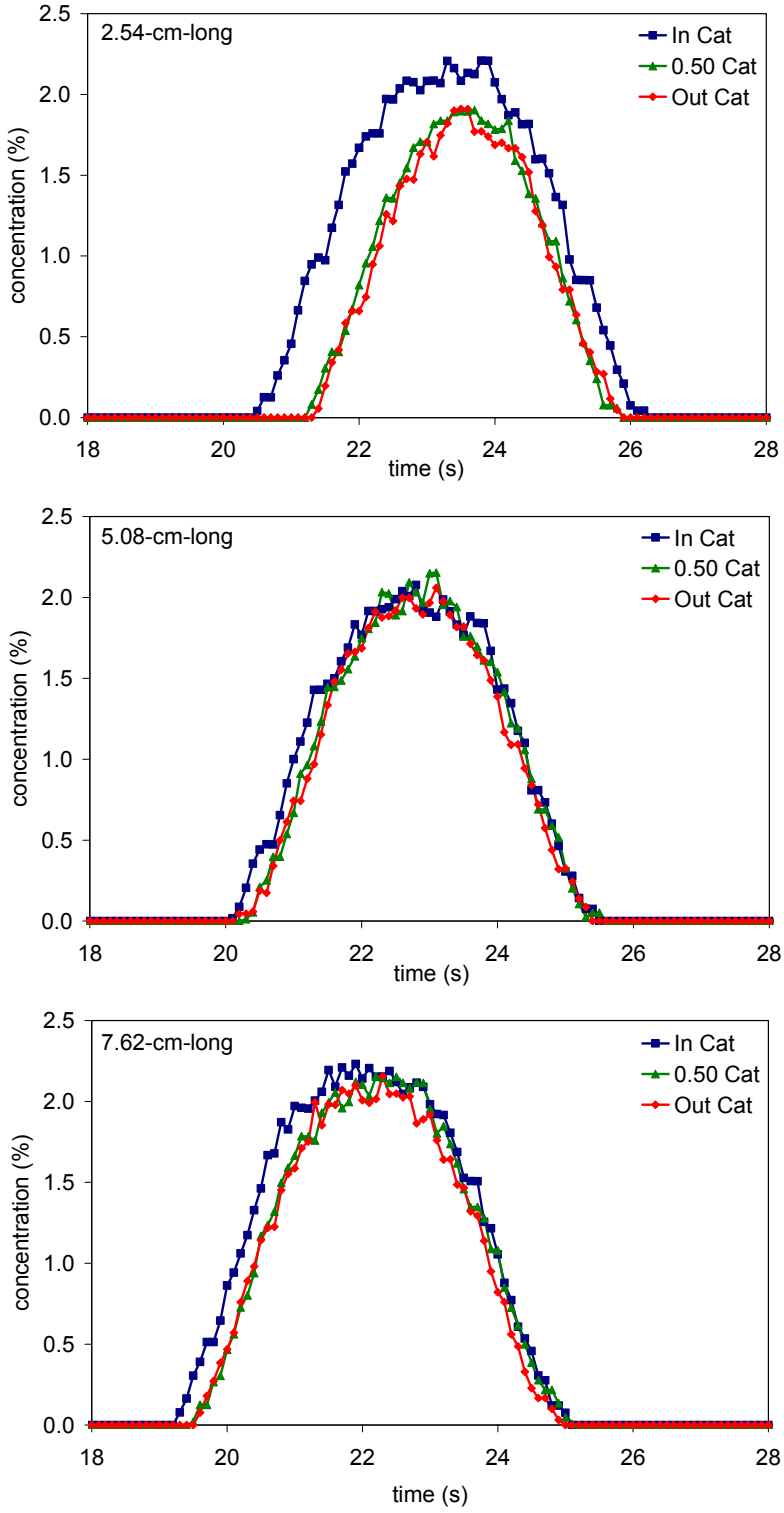

Figure 4.23. Catalyst A's H_2 consumption trends in 2.54, 5.08 and 7.62-cm-long samples in oxygen storage (without NO during lean phase) experiments with 2.0% H_2 in rich phase at 300˚C

To evaluate the extent of back-mixing, OSC experiments with a nitrogen purge of ten seconds between lean and rich pulse (referred to as back-mixing experiments) were performed. Nitrogen purge creates an inert environment between the lean and rich front, which should eliminate H_2 consumption due to lean/rich front back-mixing. As seen in Figure 4.24 nitrogen purge decreases H_2 consumption in the front half of the 2.54-cm-long sample by 35% in experiment with 1% H_2 in rich phase and by about 10% in both 5.08 and 7.62-cm-long samples. Similar results are obtained in back-mixing experiments with 2% H_2 and results are shown in Figure 4.25.

Based on OSC experiments with and without nitrogen purge, it is clear that significant amount of H_2 is consumed by the catalytic reaction between H_2 and O_2 at the interface between the rich and lean pulses. Slower moving gases result in higher degree of mixing at the lean/rich interface (as in a case of 2.54-cm-long sample), which culminates in higher H_2 consumption and lesser amount of H_2 available in reducing NO_x. As the flow rate reaches a certain level, back-mixing becomes negligible (as in the case of 5.08 and 7.62-cm-long samples) and no difference in catalyst performance is observed. In the 2.54-cm-long sample as much as 35% of H_2 is consumed from the catalytic oxidation at the lean/rich interface – compared to only 10% in the longer sample – resulting in a reduction of 15% in NO_x conversion in short-cycle experiments with 1% H_2. Based on the stoichiometry of Equations 3.1 and 3.2, for every mole of NO entering the reactor 2.5 moles of hydrogen are required to reduce the stored NO_x to N_2; therefore, 25 to 35% less availability of H_2 would result in 10 to 14% decrease in NO_x conversion when regeneration is limited by amount of H_2 available. Since in a short cycle experiments with 1% H_2 complete regeneration is determined by the availability of H_2, the reduction of NO_x conversion in shorter sample within experimental uncertainty, matches experimental results. Lower formation of NH_3 in 2.54-cm-long sample than in longer samples can be attributed to lesser availability of H_2 in shorter sample, since NH_3 production decreases with decreasing H_2 concentration [19].

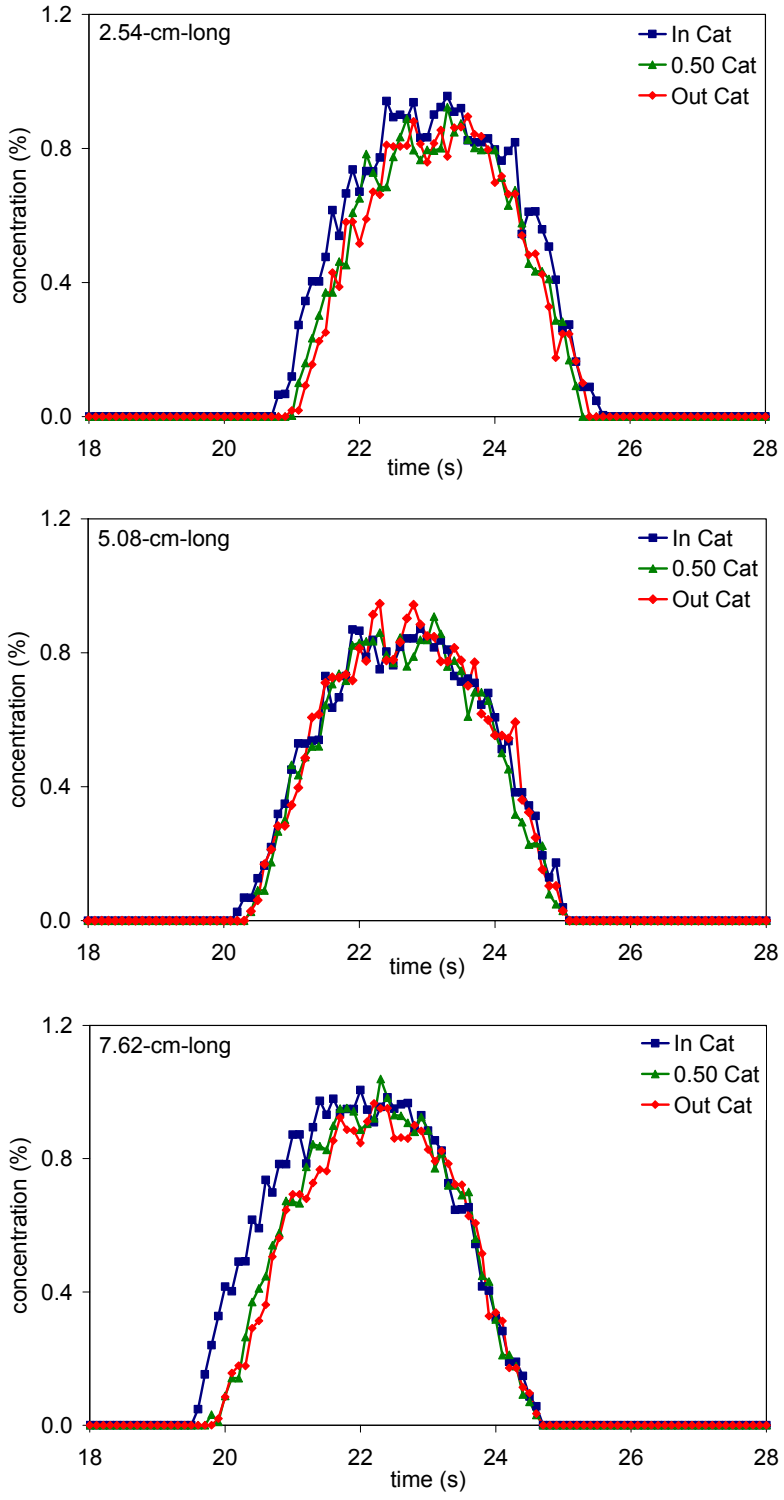

Figure 4.24. Catalyst A's H_2 consumption trends in 2.54, 5.08 and 7.62-cm-long samples in back-mixing (OSC experiments with 10s nitrogen purge) short-cycle experiments with 1.0% H_2 in rich phase at 300˚C

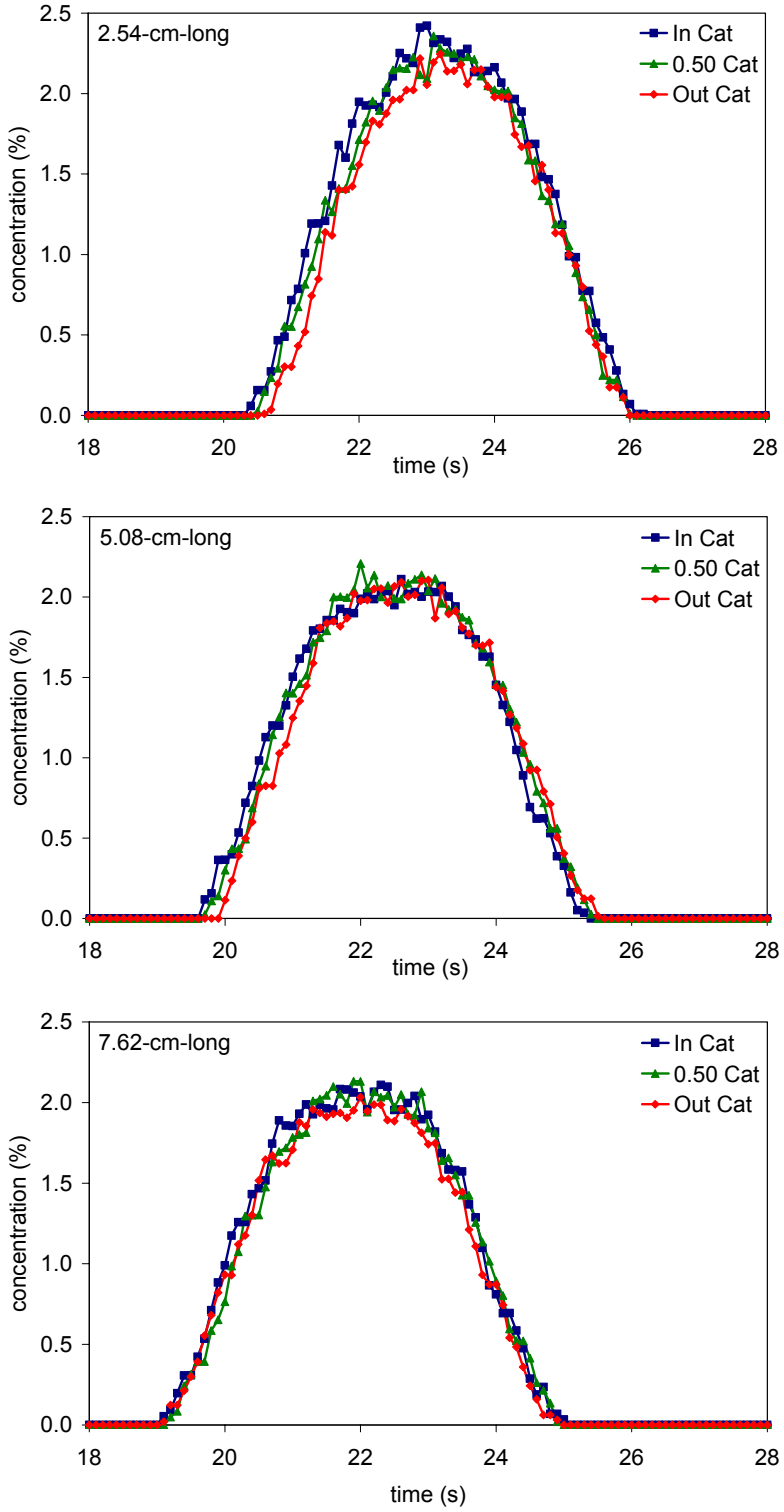

Figure 4.25. Catalyst A's H_2 consumption trends in 2.54, 5.08 and 7.62-cm-long samples in back-mixing (OSC experiments with 10s nitrogen purge) short-cycle experiments with 2.0% H_2 in rich phase at 300˚C

In general, back-mixing originates from the difference between the absolute velocity of some components in the gas mixture and the average molar velocity of the mixture: some molecules are moving faster than the molar average velocity while others slower. Thus, in addition to transport by bulk flow, each component in the mixture is transported by diffusion in the axial direction, which can be described by Fick's law of diffusion:

$$J_A = -CD_a \frac{dY_A}{dz} \tag{4.1}$$

where J_A is molar diffusive flux in mol/s·m^2, Y_A is mole fraction of component A D_a is longitudinal or axial dispersion coefficient in m^2/s and z is the axial direction. Axial dispersion coefficient characterizes the degree of back-mixing during flow, and unlike the coefficient of molecular diffusion it incorporates the effect of convective diffusion in addition to molecular diffusion [25].

The fluid phase mole balance equation for each species representing dispersion with reaction is

$$\frac{\partial}{\partial z}\left(D_a \frac{\partial C_A}{\partial z} - C_A U_z\right) + (R_A)_H - k_{m,A}\, a_c\, (C_A - C_{As}) = \frac{\partial C_A}{\partial t} \tag{4.2}$$

where $(R_A)_H$ is the rate of generation or consumption of A due to homogeneous reaction (mol/s·m^3), $k_{m,A}$ is the mass transfer coefficient (m/s), U_z is the molar average velocity (m/s), C_A is the concentration of species A (mol/m^3), C_{As} is the concentration of species A at the catalyst's surface (mol/m^3) and a_c is the ratio of wetted perimeter to cross-sectional area of the channel (m/m^2). Equation 4.2 is subject to two boundary conditions:

$$\left(-D_a \frac{\partial C_A}{\partial z}\right)_{0^-} + U_z C_A\left(0^-\right) = \left(-D_a \frac{\partial C_A}{\partial z}\right)_{0^+} + U_z C_A\left(0^+\right) \quad \text{at z=0} \tag{4.3}$$

$$\frac{\partial C_A}{\partial z} = 0 \quad \text{at z=L} \tag{4.4}$$

In Equation 4.3, 0^- indicates the position outside the catalyst at z=0, and 0^+ indicates the position inside the catalyst at z=0. Equation 4.3 originates from the continuity of molar flux at z=0, whereas Equation 4.4 from the continuity of

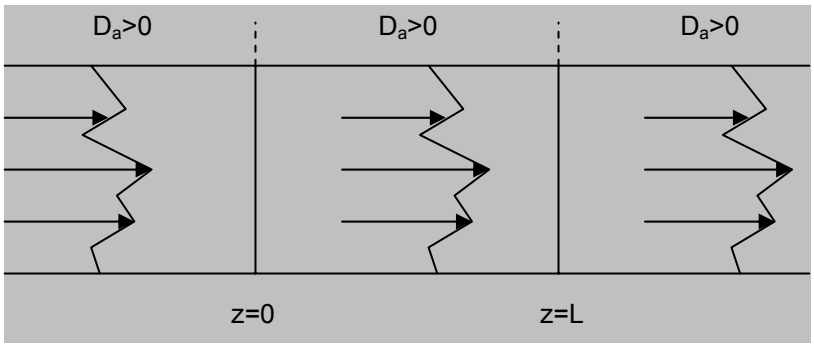

Figure 4.26. Concentration profiles with dispersion at catalyst inlet, inside catalyst and at catalyst outlet [25]

concentration at z=L [15]. The boundary conditions described by Equations 4.3 and 4.4 are graphically represented in Figure 4.26. As shown in the figure, dispersion occurs both upstream ($z=0^-$) and downstream ($z=0^+$) of the catalyst; between $z=0^+$ and $z=L^-$ (inside the catalyst) dispersion with reaction described by Equation 4.2 occurs.

Introducing $C_{As}^* = \frac{C_{As}}{C_{Ao}}$, $C_A^* = \frac{C_A}{C_{Ao}}$, $z^* = \frac{z}{L}$ and $t^* = \frac{tU_z}{L}$, and neglecting gas phase homogeneous reaction, Equations 4.2, 4.3 and 4.4 in dimensionless form become

$$\frac{D_a}{U_z L}\frac{\partial^2 C_A^*}{\partial z^{*2}} - \frac{\partial C_A^*}{\partial z^*} - \frac{L}{U_z} k_{m,A} a_c (C_A^* - C_{As}^*) = \frac{\partial C_A^*}{\partial t^*} \qquad (4.5)$$

$$\left(-\frac{D_a}{U_z L}\frac{\partial C_A^*}{\partial z^*} + \frac{\partial C_A^*}{\partial z^*}\right)_{0^-} = \left(-\frac{D_a}{U_z L}\frac{\partial C_A^*}{\partial z^*} + \frac{\partial C_A^*}{\partial z^*}\right)_{0^+} \quad \text{at } z^*=0 \qquad (4.6)$$

$$\frac{\partial C_A^*}{\partial z^*} = 0 \quad \text{at } z^*=1 \qquad (4.7)$$

The dimensionless group D_a/U_zL, referred to as the vessel dispersion number, is the parameter, which measures the extent of axial dispersion [25]. The reciprocal of D_a/U_zL is the Peclet number, Pe, which is the ratio of rate of transport by convection to rate of transport by diffusion. Rewriting Equations 4.5

and 4.6 in terms of Peclet number and replacing L/U_z by τ (space time, s), the following equations are obtained:

$$\frac{1}{Pe}\frac{\partial^2 C_A^*}{\partial z^{*2}} - \frac{\partial C_A^*}{\partial z^*} - \tau k_{m,A} a_c (C_A^* - C_{As}^*) = \frac{\partial C_A^*}{\partial t^*} \tag{4.8}$$

$$\left(-\frac{1}{Pe}\frac{\partial C_A^*}{\partial z^*} + \frac{\partial C_A^*}{\partial z^*}\right)_{0^-} = \left(-\frac{1}{Pe}\frac{\partial C_A^*}{\partial z^*} + \frac{\partial C_A^*}{\partial z^*}\right)_{0^+} \quad \text{at } z^*=0 \tag{4.9}$$

As Pe → ∞ or $D_a/U_zL \rightarrow 0$, axial dispersion becomes negligible and flow approaches plug flow. As Pe → 0 or $D_a/U_zL \rightarrow \infty$, axial dispersion becomes significant and hence back-mixing becomes important.

With negligible axial dispersion ($D_a/U_zL \rightarrow 0$), the first term in Equation 4.8 vanishes and the equation is reduced to

$$-\frac{\partial C_A^*}{\partial z^*} - \tau k_{m,A} a_c (C_A^* - C_{As}^*) = \frac{\partial C_A^*}{\partial t^*} \tag{4.10}$$

As seen in Equation 4.10, reacting system with negligible axial dispersion is governed by residence time (reciprocal of space velocity) and mass transfer coefficient. In a fully-developed laminar flow, mass transfer coefficient is constant; therefore, reacting system is governed by residence time only. Since the flow in the catalyst samples used in this study is laminar (Re<2100), changing the sample length or linear velocity should not affect the catalyst performance as long as space velocity or residence time is kept constant. However, the NO_x conversion efficiencies obtained in the present study appear to indicate the contrary – the catalyst performance is dependent on the sample length or the gas linear velocity.

Higher consumption of H_2 in 2.54-cm-long sample and lower consumption in longer samples seem to indicate a higher degree of back-mixing in shorter sample; and therefore axial dispersion should not be neglected. As the gas velocity increases with increasing length, the dispersion term, D_a/U_zL becomes less dominant. When the gas velocity reaches certain value such as those achieved in the 5.08 and 7.62-cm-long samples, the axial dispersion reaches

conditions in which the back-mixing becomes constant and the sample's performance is no longer affected by the sample's length or the gas velocity.

The investigation of the effect of length on LNT performance was extended to Catalyst B, which is of different formulation and physical properties from Catalyst A. It was evaluated in a similar manner as Catalyst A, and results are presented in Section 4.2.

4.2 Catalyst B (Umicore) Evaluation

The evaluation of Catalyst B was carried out at 230, 325 and 500˚C using similar long and short-cycle experiments in evaluating Catalyst A, from which the results obtained from 2.54, 5.08 and 7.62-cm-long samples are then compared. Results of long and short-cycle experiments are presented in Sections 4.2.1 and 4.2.2, respectively.

4.2.1 Long-Cycle Experiments

Figures 4.27 to 4.29 show the catalyst outlet gas concentrations and temperature profiles for long-cycle experiments performed at 230, 325 and 500˚C. Three cycles were run, and the results are shown only for the third cycle. Each long cycle consists of 15 minutes of NO_x capture (300 ppm NO, 10% O_2, 5% H_2O, 5% CO_2 and balance N_2) and 10 minutes regeneration (0.4% H_2, 5% H_2O, 5% CO_2 and balance N_2).

The general trends are similar to the ones presented for Catalyst A, i.e., NO_x is stored on the catalyst surface during the lean period and released from the surface and reduced to N_2 (not measured) and other products during the subsequent rich period. Immediately after switching from lean to rich condition, N_2O is formed and followed shortly by NH_3. Formation of N_2O and NH_3 decreases with increasing temperature.

The cycle average NO_x conversion efficiencies for 2.54, 5.08 and 7.62-cm-long samples are given in Table 4.9. At 500˚C rapid decomposition of highly unstable nitrate species overwhelms the reduction process, resulting in large NO_x

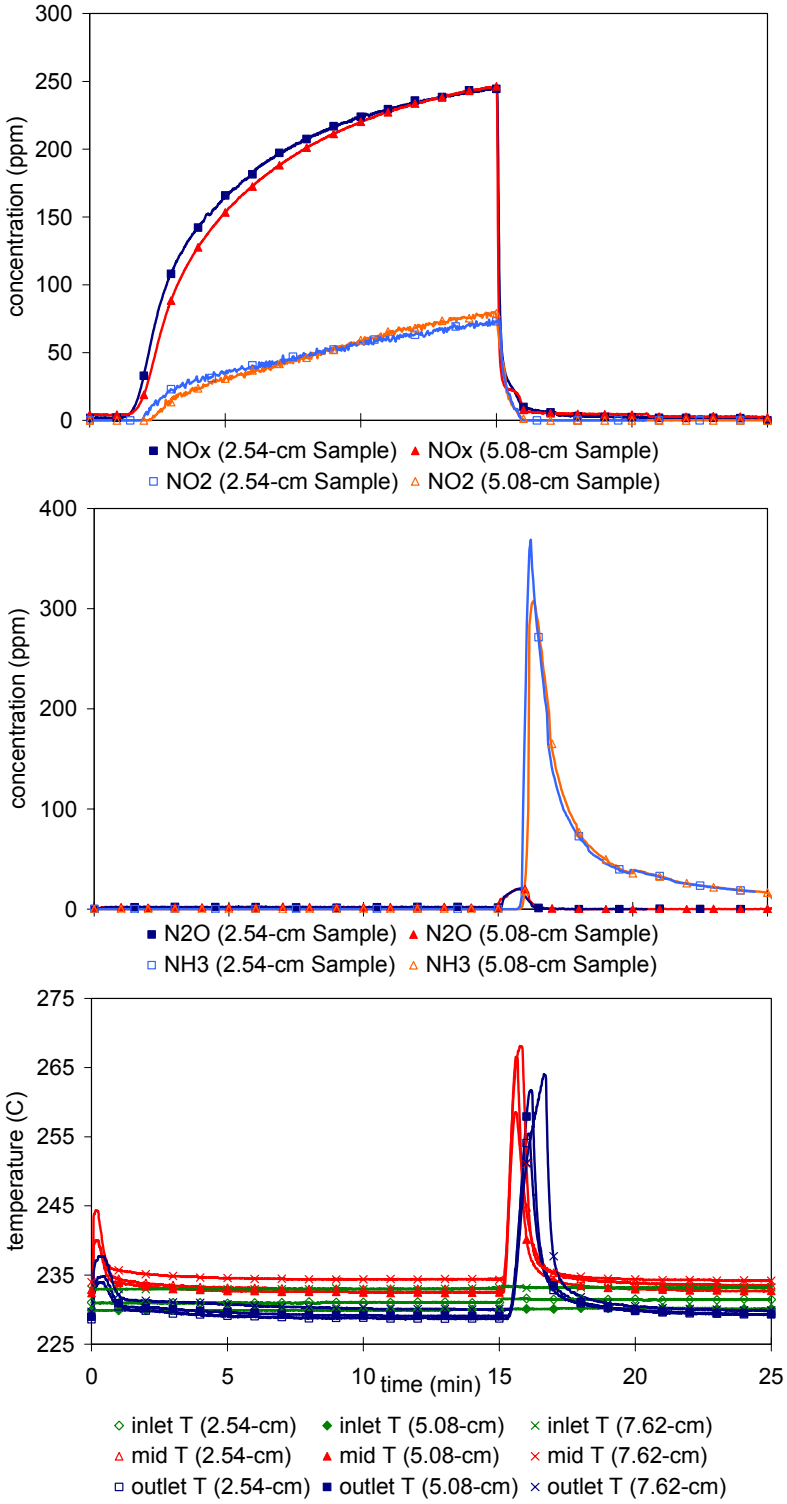

Figure 4.27. Catalyst B's outlet gas concentrations and temperature profiles for 2.54, 5.08 and 7.62-cm-long samples in long-cycle experiments with 0.4% H_2 in rich phase at 230˚C (Note: data for 7.62-cm-long sample was not taken)

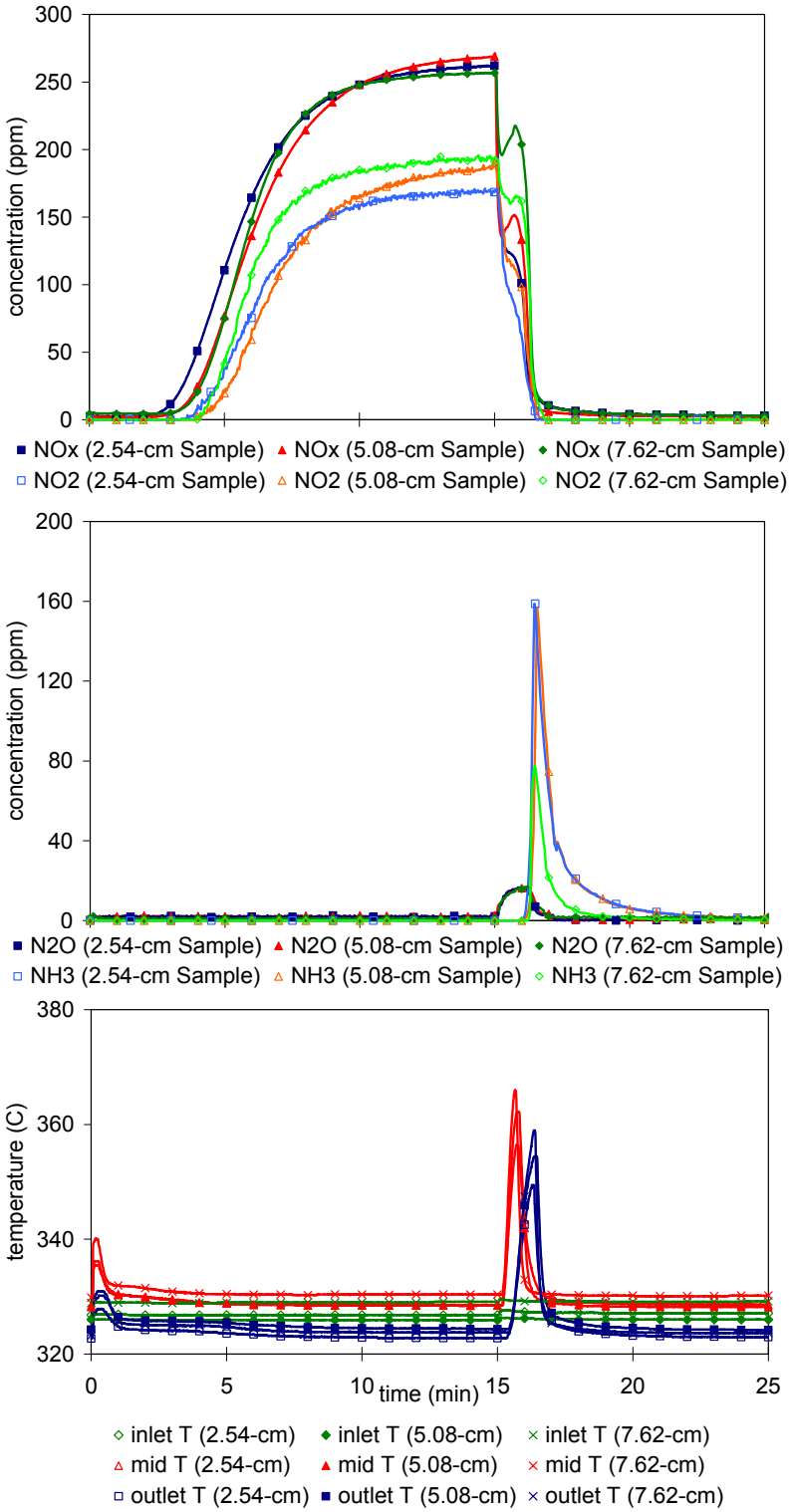

Figure 4.28. Catalyst B's outlet gas concentrations and temperature profiles for 2.54, 5.08 and 7.62-cm-long samples in long-cycle experiments with 0.4% H_2 in rich phase at 325˚C

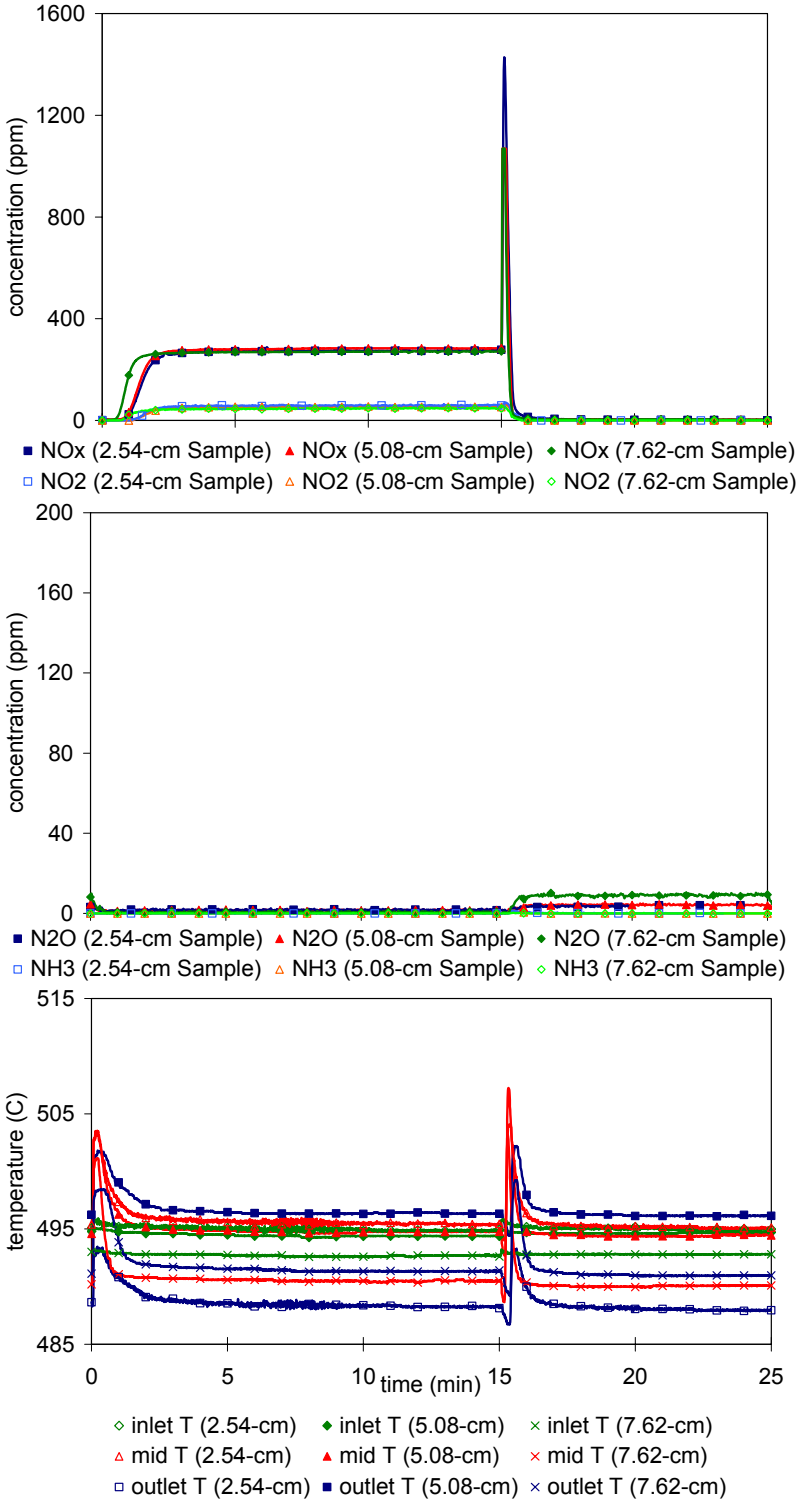

Figure 4.29. Catalyst B's outlet gas concentrations and temperature profiles for 2.54, 5.08 and 7.62-cm-long samples in long-cycle experiments with 0.4% H_2 in rich phase at 500˚C

Table 4.9. NO_x conversion efficiencies of Catalyst B in long-cycle experiments with 0.4% H_2 in rich phase

Temperature / Length	230˚C	325˚C	500˚C
2.54-cm	36.6%	36.5%	1.6%
5.08-cm	40.7%	40.8%	1.9%
7.62-cm	—	35.8%	1.8%

release and negligible NO_x conversion. The time delay in the NO_x outlet concentration at 325˚C is twice as long as at 230˚C (approximately 3 vs. 1.5 minutes), suggesting that at 325˚C prior to NO_x breakthrough more NO_x is stored and less vacant storage sites available culminating in a higher rate of increase in NO_x outlet concentration after breakthrough. Higher NO_x storage prior to breakthrough and higher rate of increase in NO_x outlet concentration after breakthrough at 325˚C as opposed to results at 230˚C – lower NO_x storage and lower rate of increase in NO_x outlet concentration before and after breakthrough – in effect giving rise to similar NO_x conversion efficiency at these two temperatures. The temperature increase at the beginning of lean cycle is possibly due to the oxidation of surface H_2 stored from the previous cycle and re-oxidation of ceria component of the catalyst's washcoat [26].

Figures 4.27 to 4.29 and Table 4.9 show no significant difference in the catalyst outlet gas concentrations, temperature profiles and NO_x conversion efficiencies between 2.54, 5.08 and 7.62-cm-long samples. It is, therefore, concluded that the performance of Catalyst B is not affected by sample's length in long-cycle experiments as in the case of Catalyst A.

4.2.2 Short-Cycle Experiments

Short-cycle experiments were conducted at the same temperatures as the long-cycle experiments. Each cycle consists of 60 s capture with the same gas

Table 4.10. NO_x conversion efficiencies of Catalyst B in short-cycle experiments with 1.4% H_2 in rich phase

Temperature / Length	230˚C	325˚C	500˚C
2.54-cm	64.3%	75.3%	43.0%
5.08-cm	76.9%	85.1%	45.1%
7.62-cm	86.4%	93.1%	49.1%

Table 4.11. NO_x conversion efficiencies of Catalyst B in short-cycle experiments with 3.4% H_2 in rich phase

Temperature / Length	230˚C	325˚C	500˚C
2.54-cm	96.0%	99.5%	72.9%
5.08-cm	98.5%	99.4%	71.3%
7.62-cm	99.8%	99.2%	62.9%

composition as in the long-cycle experiments and 5 s of regeneration with H_2 concentration of 1.4% and 3.4%. As in the case of Catalyst A evaluation, lower H_2 concentration (1.4%) was used to investigate the effect of partial regeneration on Catalyst B performance and higher concentration (3.4%) for full regeneration. Figures 4.30 to 4.32 show the catalyst outlet gas concentrations and temperature profiles for short-cycle experiments with 1.4% H_2 in the rich phase, while Figures 4.33 to 4.35 for 3.4% H_2. Tables 4.10 and 4.11 show the cycle average NO_x conversion efficiencies of Catalyst B obtained from the short-cycle experiments with 1.4% and 3.4% H_2, respectively.

The effect of length on Catalyst B performance in short-cycle experiments follows the same trend observed in Catalyst A: the longer the sample the better the performance when regeneration is limited by the amount of H_2 available. A

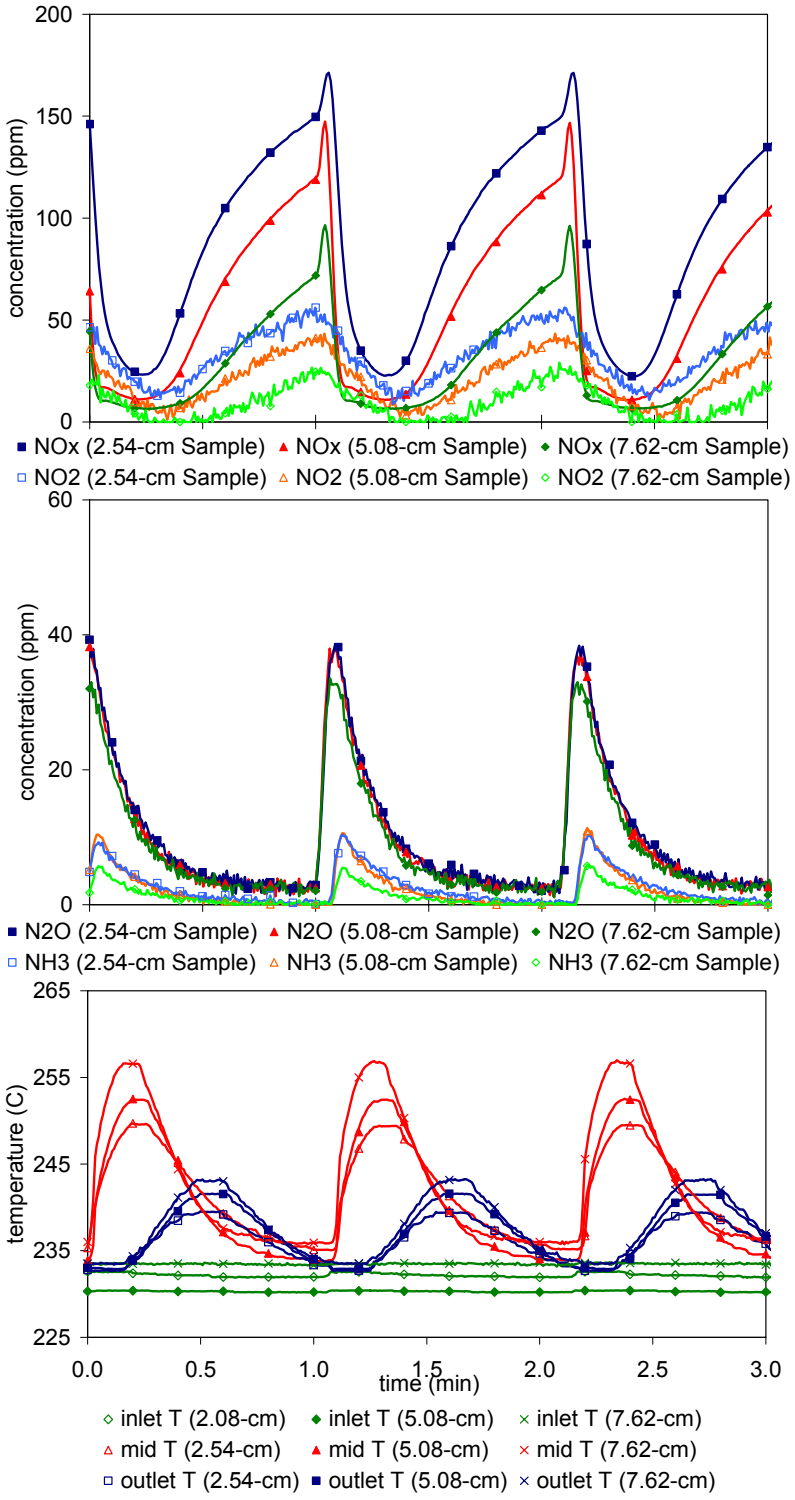

Figure 4.30. Catalyst B's outlet gas concentrations and temperature profiles for 2.54, 5.08 and 7.62-cm-long samples in short-cycle experiments with 1.4% H_2 in rich phase at 230°C

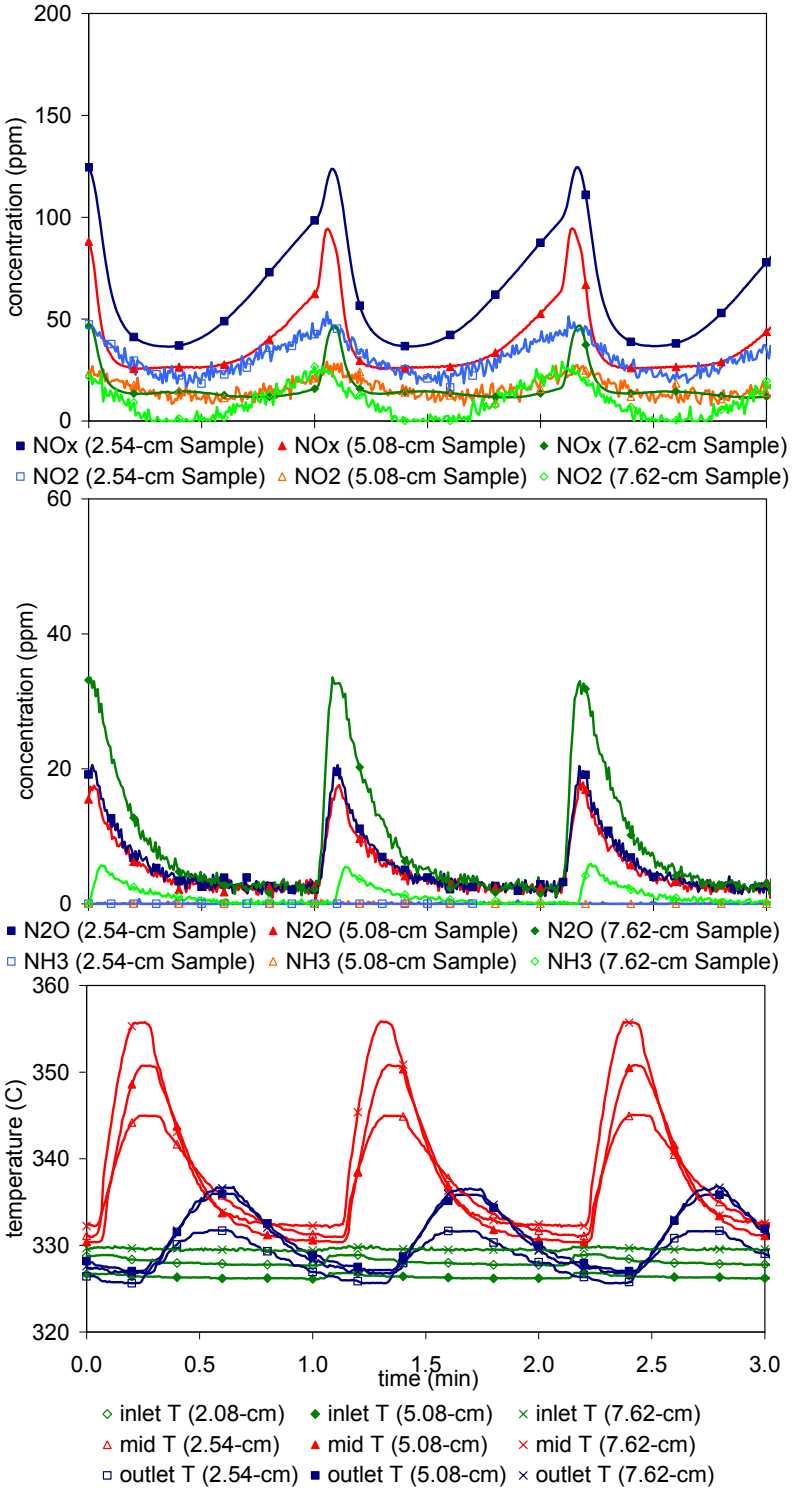

Figure 4.31. Catalyst B's outlet gas concentrations and temperature profiles for 2.54, 5.08 and 7.62-cm-long samples in short-cycle experiments with 1.4% H_2 in rich phase at 325°C

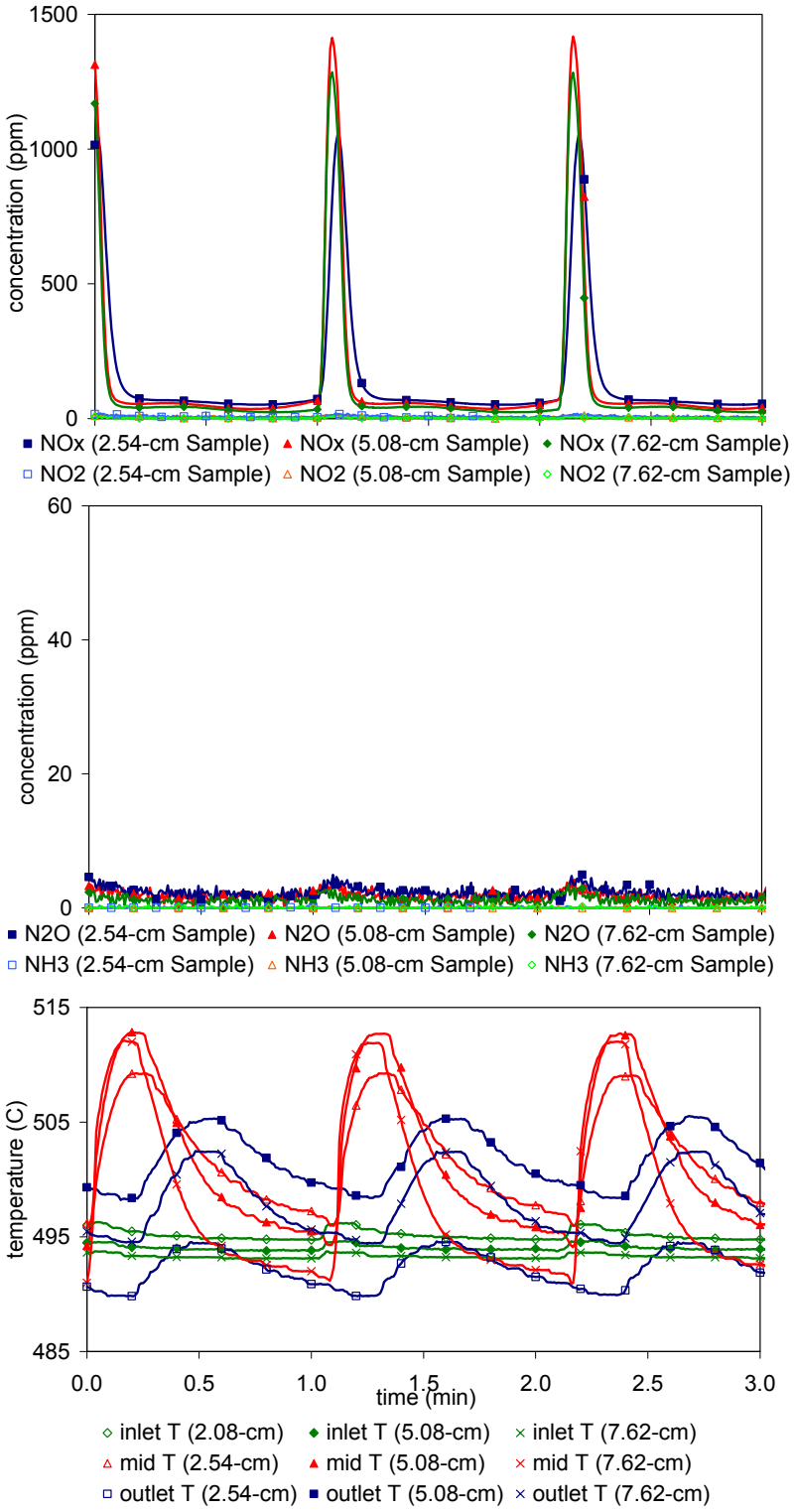

Figure 4.32. Catalyst B's outlet gas concentrations and temperature profiles for 2.54, 5.08 and 7.62-cm-long samples in short-cycle experiments with 1.4% H_2 in rich phase at 500˚C

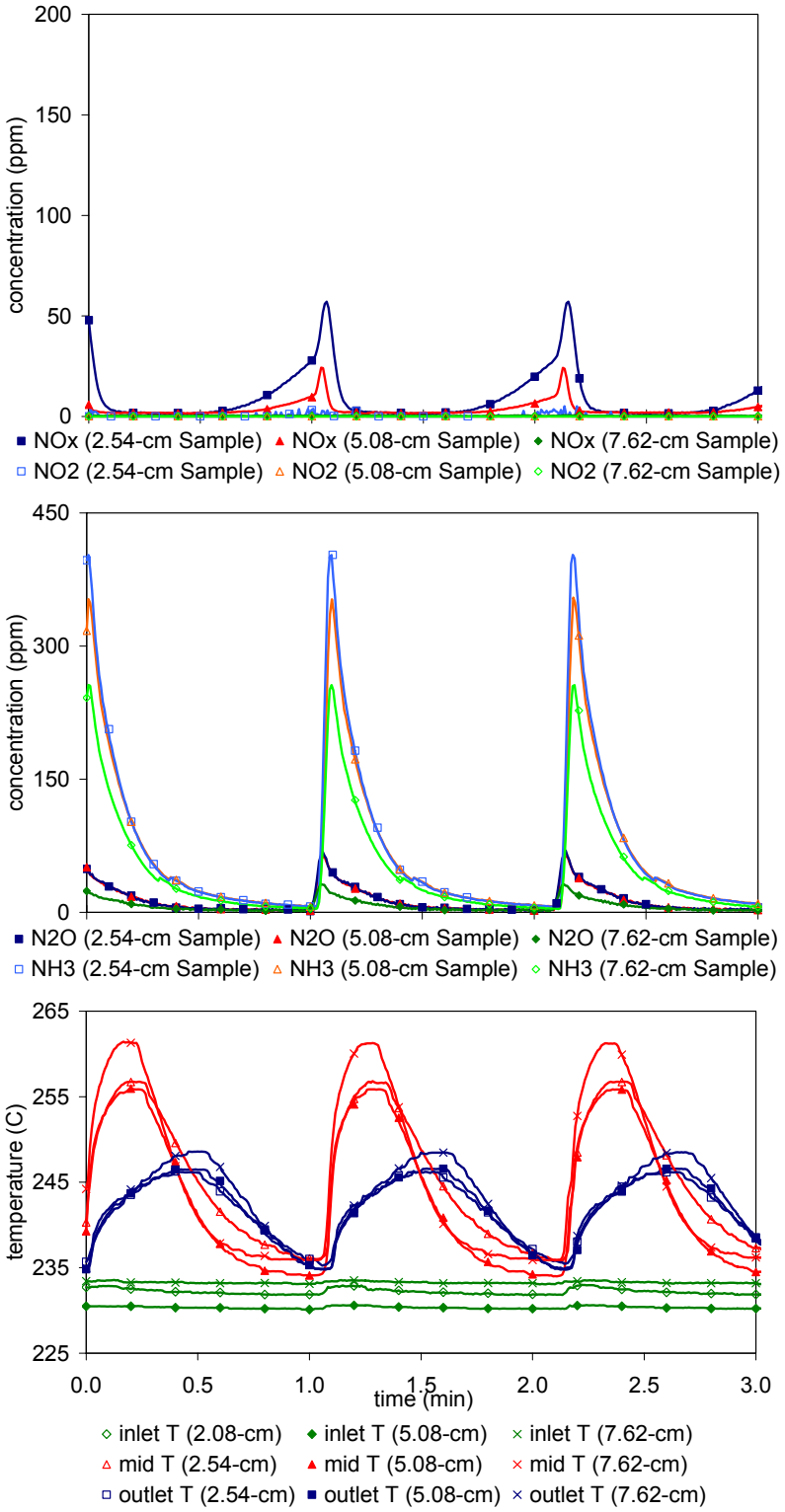

Figure 4.33. Catalyst B's outlet gas concentrations and temperature profiles for 2.54, 5.08 and 7.62-cm-long samples in short-cycle experiments with 3.4% H_2 in rich phase at 230˚C

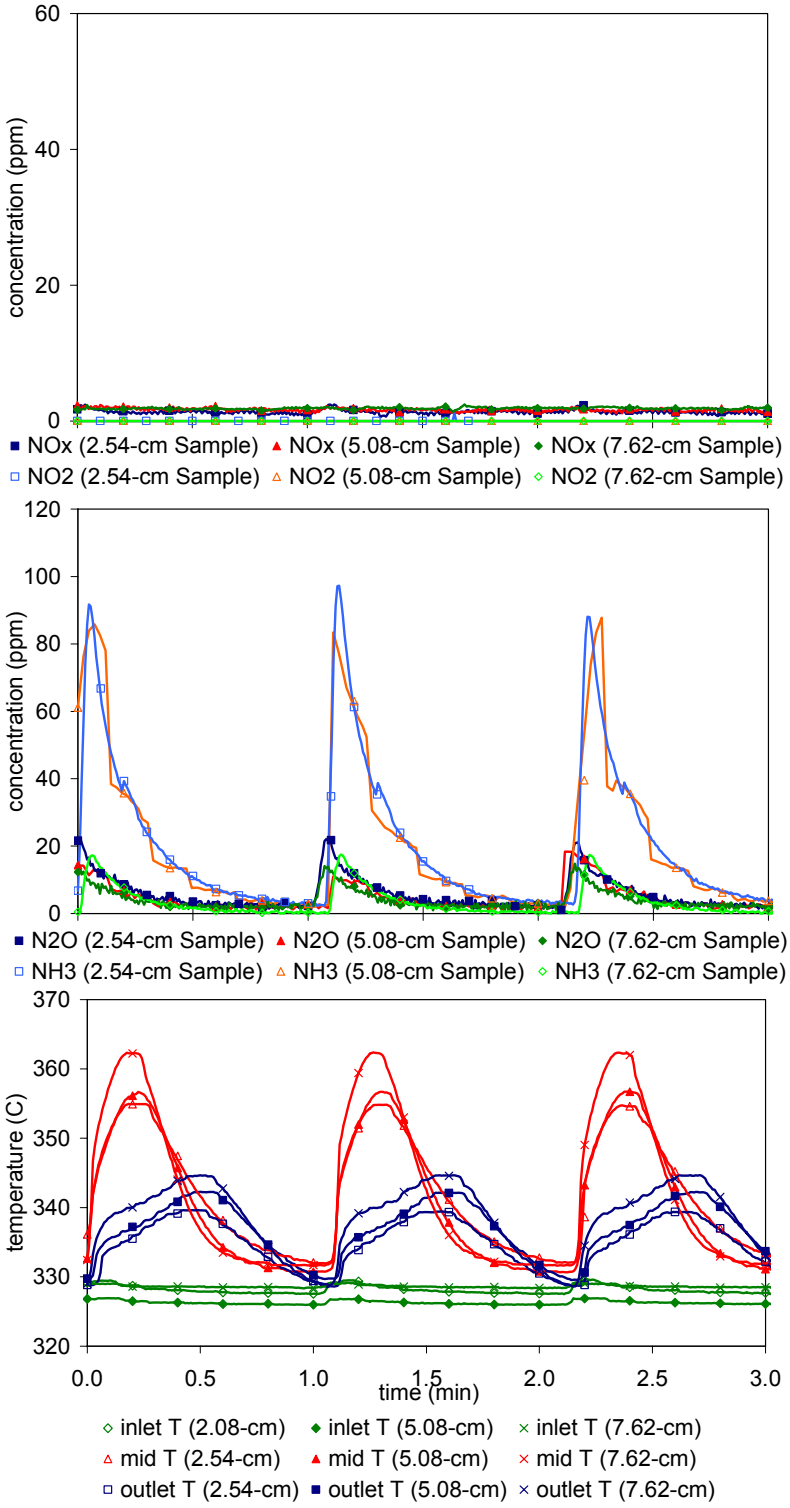

Figure 4.34. Catalyst B's outlet gas concentrations and temperature profiles for 2.54, 5.08 and 7.62-cm-long samples in short-cycle experiments with 3.4% H_2 in rich phase at 325˚C

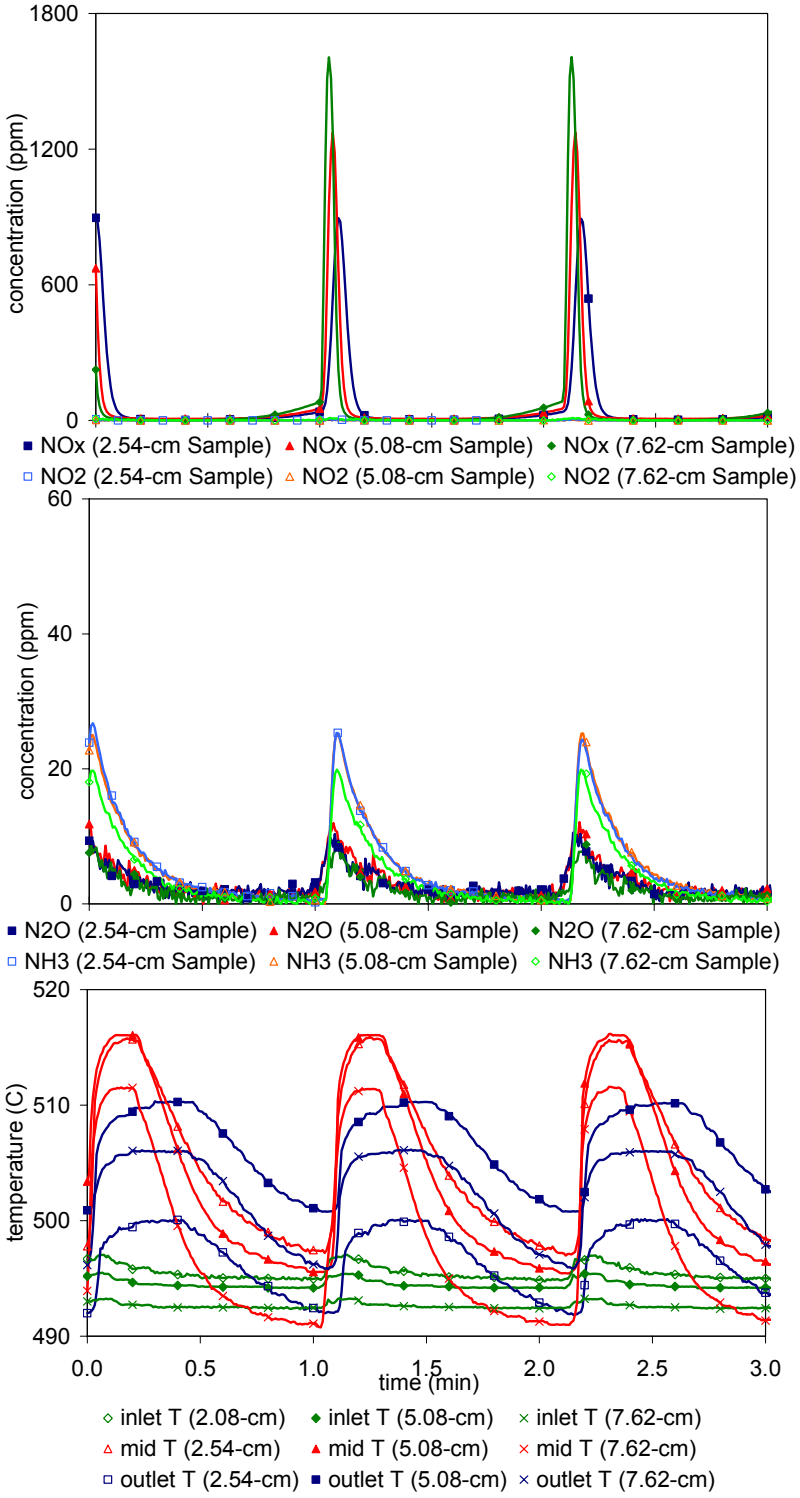

Figure 4.35. Catalyst B's outlet gas concentrations and temperature profiles for 2.54, 5.08 and 7.62-cm-long samples in short-cycle experiments with 3.4% H_2 in rich phase at 500˚C

difference of 13% is observed between 2.54 and 5.08-cm-long samples in short-cycle experiments with 1.4% H_2 in rich phase at 230˚C and 10% at 325˚C. For 5.08 and 7.62-cm-long samples a difference of 9.5% and 8% is observed at 230 and 325˚C, respectively. The difference between these two samples could possibly be lower if the inlet NO in both samples could be maintained at the same concentration – the concentration of inlet NO in 7.62-cm-long sample was 30 ppm lower than in 5.08-cm-long sample as measured through the bypass (253 ppm vs. 284 ppm). On the other hand, concentration of inlet NO in 2.54-cm-long sample, as measured through bypass, was similar to 5.08-cm-long sample. Variation in inlet concentration of NO is due to the use of different gas cylinders in preparing the simulated exhaust gases. Lower concentration of inlet NO in 7.62-cm-long sample may also be responsible for the higher production of NH_3 and N_2O than what it would otherwise be if inlet NO in 7.62-cm-long sample was at the same concentration as in 2.54 and 5.08-cm-long samples (see Figure 4.31), since less H_2 is consumed with lower inlet NO and production of both NH_3 and N_2O increases with increasing H_2. No significant difference in NO_x conversion efficiency is observed between three samples at 500˚C probably because the NO_x desorption dominates the reduction process making variation in H_2 availability due to back-mixing insignificant (reduction loss due to back-mixing is discussed later in this section).

Increasing H_2 concentration to 3.4% in rich phase results in nearly 100% NO_x conversion in short-cycle experiments at 230 and 325˚C and 30% increase at 500˚C. No significant difference in average cycle NO_x conversion efficiency is observed between 2.54, 5.08 and 7.62-cm-long samples with 3.4% H_2 at a given temperature as seen in Table 4.11. It is not clear why NO_x conversion in 7.62-cm-long sample at 500˚C is 9% lower than in 2.54 and 5.08-cm-long samples. The differences in NO_x profiles and NO_x conversion efficiencies between samples of three different lengths at 230˚C follow the trend observed in short-cycle experiments with 1.4% H_2, in which the longer the sample the better the

performance. However, the differences are within the experimental uncertainty, and thus it is inconclusive to attribute these differences to variation in length.

The intra-catalyst concentration of H_2 measured by SpaciMS at four different axial locations – catalyst inlet, quarter from the inlet, mid-section and exit – provides information on the consumption of H_2 along the length of 2.54, 5.08 and 7.62-cm-long-samples. Figures 4.36 and 4.37 show the profiles of H_2 in short-cycle experiments with 1.4 and 3.4% H_2 in rich phase at 325˚C, respectively. Results obtained at 230 and 500˚C are given in Appendix A (Figures A.6 to A.9). As seen in these figures, consumption of H_2 along the length of 2.54, 5.08 and 7.62-cm-long samples in short-cycle experiments with 1.4 and 3.4% H_2 follows the previously observed trend in Catalyst A: more H_2 is consumed in shorter sample. For example, in short-cycle experiments at 325˚C with 1.4% H_2 in the rich phase, as seen in Figure 4.36, H_2 is completely consumed in the front quarter of the 2.54-cm-long sample; whereas about 23% of H_2 remains in the 5.08 and 14% in 7.62-cm long samples.

Different slopes in catalyst's inlet H_2 profiles suggest different degree of lean/rich front back-mixing which may contribute to significant reductant loss as previously seen in Catalyst A. Steeper slope of inlet H_2 profile in 7.62-cm-long sample suggests that the flow approaches plug flow at higher linear velocity resulting in negligible back-mixing. Also, as seen in Table 4.12 and Figures 4.36 and 4.37, the average concentration of inlet H_2 in short-cycle experiments measured by SpaciMS is different between samples of different lengths. Average inlet concentration of H_2 is calculated by dividing area under H_2 vs. time curve by the duration of the regeneration pulse of 5 s. Variation of inlet H_2 from intended value indicates that some H_2 might be consumed upstream of the catalyst. Consumption of H_2 upstream of the catalyst can be attributed to the oxidation reaction on the metallic surface of the guide tube used for SpaciMS probes and possibly on the surface of stainless steel tubing of the Bench-Flow Reactor. Loss of H_2 upstream of the catalyst decreases with increasing length,

Table 4.12. Average concentration of inlet H_2 as measured by SpaciMS at 325˚C with 1.4% or 3.4% H_2 in rich phase

Concentration / Length	1.4%	3.4%
2.54-cm	1.02%	2.89%
5.08-cm	1.20%	3.22%
7.62-cm	1.25%	3.23%

and inlet concentration of H_2 approaches intended value, which seem to indicate that back-mixing decreases with increasing length or linear velocity.

Short-cycle experiments without NO in the lean phase, similar to those performed on Catalyst A (OSC experiments), were carried out in order to determine Catalyst B's oxygen storage capacity. In addition, OSC experiments with a nitrogen purge of ten seconds between lean and rich (back-mixing experiments) were carried out in order to evaluate the extent of back-mixing. All of H_2 is consumed in OSC experiments with 1.4% H_2 in rich phase at all temperatures; whereas between 45 to 60% is consumed with 3.4% H_2. It is difficult to quantify the amount of H_2 consumed due to lean/rich front mixing from OSC and back-mixing experiments since significant stored oxygen and possibly H_2 may also desorb during neutral purge. Nevertheless, the trends of H_2 consumption in short-cycle experiments indicate different degree of lean/rich front back-mixing depending on catalyst's length or linear velocity, which in turn affects catalyst's NO_x conversion efficiency. Since the flow rates used in Catalyst B's evaluation are similar to those in Catalyst A, and the discrepancies observed in NO_x conversion between samples of three different lengths closely match the ones observed in Catalyst A, it is safe to assume that differences in NO_x conversion are solely due to loss of H_2 as a result of back-mixing.

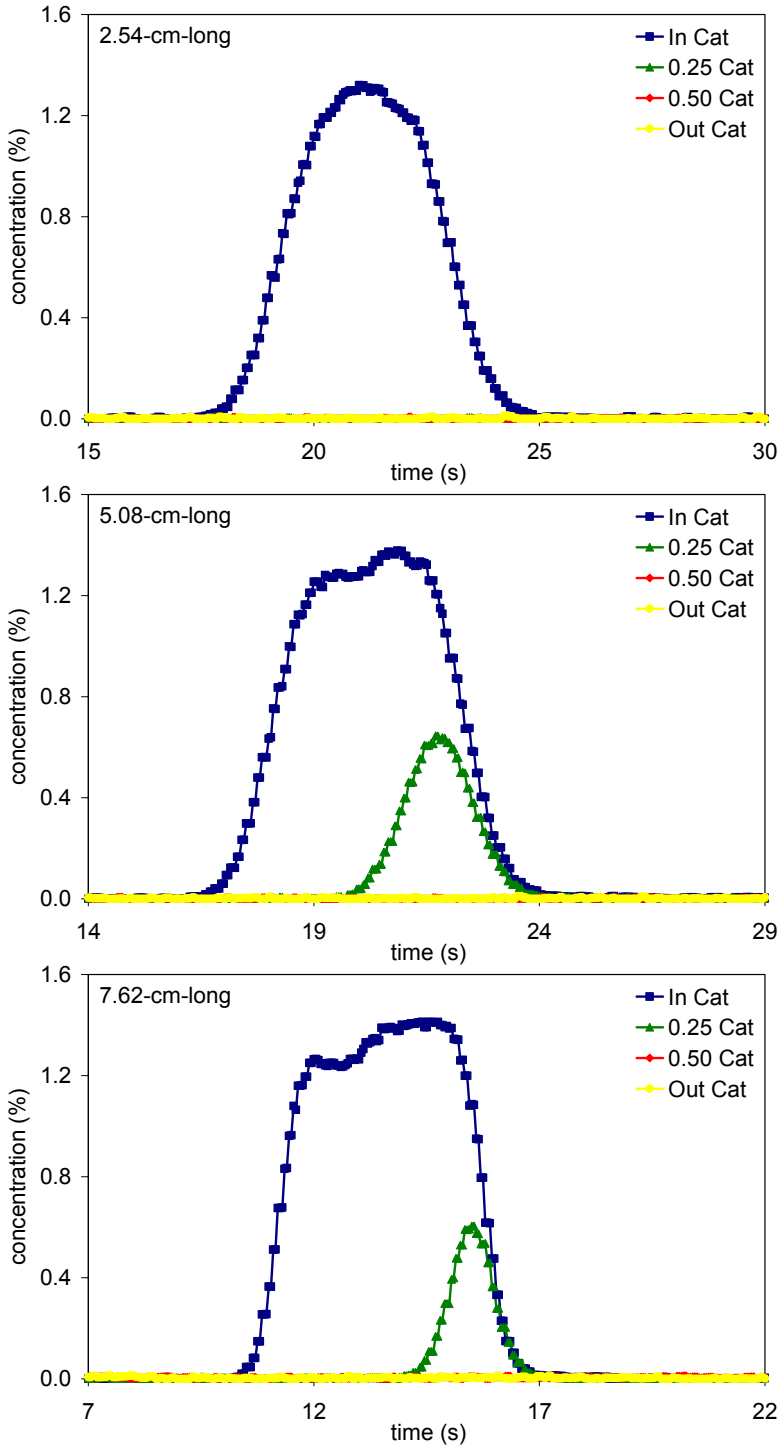

Figure 4.36. Catalyst B's H_2 consumption trends in 2.54, 5.08 and 7.62-cm-long samples in short-cycle experiments with 1.4% H_2 in rich phase at 325˚C

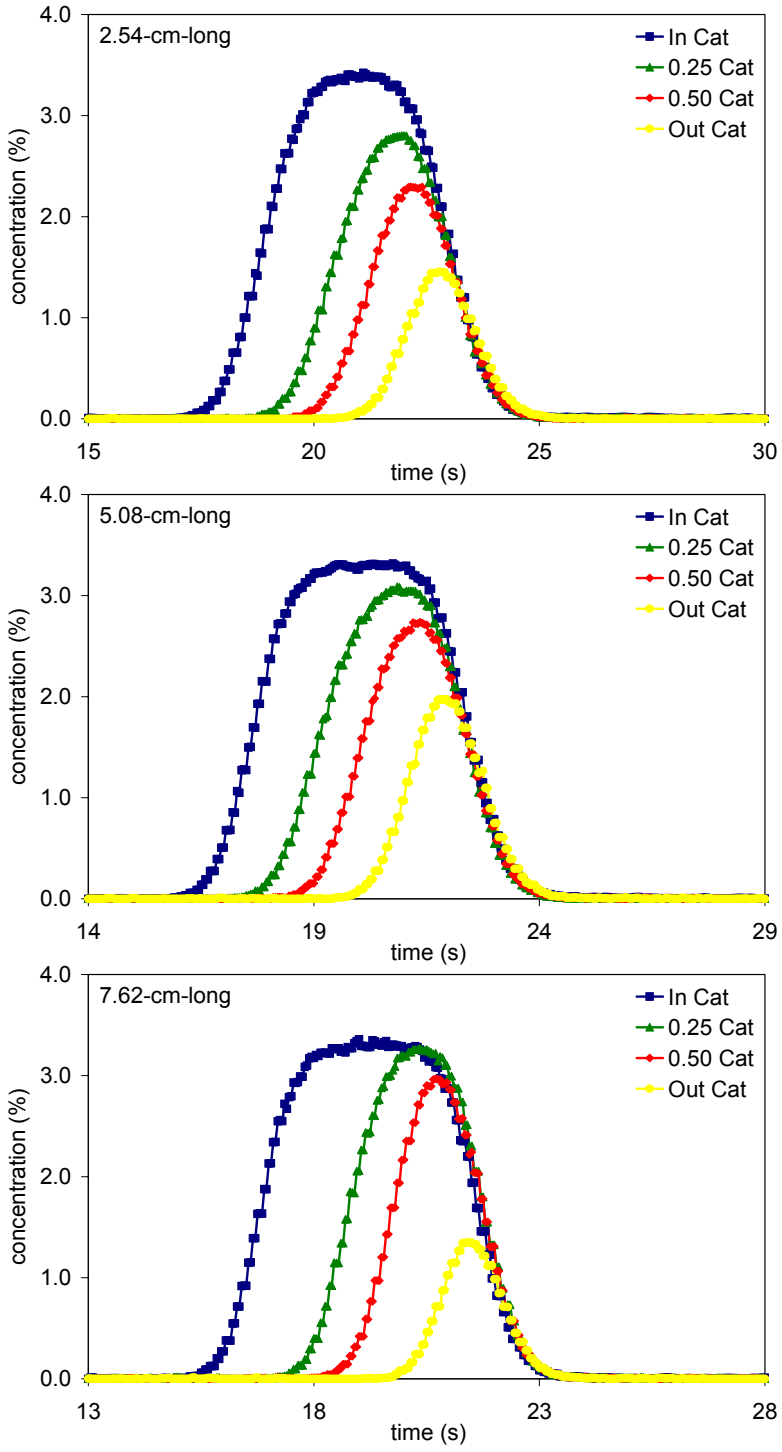

Figure 4.37. Catalyst B's H_2 consumption trends in 2.54, 5.08 and 7.62-cm-long samples in short-cycle experiments with 3.4% H_2 in rich phase at 325˚C

CHAPTER 5

CONCLUSIONS

The effect of monolith length on the NO_x performance of two different Lean NO_x Traps was investigated in the present study. Samples of three different lengths within each LNT were evaluated with long and short-cycle experiments at a fixed gas hourly space velocity, and results were compared between samples of different lengths. No significant difference in performance was observed in long and short-cycle experiments with full regeneration. On a contrary, significant difference is observed in short-cycle experiments with partial regeneration: the longer the sample the better the performance. A difference as large as 20% in NO_x conversion efficiency was observed between 2.54 and 7.62-cm-long samples with worse performance in shorter sample.

Reductant (H_2) consumption trends during short-cycle experiments indicate different degrees of lean and rich front back-mixing for samples of different sizes. Higher back-mixing results in a higher H_2 loss via its oxidation by O_2 and lesser H_2 availability for reducing stored NO_x, which in turn affects catalyst's performance when regeneration is limited by amount of H_2 available. In 2.54-cm-long sample as much as 35% of H_2 is consumed from the catalytic oxidation at the lean/rich interface resulting in a reduction of 15% in NO_x conversion in short-cycle experiments with partial regeneration.

Back-mixing is attributed to the axial diffusion of chemical species in the gas mixture which occurs to a greater extent in the mixtures moving with the lower linear velocity; therefore, the observed "length effect" is the result of greater axial diffusion in slower moving gases (at a fixed gas hourly space velocity and catalyst diameter, gas velocity or flow rate decreases with decreasing sample length). The dimensionless group D_a/U_zL where D_a is the axial dispersion coefficient, U_z is the molar average velocity and L is the length of the catalyst,

referred to as the vessel dispersion number, is the parameter, which measures the extent of axial mixing. With increasing length and linear velocity, D_a/U_zL decreases and back-mixing becomes negligible; thus, the flow approaches plug flow and the sample's performance is no longer affected by the sample's length or the gas velocity.

REFERENCES

1. R. E. Hayes and S. T. Kolaczkowski, Introduction to Catalytic Combustion, Gordon and Breach Science Publishers (1997)
2. Masahiko Takeuchi and Shinichi Matsumoto, Topics in Catalysis, 28 (2004)
3. L. Liotta, A. Macaluso, G. Arena, M. Livi, G. Centi and G. Deganello, Catalysis Today, 75, 439 (2002)
4. H. Ohtsuka, Applied Catalysis B: Environmental, 33, 325 (2001)
5. N. Miyoshi, S. Matsumoto, K. Katoh, T. Tanaka, J. Harada, N. Takahashi, K. Yokota, M. Sugiura, K. Kasahara, SAE Technical Paper Series 950809 (1995)
6. N. Takahashi, H. Shinjoh, T. Iijima, T. Suzuki, K. Yamazaki, K. Yokota, H. Suzuki, N. Miyoshi, S. Matsumote, T. Tanizawa, T. Tanaka, S. Tateishi, K. Kasahara, Catalysis Today, 27, 63 (1996)
7. L. Olsson, H. Persson, E. Fridell, M. Skoglundh and B. Andersson, J. Phys. Chem. B, 105 (2001)
8. M. Takeuchi and S. Matsumoto, Topics in Catalysis, 28 (2004)
9. N. W. Cant and M. J. Patterson, Catalysis Today, 73, 271-278 (2002)
10. S. Salasc, M. Skoglundh and E. Fridell, Applied Catalysis B: Environmental, 36, 145-160, (2002)
11. W. S. Epling, L. E. Campbell, A. Yezerets, N. W. Currier and J. E. Parks, Catalysis Reviews, 46, 2, 163-245 (2004)
12. I. Nova, L. Castoldi, L. Lietti, E. Tronconi and P. Forzatti, Catal. Today, 75, 431 (2002)
13. I. Nova, L. Castoldi, F. Prinetto, V. Dal Santc, L. Lietti, E. Tronconi, P. Forzatti, G. Ghiotti, R. Psaro, and S. Recchia, Topics in Catalysis, 30/31 (2004)
14. Y. Su and M. Amiridis, Catalysis Today, 96, 31-41 (2004)
15. L. Lietti, P. Forzatti, I. Nova and E. Tronconi, J. Catalysis, 204, 175-191 (2001)

16. B. West, S. Huff, J. Parks, S. Lewis, J. Choi, W. Partridge and J. Storey, SAE Technical Paper Series 2004-01-3023 (2004)
17. I. Nova, L. Lietti, L. Castoldi, E. Tronconi and P. Forzatti, Journal of Catalysis, 239, 244-254 (2006)
18. R. Muncrief, K. Coym and M. Harold, 18th North American Meeting of the North American Catalysis Society, Cancun, Mexico (2003)
19. Josh Pihl, Master's Thesis, University of Wisconsin (2005)
20. H. Kim, Master's Thesis, University of Tennessee (2006)
21. J. Hoard and S. Daw, 8th DOE Cross-Cut Lean Exhaust Emissions Reductions Simulations (CLEERS), Detroit, MI (2005)
22. W. Partridge, J. Storey, S. Lewis, R. Smithwick, G. DeVault, M. Cunnigham, N. Currier, T. Yohushonis, SAE Technical Paper Series 2000-01-2952 (2000)
23. http://www.cleers.org
24. A. Knafl, S. Busch, M. Han, S. Bohac, D. Assanis, P. Szymkowicz, R. Blint, SAE Technical Paper Series 2006-01-0209 (2006)
25. H. S. Fogler, Elements of Chemical Reaction Engineering, Pearson Education (2006)
26. J. R. Theis, J. A. Ura, J. J. Li, G. G. Surnilla, J. M. Roth and C. T. Goralski Jr., SAE Technical Paper Series 2003-01-1159 (2003)
27. L. Olsson, B. Westerberg, H. Persson, E. Fridell, M. Skoglundh and B. Andersson, J. Phys. Chem. B, 103, 10433 (1999)
28. L. Cumaranatunge, S. Mulla, A. Yezerets, N. Currier, W. Delgass and F. Ribeiro, Journal of Catalysis, 246, 29-34 (2007)
29. J. Choi, W. Partridge, W. Epling, N. Currier and T. Yonushonis, Catalysis Today, 114, 102-111 (2006)
30. W. Epling, A. Yezerets and N. Currier, Catalysis Letter, 110 (2006)
31. T. Collier, C. Burgess and M. Brogan, SAE Technical Paper Series 2004-01-0592 (2004)
32. S. Poulston and R. Rajaram, Catalysis Today, 81, 603-610 (2003)

33. K. Nakatani, S. Hirota, S. Takeshima, K. Itoh, T. Tanaka and K. Dohmae, SAE Technical Paper Series 2002-01-0957 (2002)
34. E. Fridell, H. Persson, L. Olsson, B. Westerberg, A. Amberntsson and M. Skoglundh, Topics in Catalysis, 16/17 (2001)
35. E. Fridell, H. Persson, B. Westerberg, L. Olsson and M. Skoglundh, Catalysis Letters, 66, 71-74 (2000)
36. H. Mahzoul, J. Brilhac and P. Gilot, Applied Catalysis B: Environmental, 20, 47-55 (1999)

APPENDIX

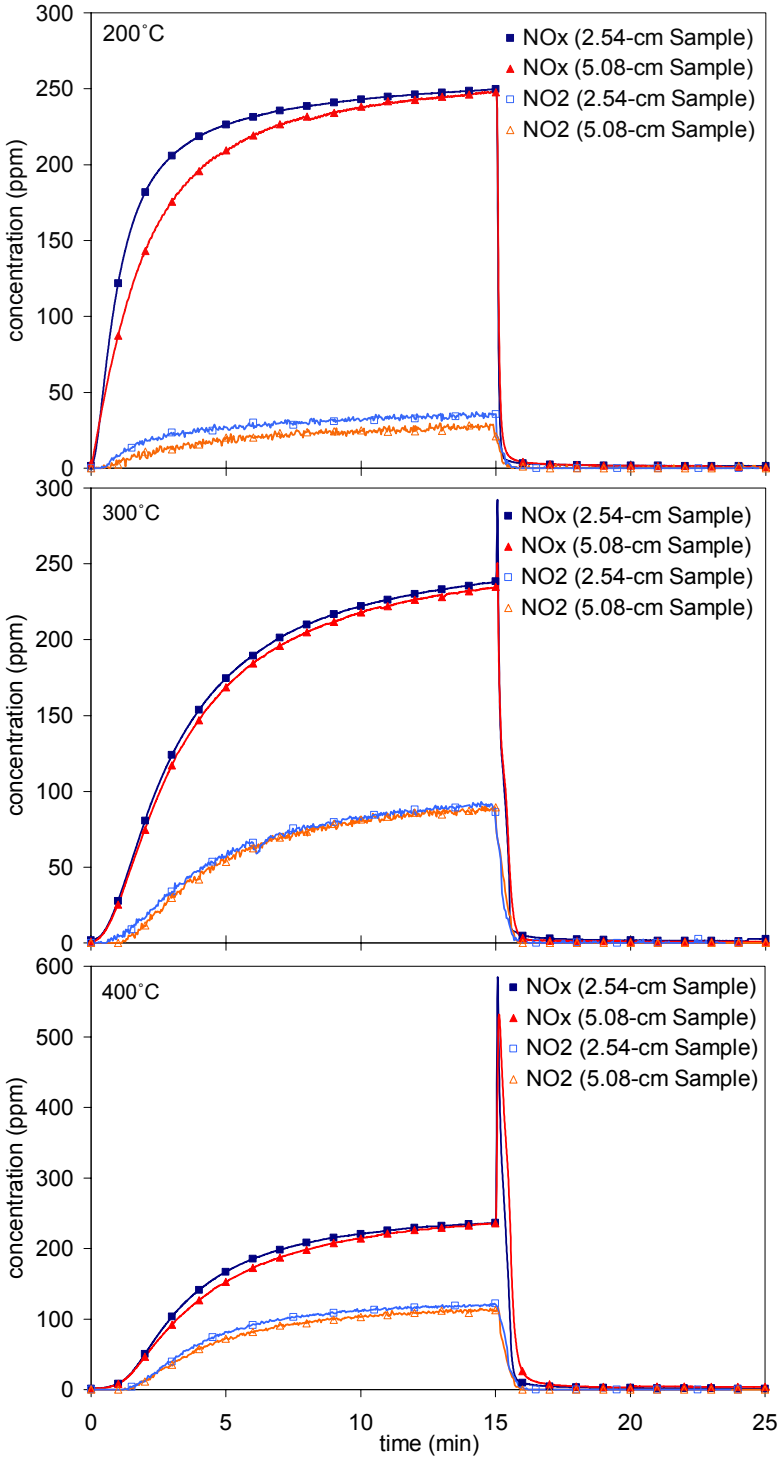

Figure A.1. Catalyst A's outlet concentrations of NO_2 and NO_x in long-cycle experiments with 0.5% H_2 during rich phase at 200, 300 and 400˚C

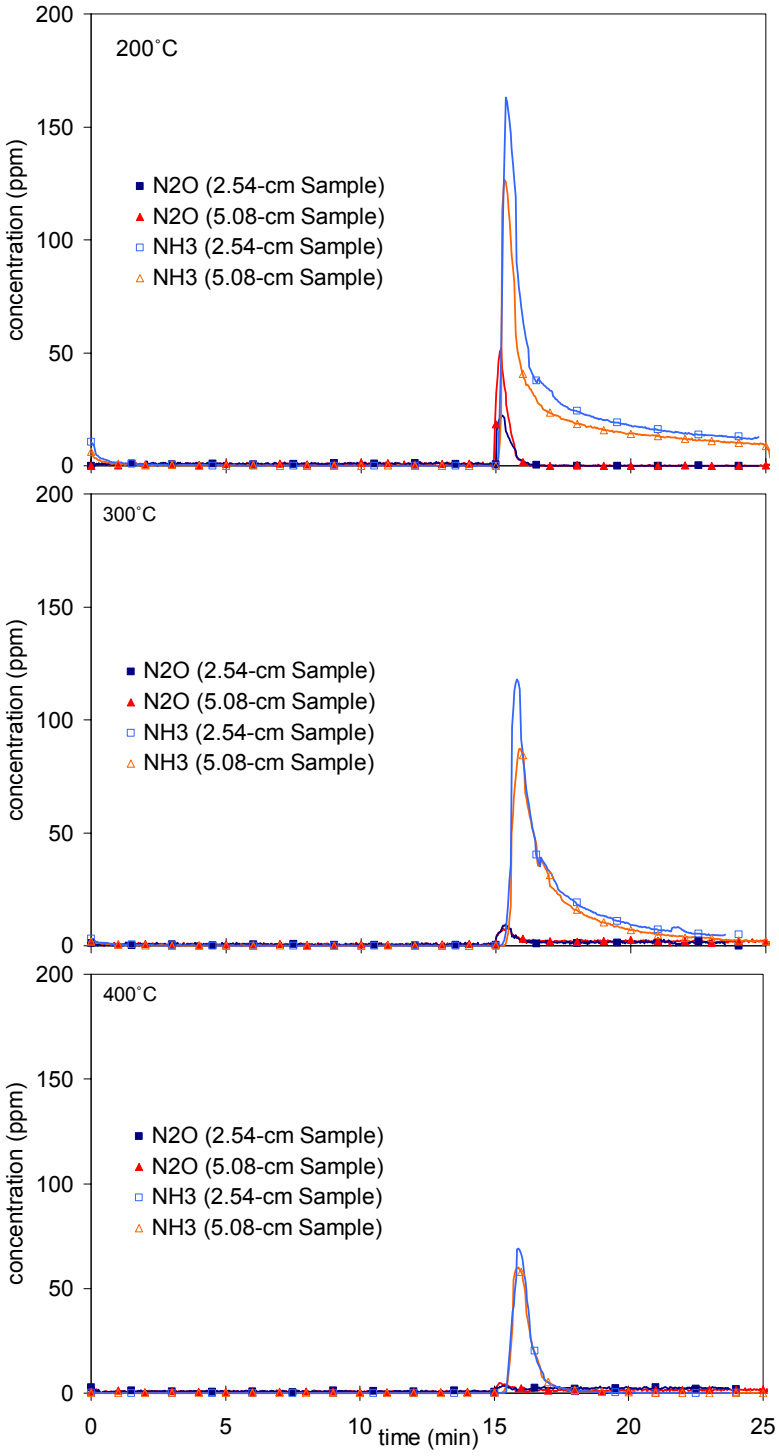

Figure A.2. Catalyst A's outlet concentrations of N_2O and NH_3 in long-cycle experiments operating with 0.5% H_2 during rich phase at 200, 300 and 400˚C

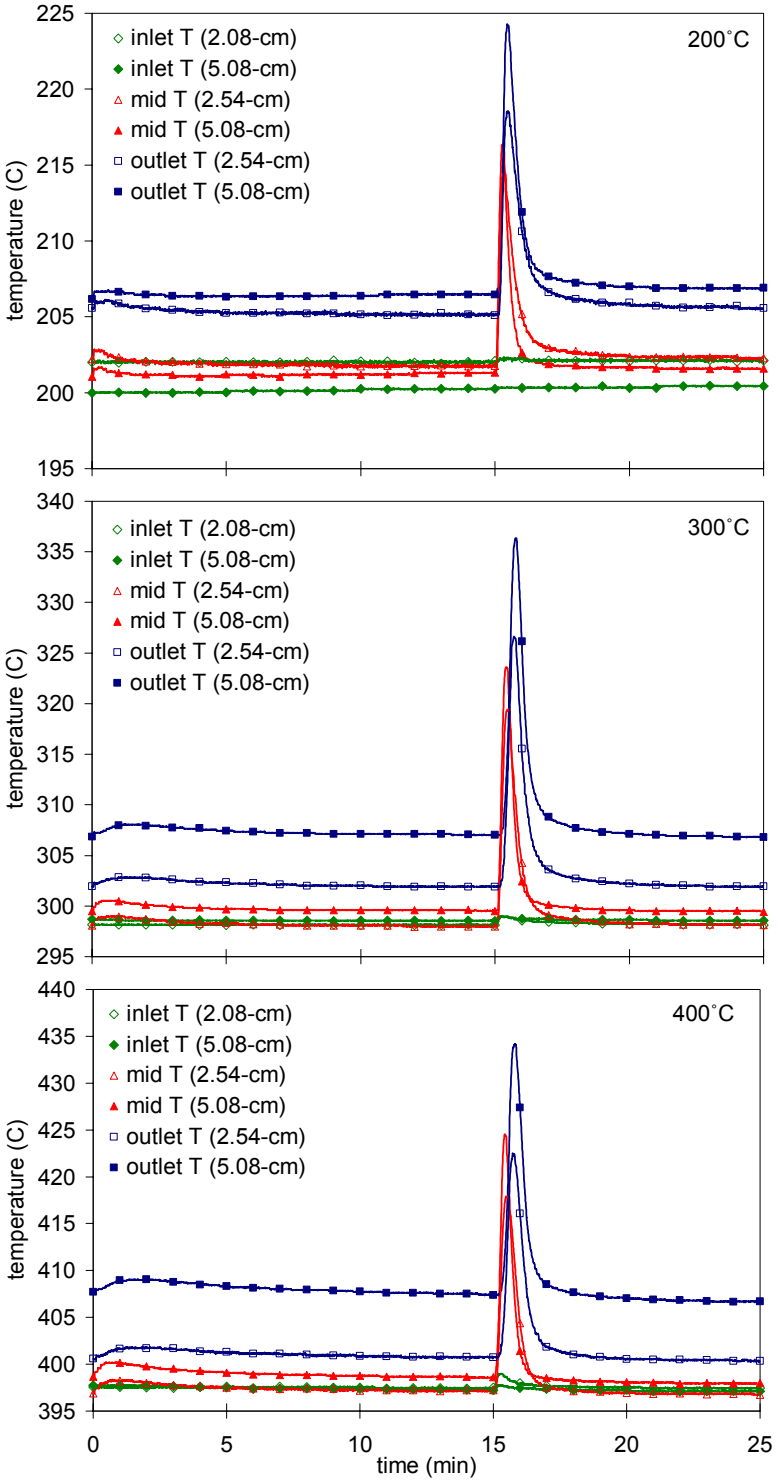

Figure A.3. Catalyst A's temperature profiles in long-cycle experiments with 0.5% H_2 during rich phase at 200, 300 and 400˚C

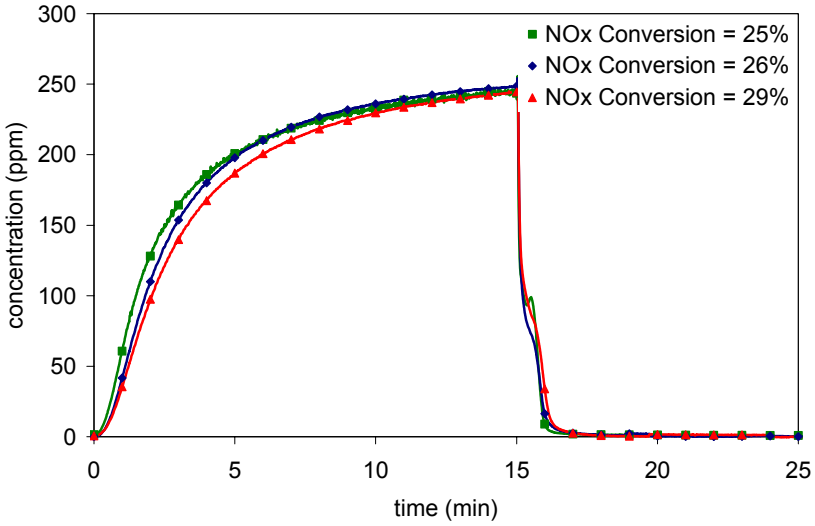

Figure A.4. Catalyst A's outlet concentrations of NO_x for 2.54-cm-long samples in long-cycle baseline experiments with 0.2% H_2 in rich phase at 300˚C and 30,000 h^{-1} space velocity (sample-to-sample variation)

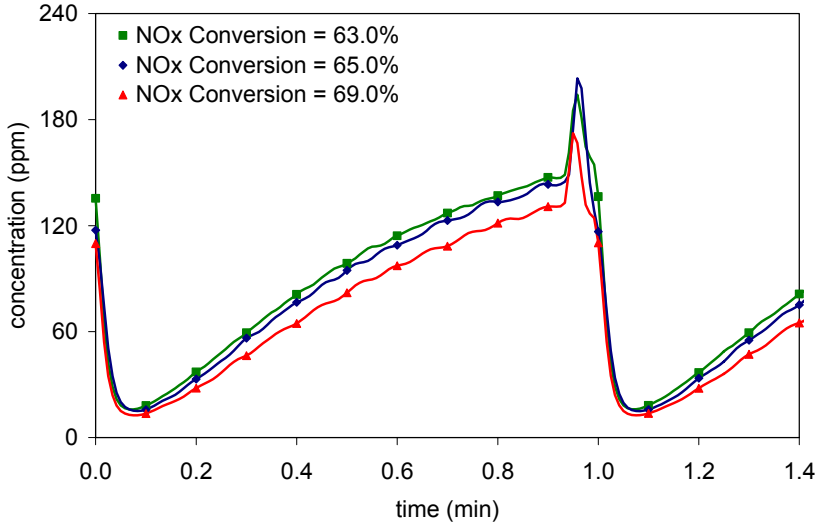

Figure A.5. Catalyst A's outlet concentrations of NO_x for 2.54-cm-long samples in short-cycle baseline experiments with 1.0% H_2 in rich phase at 300˚C and 30,000 h^{-1} space velocity (sample-to-sample variation)

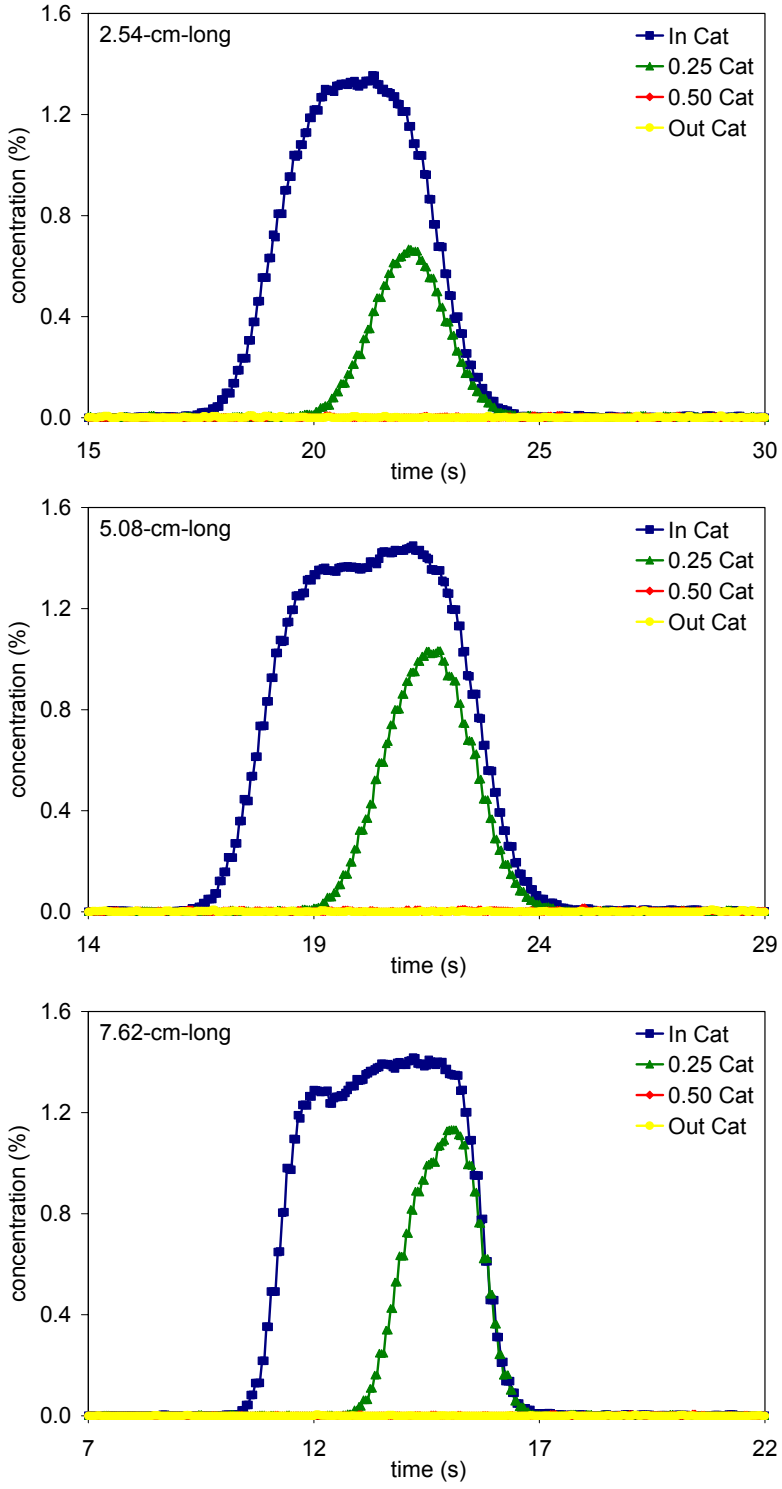

Figure A.6. Catalyst B's H_2 consumption trends in 2.54, 5.08 and 7.62-cm-long samples in short-cycle experiments with 1.4% H_2 in rich phase at 230˚C

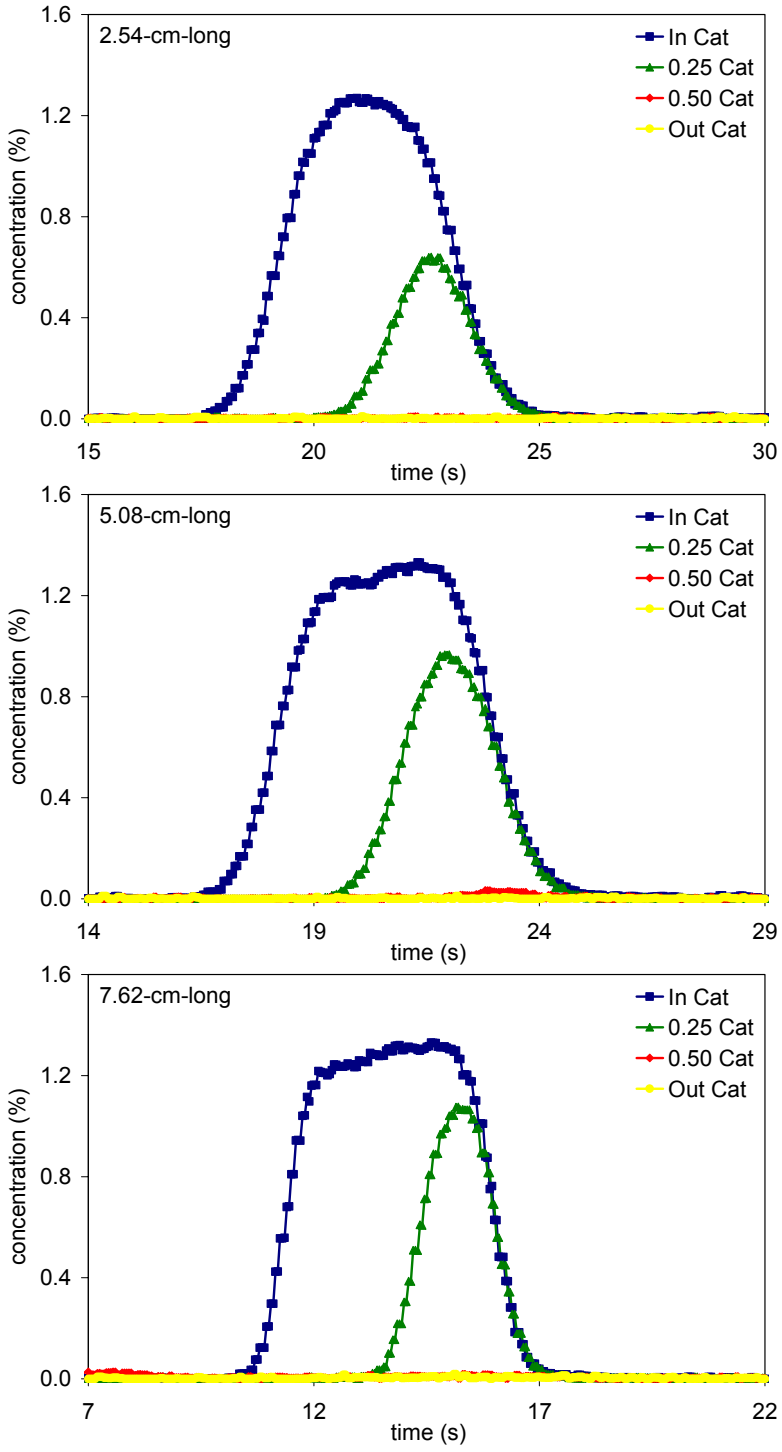

Figure A.7. Catalyst B's H_2 consumption trends in 2.54, 5.08 and 7.62-cm-long samples in short-cycle experiments with 1.4% H_2 in rich phase at 500˚C

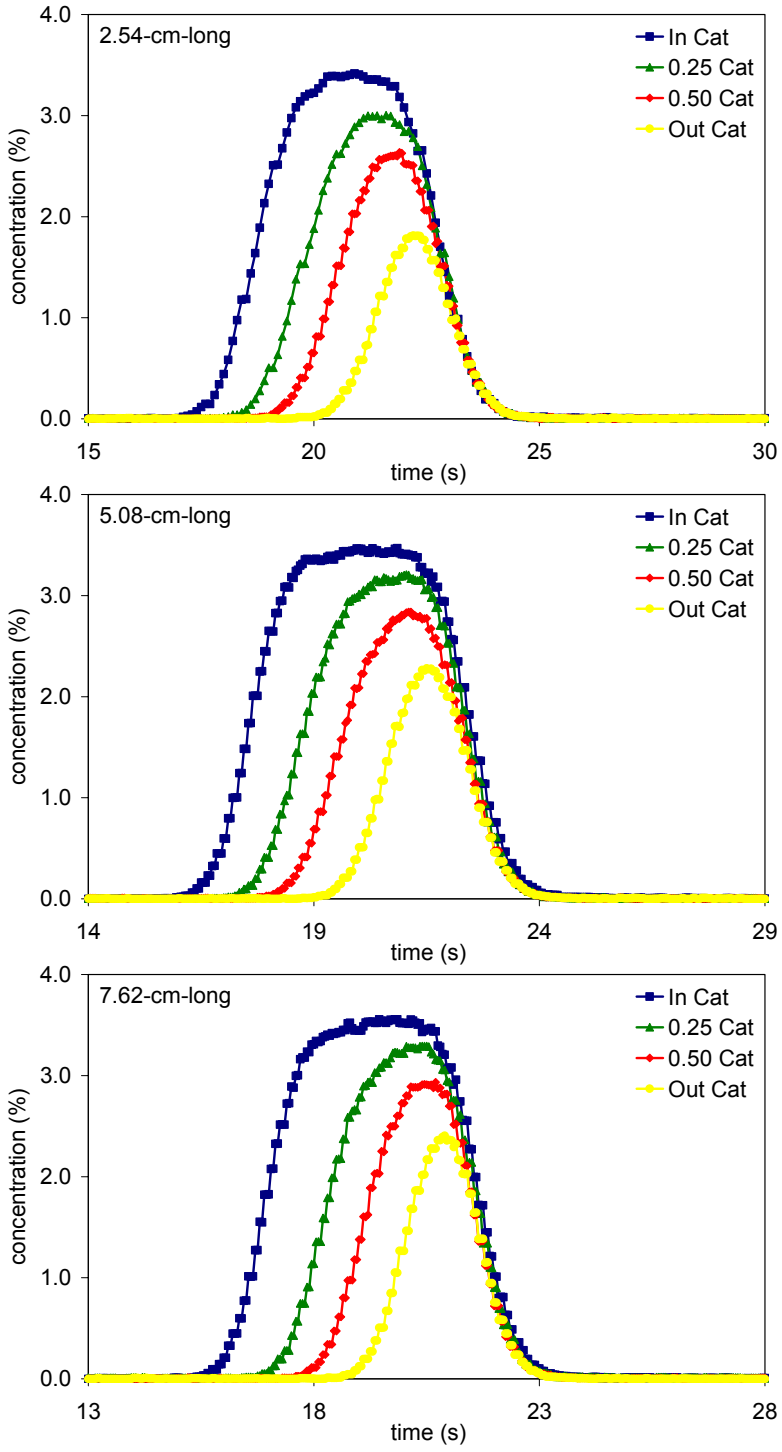

Figure A.8. Catalyst B's H_2 consumption trends in 2.54, 5.08 and 7.62-cm-long samples in short-cycle experiments with 3.4% H_2 in rich phase at 230˚C

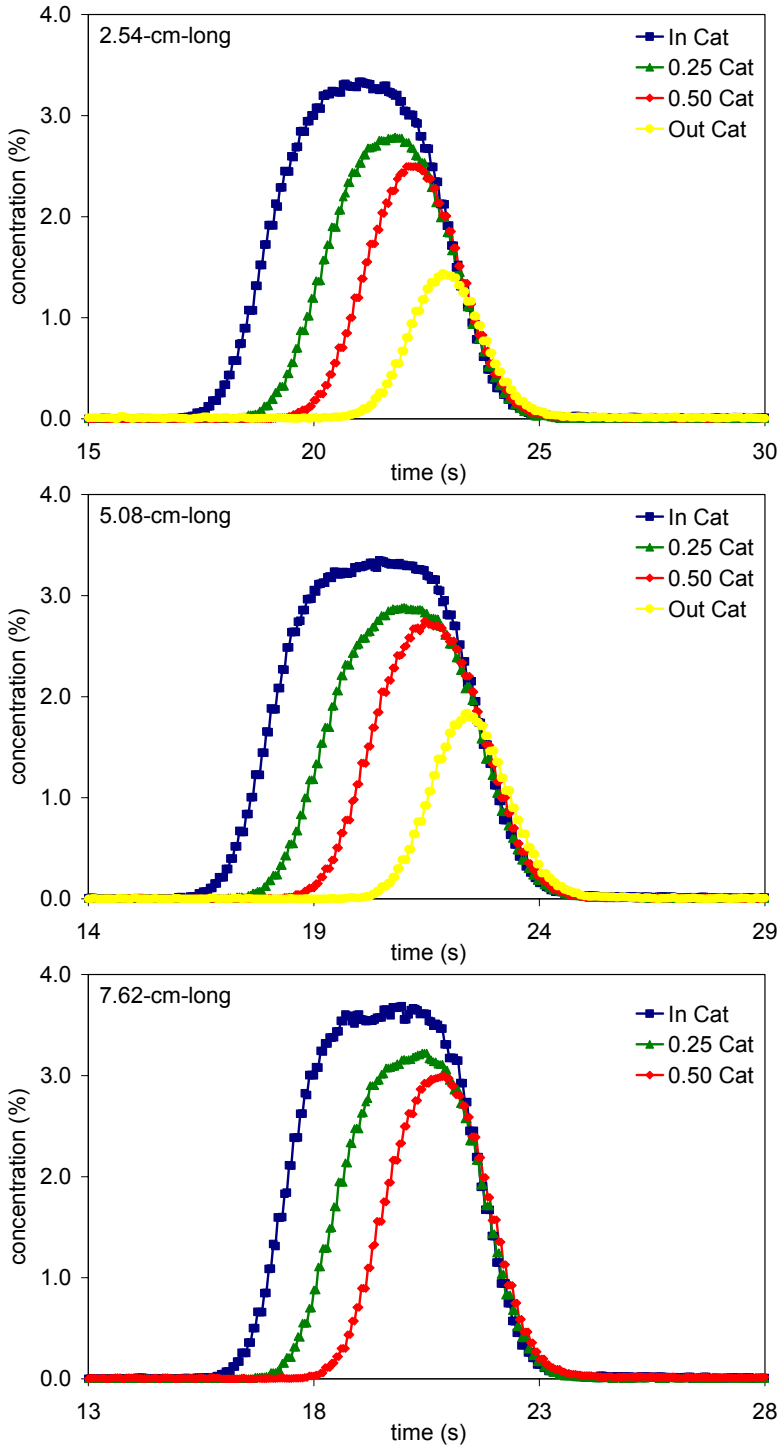

Figure A.9. Catalyst B's H_2 consumption trends in 2.54, 5.08 and 7.62-cm-long samples in short-cycle experiments with 3.4% H_2 in rich phase at 500˚C

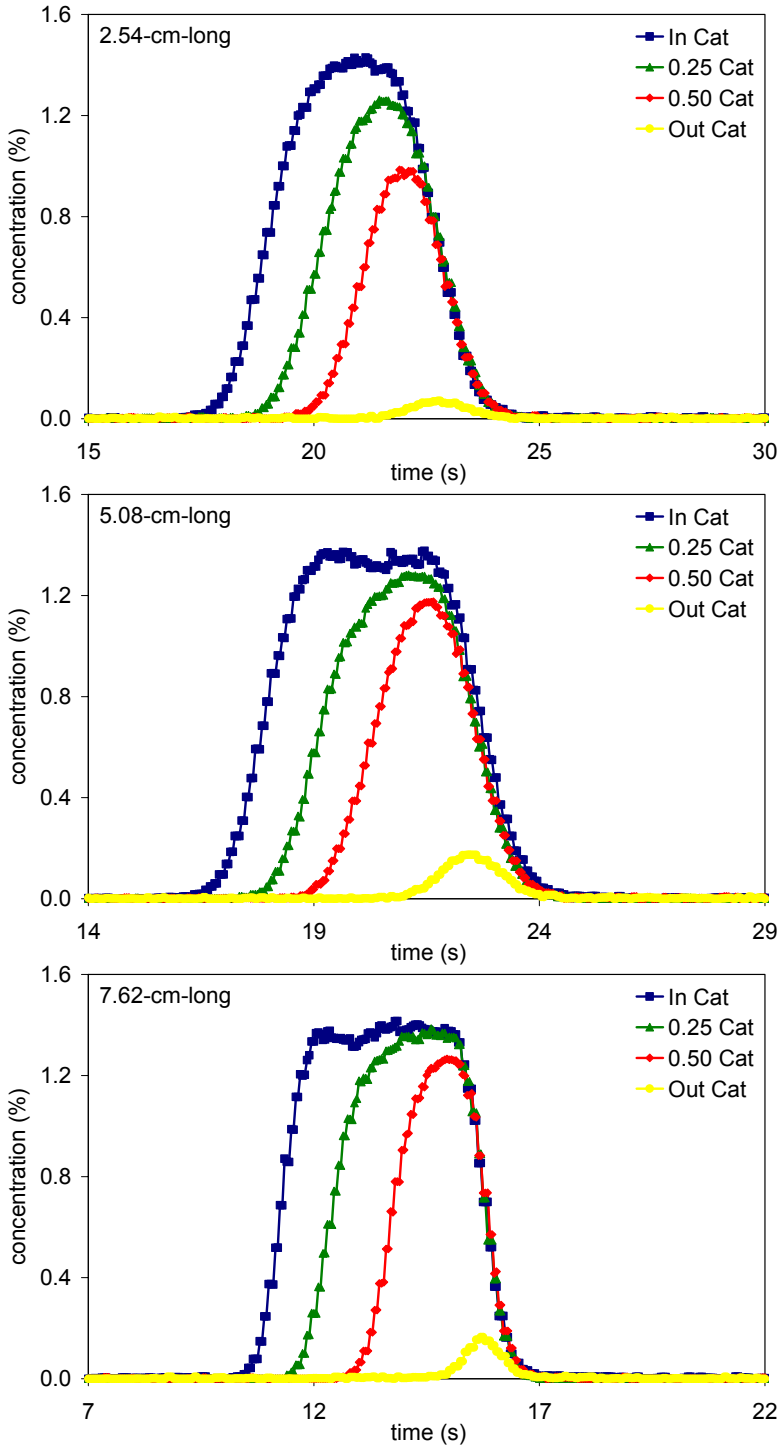

Figure A.10. Catalyst B's H_2 consumption trends in 2.54, 5.08 and 7.62-cm-long samples in oxygen storage (without NO during lean phase) experiments with 1.4% H_2 in rich phase at 230˚C

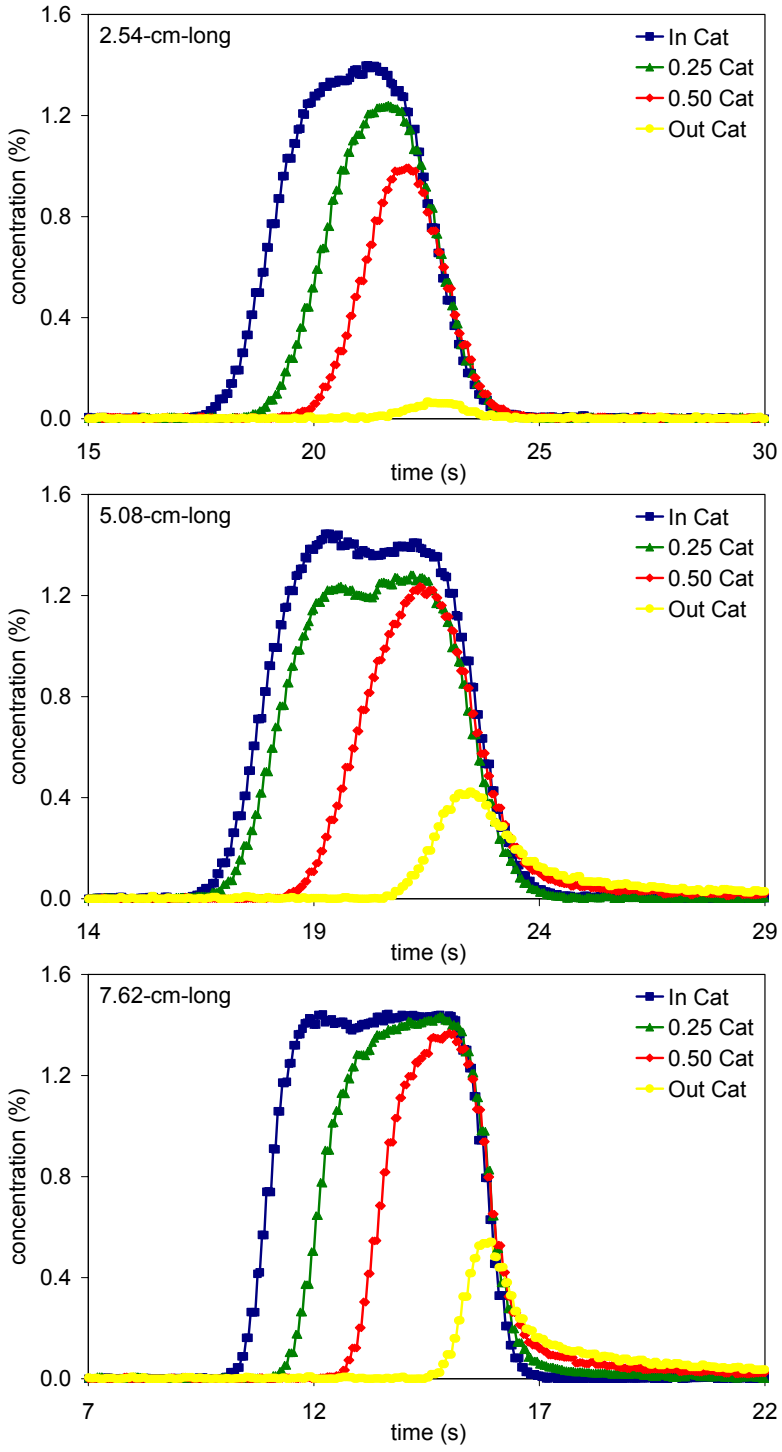

Figure A.11. Catalyst B's H_2 consumption trends in 2.54, 5.08 and 7.62-cm-long samples in back-mixing (OSC experiments with 10s nitrogen purge) short-cycle experiments with 1.4% H_2 in rich phase at 230˚C

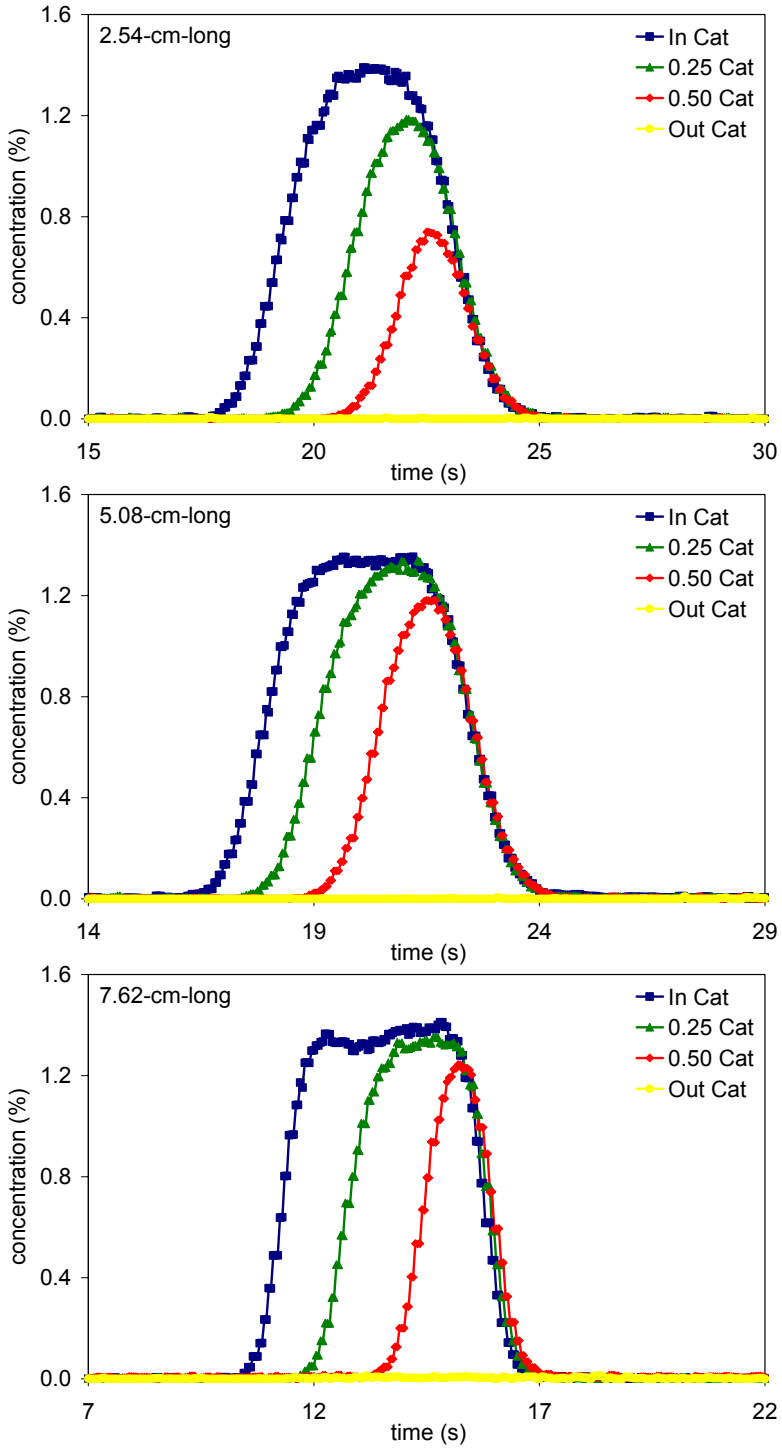

Figure A.12. Catalyst B's H_2 consumption trends in 2.54, 5.08 and 7.62-cm-long samples in oxygen storage (without NO during lean phase) experiments with 1.4% H_2 in rich phase at 325˚C

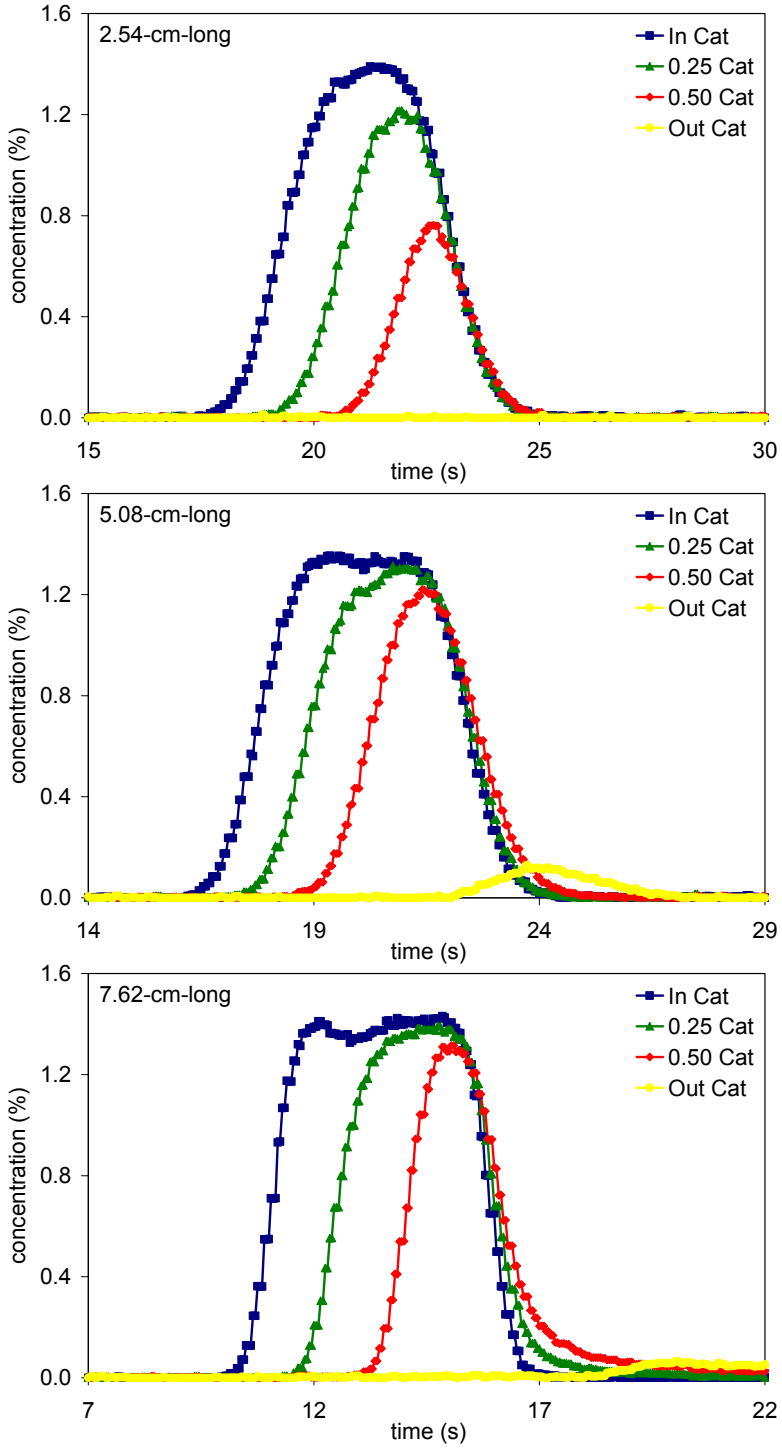

Figure A.13. Catalyst B's H_2 consumption trends in 2.54, 5.08 and 7.62-cm-long samples in back-mixing (OSC experiments with 10s nitrogen purge) short-cycle experiments with 1.4% H_2 in rich phase at 325°C

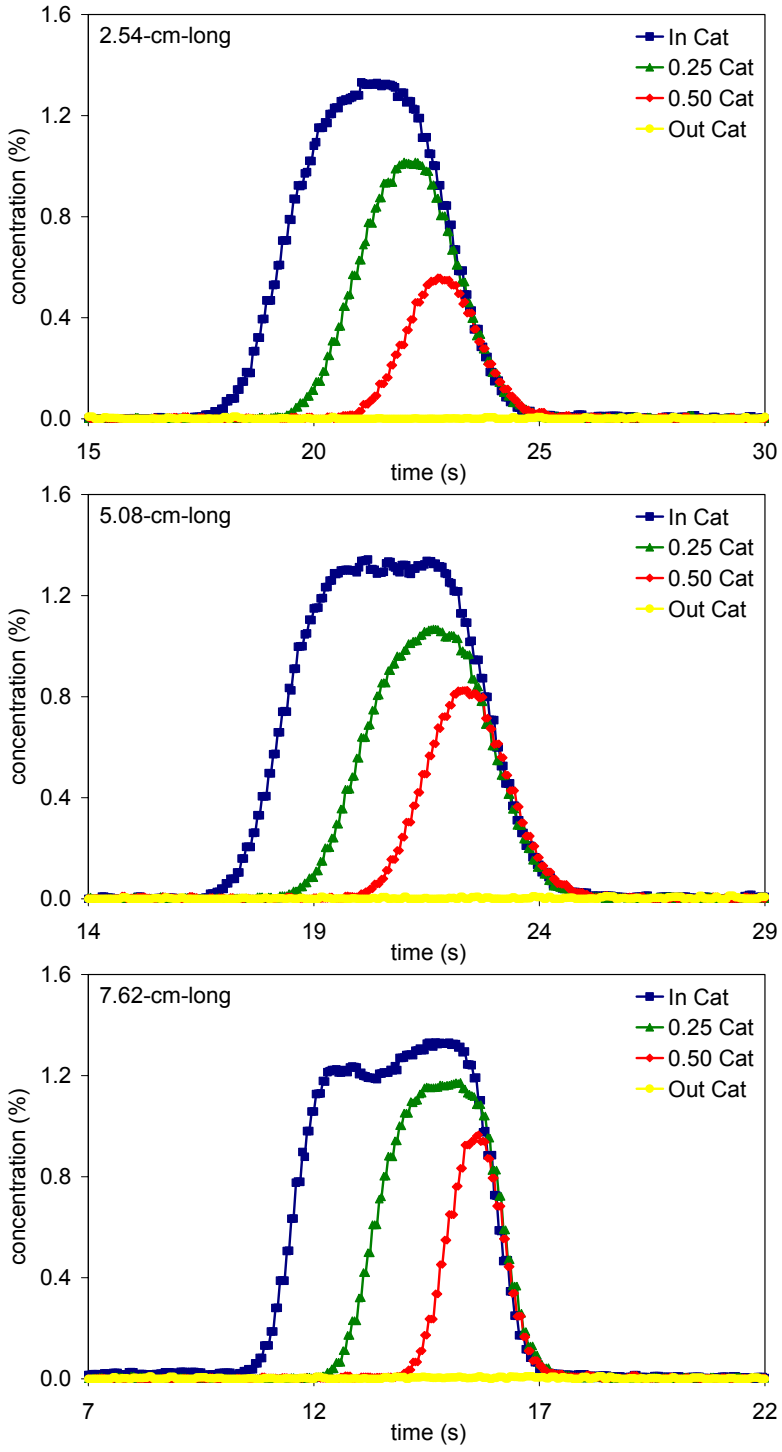

Figure A.14. Catalyst B's H_2 consumption trends in 2.54, 5.08 and 7.62-cm-long samples in oxygen storage (without NO during lean phase) experiments with 1.4% H_2 in rich phase at 500˚C

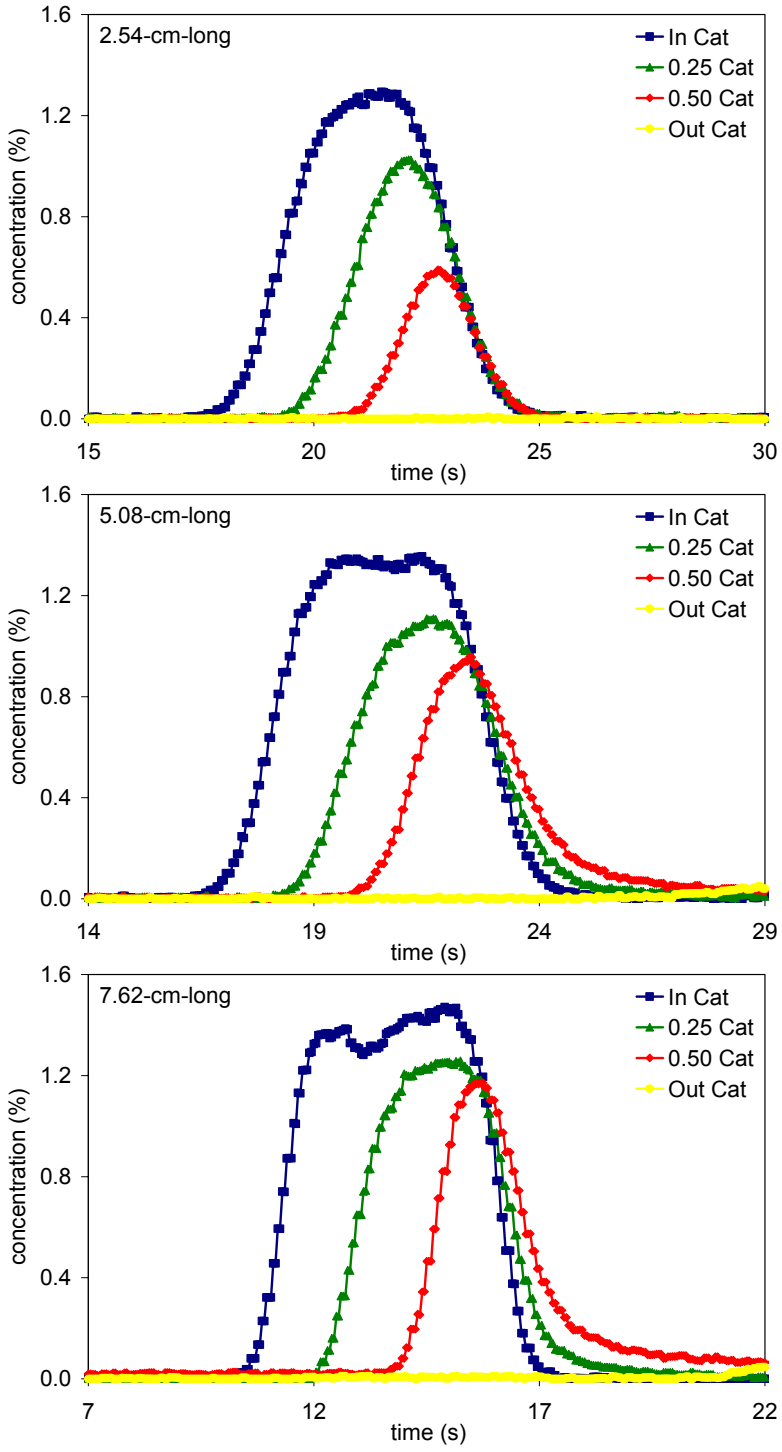

Figure A.15. Catalyst B's H_2 consumption trends in 2.54, 5.08 and 7.62-cm-long samples in back-mixing (OSC experiments with 10s nitrogen purge) short-cycle experiments with 1.4% H_2 in rich phase at 500˚C

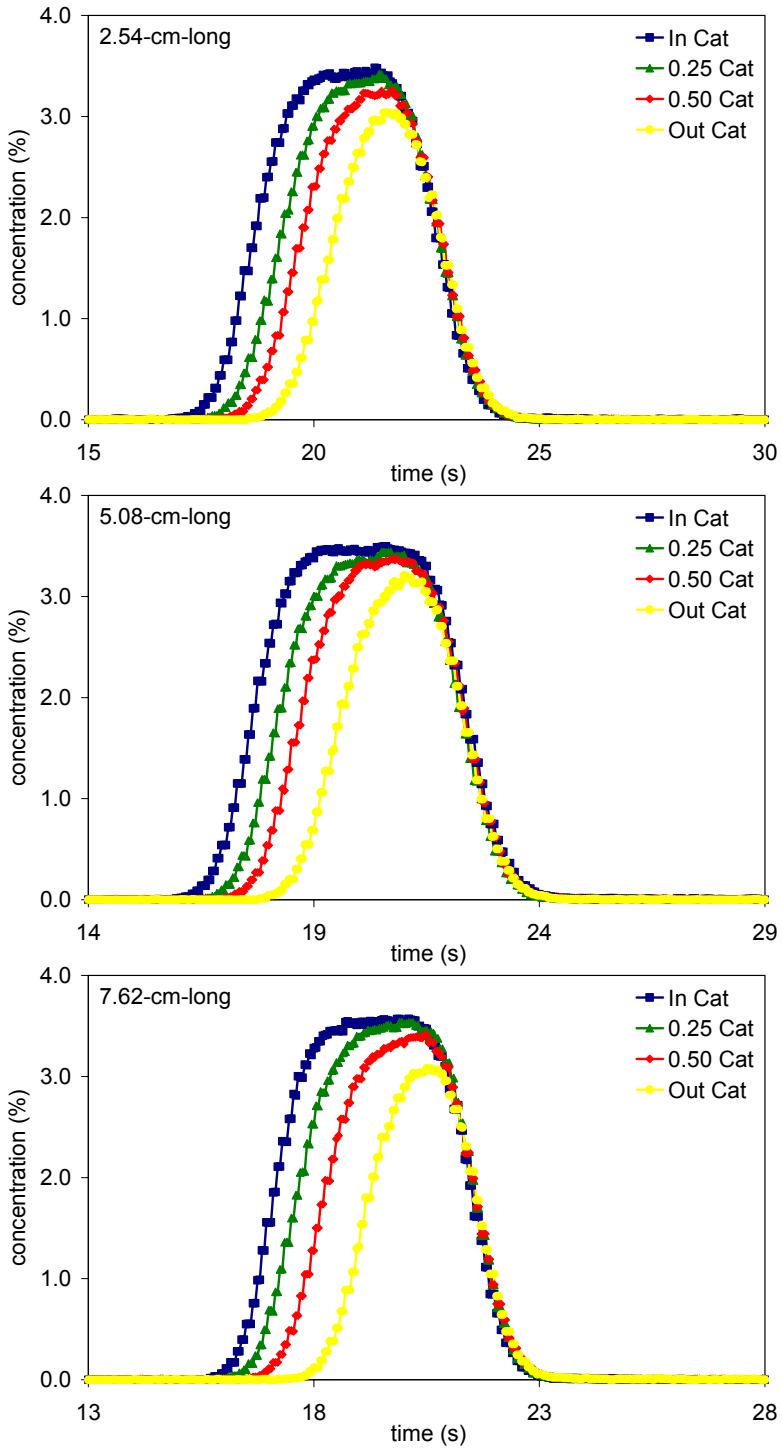

Figure A.16. Catalyst B's H_2 consumption trends in 2.54, 5.08 and 7.62-cm-long samples in oxygen storage (without NO during lean phase) experiments with 3.4% H_2 in rich phase at 230˚C

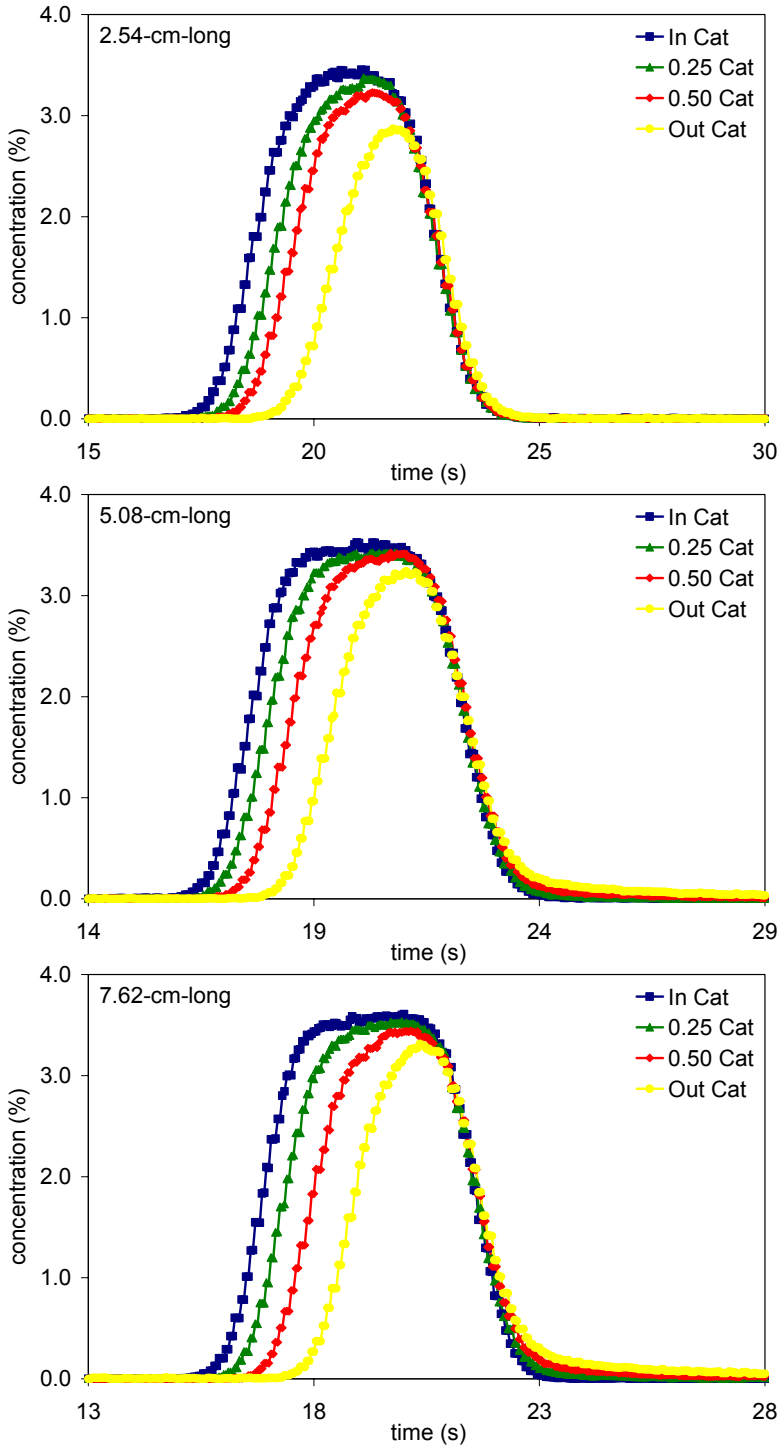

Figure A.17. Catalyst B's H_2 consumption trends in 2.54, 5.08 and 7.62-cm-long samples in back-mixing (OSC experiments with 10s nitrogen purge) short-cycle experiments with 3.4% H_2 in rich phase at 230˚C

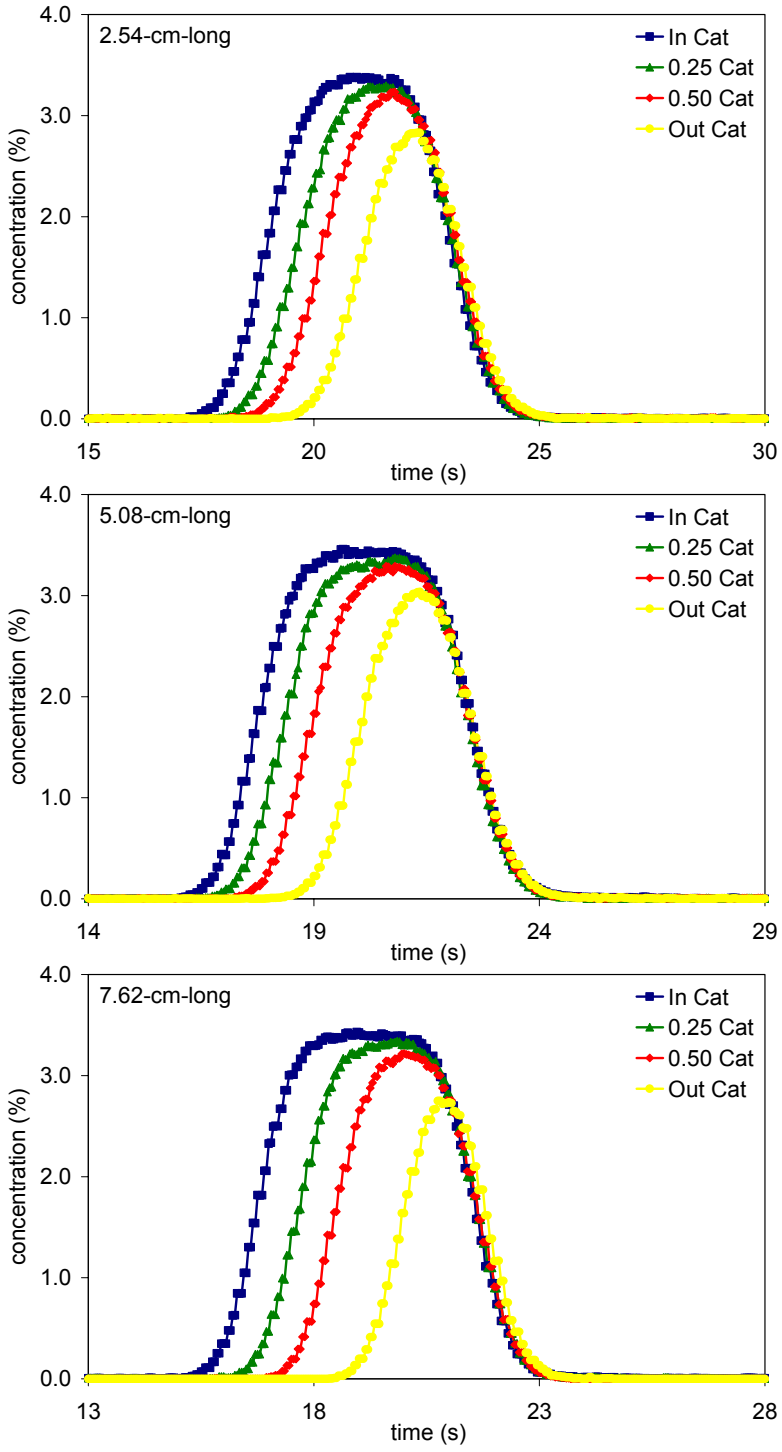

Figure A.18. Catalyst B's H_2 consumption trends in 2.54, 5.08 and 7.62-cm-long samples in oxygen storage (without NO during lean phase) experiments with 3.4% H_2 in rich phase at 325˚C

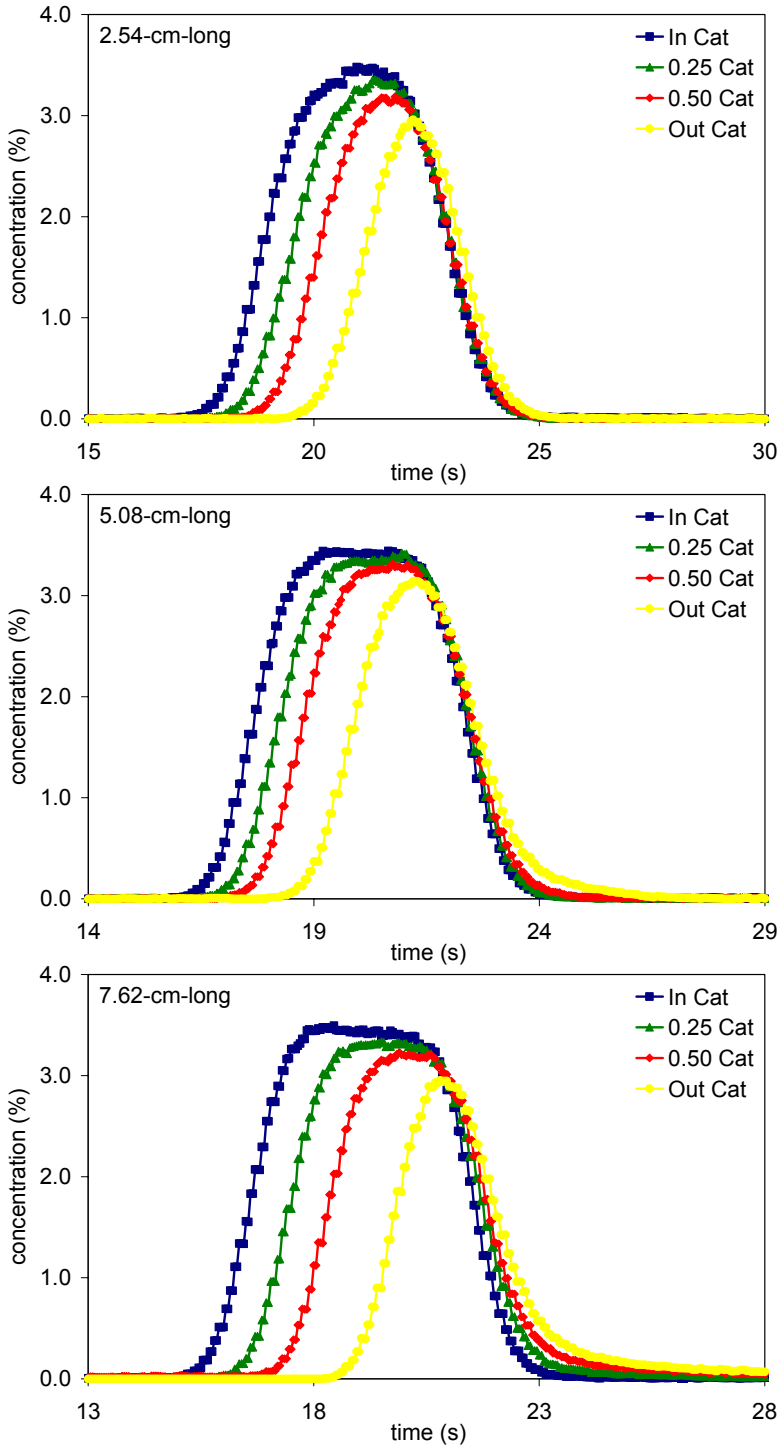

Figure A.19. Catalyst B's H_2 consumption trends in 2.54, 5.08 and 7.62-cm-long samples in back-mixing (OSC experiments with 10s nitrogen purge) short-cycle experiments with 3.4% H_2 in rich phase at 325˚C

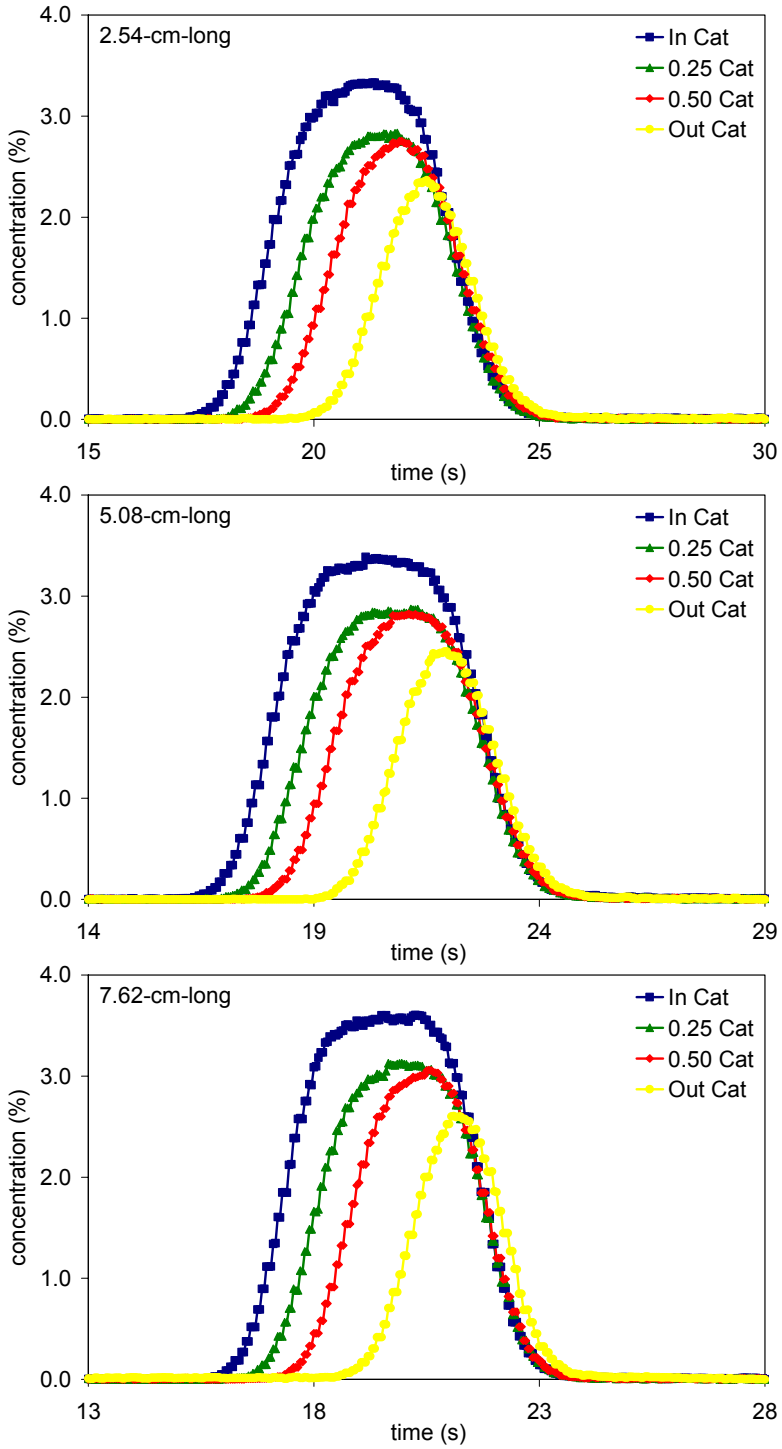

Figure A.20. Catalyst B's H_2 consumption trends in 2.54, 5.08 and 7.62-cm-long samples in oxygen storage (without NO during lean phase) experiments with 3.4% H_2 in rich phase at 500˚C

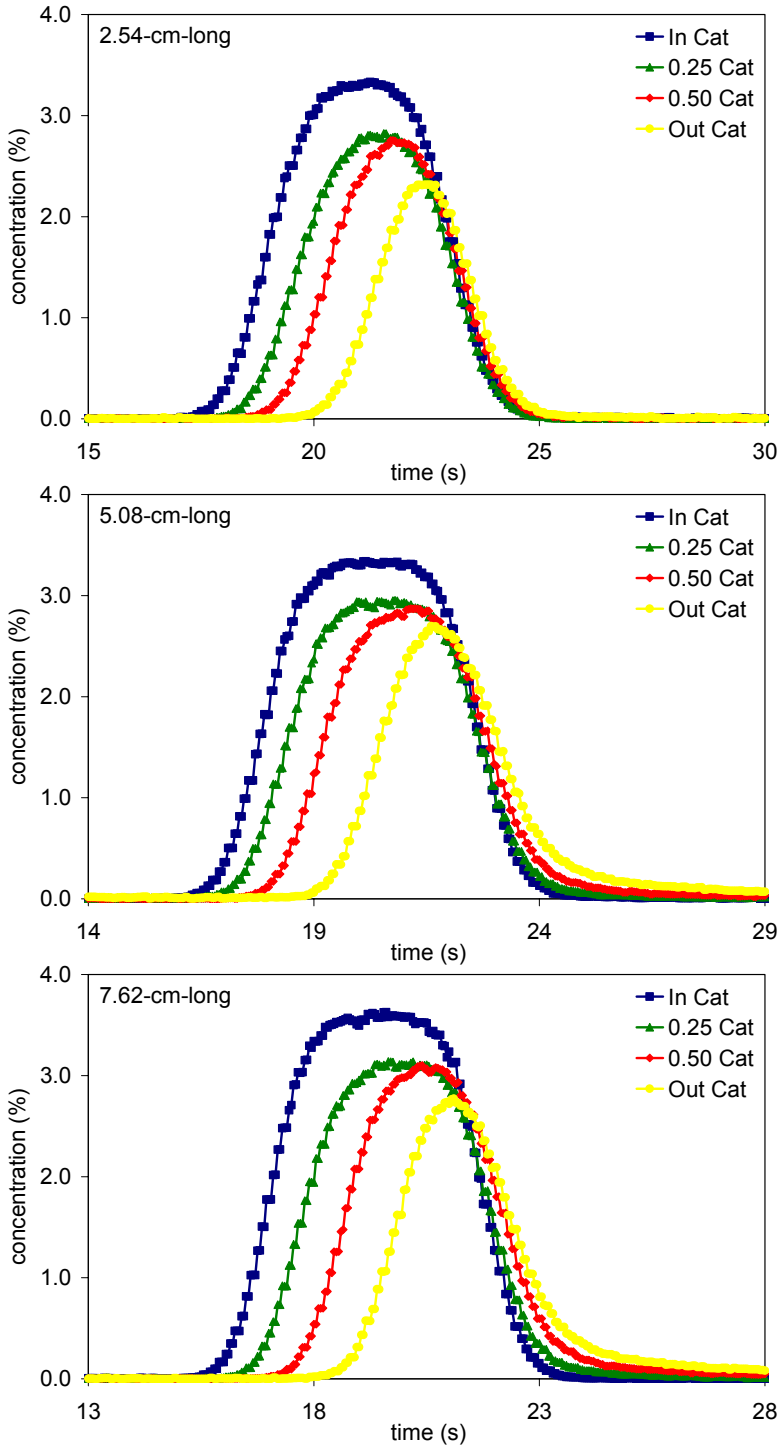

Figure A.21. Catalyst B's H_2 consumption trends in 2.54, 5.08 and 7.62-cm-long samples in back-mixing (OSC experiments with 10s nitrogen purge) short-cycle experiments with 3.4% H_2 in rich phase at 500˚C

VITA

Vitaly Y. Prikhodko was born in Zernograd, Russia on October 5, 1979. He came to the USA in 1997 as a high school exchange student in Bedford, Virginia. After completing high school he began studying computer science and business at the Maryville College, Maryville, Tennessee. In May 2002 he received a Bachelor of Arts degree from the Maryville College. Upon completion of his undergraduate studies he worked at the National Transportation Research Center, Knoxville, Tennessee for a year, and in 2003 he enrolled in the graduate studies program at the University of Tennessee, Knoxville. Vitaly received his Masters of Science degree in Mechanical Engineering from the University of Tennessee in August 2007.